uOttawa

L'Université canadienne
Canada's university

FACULTÉ DES ÉTUDES SUPÉRIEURES ET POSTOCTORALES

uOttawa

L'Université canadienne
Canada's university

FACULTY OF GRADUATE AND POSDOCTORAL STUDIES

Line Bouchard

AUTEUR DE LA THÈSE / AUTHOR OF THESIS

M.Sc. (Physics)

GRADE / DEGREE

Department of Physics

FACULTÉ, ÉCOLE, DÉPARTEMENT / FACULTY, SCHOOL, DEPARTMENT

Stabilization of an FM Active Harmonic Mode-Locked Fiber Laser at High Repetition Rates

TITRE DE LA THÈSE / TITLE OF THESIS

X. Bao

DIRECTEUR (DIRECTRICE) DE LA THÈSE / THESIS SUPERVISOR

CO-DIRECTEUR (CO-DIRECTRICE) DE LA THÈSE / THESIS CO-SUPERVISOR

EXAMINATEURS (EXAMINATRICES) DE LA THÈSE / THESIS EXAMINERS

J. Armitage

A. Czajkowski

E. Fortin

Gary W. Slater

LE DOYEN DE LA FACULTÉ DES ÉTUDES SUPÉRIEURES ET POSTDOCTORALES /
DEAN OF THE FACULTY OF GRADUATE AND POSTDOCORAL STUDIES

ATH

Stabilization of an FM Active Harmonic Mode-Locked Fiber Laser at High Repetition Rates

Line Bouchard

Thesis submitted to the
Faculty of Graduate and Postdoctoral Studies
In partial fulfilment of the requirements
For the MSc degree in Physics

Department of Physics
Faculty of Science
University of Ottawa

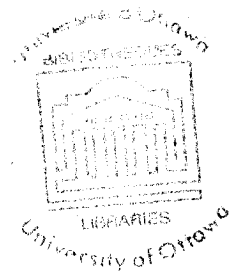

Your file Votre référence
ISBN: 978-0-494-41788-1
Our file Notre référence
ISBN: 978-0-494-41788-1

Abstract

A new and simple approach was optimized for stabilizing a harmonic active mode-locked fiber laser at 40GHz. A computer tunes the modulation frequency in a 500kHz band near 40GHz to follow variations in the optical cavity length. A second approach based on a Proportional-Integral (*PI*) controller and a piezo fiber stretcher was also developed and optimized. This approach uses a circuit-controlled piezo (PZT) device to physically counteract optical cavity length variations.

The optimized circuit-controlled and computer-controlled approaches were compared to draw conclusions on their performance. Results for the pulse characteristics, the side mode suppression ratio and the time jitter show that both approaches provide an efficient method for stabilizing a harmonic FM active mode-locked fiber laser at 40GHz. Finally, the versatility of both approaches was used to attempt to generalize the two methods for use at any modulation frequency up to 40GHz.

This work contains no material which has been accepted for the award of any other degree of diploma in any University or other tertiary institution and, to the best of my knowledge and belief, contains no material previously published or written by another person, except where due reference has been made in the text.

I give consent to this copy of my thesis, when deposited in the University Library, being available for loan and photocopying.

SIGNED:.....

DATE:.....

Supervisor: Dr. Xiaoyi Bao

Acknowledgement

I am grateful to many people for helping me over the two last years with the various aspects of this project and the realization of this thesis.

First, I would like to thank my supervisor Dr. Xiaoyi Bao for having given me the opportunity to undertake this project. It has been a privilege for me to work with her. She was exactly the supervisor that I was hoping to find: always present, supportive and encouraging of my work. Indeed, I found in Dr. Bao more than a supervisor, I found a friend.

Second, my colleagues provided me with many comments and suggestions that have greatly benefited me. I would like to thank Dr. Shiquan Yang who endured my endless questions and who always replied with helpful suggestions and comments on my work. I would also like to thank Dr. Evgueni A. Ponomarev for his many ideas and insightful comments; Balchoya spaciba! Finally, I would like to thank Fabien Ravet for his help and patience but perhaps more so for his smile and cheerfulness. He made the Fiber Optic Lab a pleasant place for me to work.

Third, I would like to thank my family, especially my parents Denis Bouchard and Madeleine Tremblay who have encouraged me in every endeavour I have ever undertaken. For being my sister, in all that this entails, and for her sympathetic ear, I would also like to thank Anik Bouchard.

I would be remiss to forget the support that I have received from my friends, and so I would like to thank Oscar and Ana for their encouragement and support over the last two years and the Laflammes for their constant interest and optimism.

Finally, I am deeply indebted to the love of my life, Dana Smith, whose uncanny ability to find the silver lining in even the stormiest of clouds has given me the strength to overcome the challenges of undertaking a project in a new field and in a new language. Without him, this thesis could not have been written. Dana, for all of the help that you have given me and for all of the patience that you have shown and continue to show, I would like to offer my heartfelt thanks.

Table of Contents

List of Figures

1. Introduction

Active harmonic mode-locked fiber lasers have become popular in recent years because of their ability to generate ultrashort optical pulses with high repetition rates. The principal interest in such lasers is for application in high-speed telecommunication systems. These lasers are generally used for producing high signal-to-noise ratio pulses. However, the very long cavity length required for these applications, and hence the small inter-mode frequency spacing, means that the lasers are sensitive to changes in temperature. A stabilization process is thus required to get transform-limited optical pulses of picosecond duration or less.

Much research has been undertaken to find a way of stabilizing active harmonic fiber lasers due to temperature fluctuations. In 1992, stabilization of a fiber laser with a piezo fiber stretcher was achieved for the first time by Shan [15]. The piezo (PZT) was wound around an erbium-doped fiber and stretched using an amplified signal with a response proportional to the mixing of the electrical output signal from the laser and the synthesizer. The stretched fiber length produced a change in the optical cavity length that could counteract the effect of temperature variations and stabilize the laser.

In 1997, a new method based on the same principle was developed by Nakazawa [17]. In this approach, a Proportional-Integral *PI* controller was used instead of a gain amplifier to control the PZT. In addition, the modulation frequency applied to the modulator was produced using a clock extraction circuit.

It should be noted that the signal from the modulator, which can be extracted differently depending on the kind of fiber laser, plays a critical role in the process of stabilization. The modulation frequency used by Nakazawa was extracted by passing the signal from the laser output through a narrowband electrical filter (i.e. a clock extraction circuit). This method allows at least one multiple integer of the inter-mode beat frequency separation to coincide with the modulation frequency at any moment in time. In order to avoid amplification of side modes however, either the electrical filter must have a bandwidth smaller than the mode spacing inside the cavity, or there must be an effective side mode suppression mechanism. The signal that drives the modulator, as described by Shan [15], and used in this thesis, differs from the one used by Nakazawa [17] in that an external RF synthesizer with a known frequency sets the signal, which avoids the need for a clock extraction circuit.

External temperature variations – such as those caused by an air conditioner – alter the laser's optical cavity length and hence cause the inter-mode frequency spacing to change. Since the fiber laser is modulated at high repetition rates, which requires the use of a multiple integer of the fundamental inter-mode frequency spacing, even a small change in this frequency spacing due to temperature fluctuations can cause significant instability. For the mode-locked fiber laser used in this thesis, the synthesizer-driven modulation frequency is fixed at a multiple integer of the inter-mode frequency spacing. Since this latter varies with the temperature, the fiber laser thus becomes unstable and a method of stabilization was required.

The goals of this project were threefold: to optimize a new and simple method of stabilization developed by Ponomarev for a 40GHz mode-locked fiber laser [14]; to build a second stabilization approach based on Shan [15] and Nakazawa [17] to compare it with the

new approach; and, to draw conclusions on the performance of both approaches at different modulation frequencies.

The new approach [14] uses computer control to adjust the modulation frequency to track changes in the inter-mode frequency spacing. This method does not counteract the effects of temperature then, but rather follows the variations in order to keep the laser stable. The second approach (adding an *I*, or integral, controller to that used by Shan [15] and using an external synthesizer to obviate the need for a clock extraction circuit as in Nakazawa [17]) uses a piezo fiber stretcher, driven by an electronic circuit, to physically increase or decrease the cavity length to keep the total optical cavity length constant.

A hybrid approach, used as a transition between the first and the second approaches, was also developed and used to stabilize the fiber laser. It uses a computer to control the piezo fiber stretcher to maintain the optical cavity length constant. This hybrid method will be introduced but not compared with the other two methods due the strong similarity of its performance with the first method.

The first two chapters introduce the mode-locking phenomenon and the components that comprise an FM harmonic active mode-locked fiber laser, including the causes and consequences of instabilities. The three methods of stabilization are explained in detail in Chapter 3, followed by the results and optimization in Chapter 4. The comparison between the computer-controlled method and the circuit-controlled method is undertaken in Chapter 6. The generalization of the two methods to modulation frequencies of 10GHz, 5GHz and 2.5GHz is presented in Chapter 7.

2. Mode-locked Fiber Lasers

2.1. Historical Background

Snitzer first proposed a cavity laser using fiber in 1961 [34], and in 1964 demonstrated an optical fiber amplifier using Nd-doped fiber [11]. The first demonstration of a rare-earth single-mode fiber was in 1983 [11], followed two years later by the development of a Nd-doped single-mode fiber laser. It took more than 20 years and the development of rare-earth-doped fiber amplifiers before fiber lasers became popular. The key breakthrough was in 1987 when Er-doped fiber amplifiers (EDFAs) were demonstrated, which eventually led to development of mode-locked Er-doped fiber lasers (EDFL).

EDFAs became very popular due to their wide spectrum bandwidth and their capacity to amplify the signal in the spectral region around 1.55μm, the optimum window for signal transmission in optical fiber. These same characteristics make EDFAs good candidates for gain amplification in mode-locked fiber laser cavities. EDFLs have been used in telecommunication and sensing applications and also have potential for use in laser cutting, drilling, and medical applications. Research continues in each of these domains with the objective of generating the shortest pulse duration and the highest peak power possible.

Two distinct techniques are generally used to generate short optical pulses with fiber lasers, depending on the application. One technique, involving mode-locking of the fiber laser, is usually used for applications that require a pulse duration in the femtosecond range but do not necessarily require a high peak power. Telecommunications and medical

research are the prime applications for mode-locked fiber lasers. Another technique, called Q-switching, generates bursts of pulses with widths in the nanosecond range. The Q-switching technique is primarily used in laser cutting or drilling applications where high peak power is required.

Following a short review of the principles of a laser, the concept and techniques of mode-locking will be introduced, followed by a discussion of Q-switching.

2.2. Fiber Laser Principles and Design

Lasers, or light amplification by stimulated emission of radiation, produce a high-energy, monochromatic, coherent beam of electromagnetic radiation. The essential elements of a laser are the gain medium formed by ions or atoms, a pumping process to excite these molecules to a higher energy level, and a reflection system to allow the radiation to bounce back and forth inside the cavity coherently, and eventually to leave the laser cavity (see Figure 2.1).

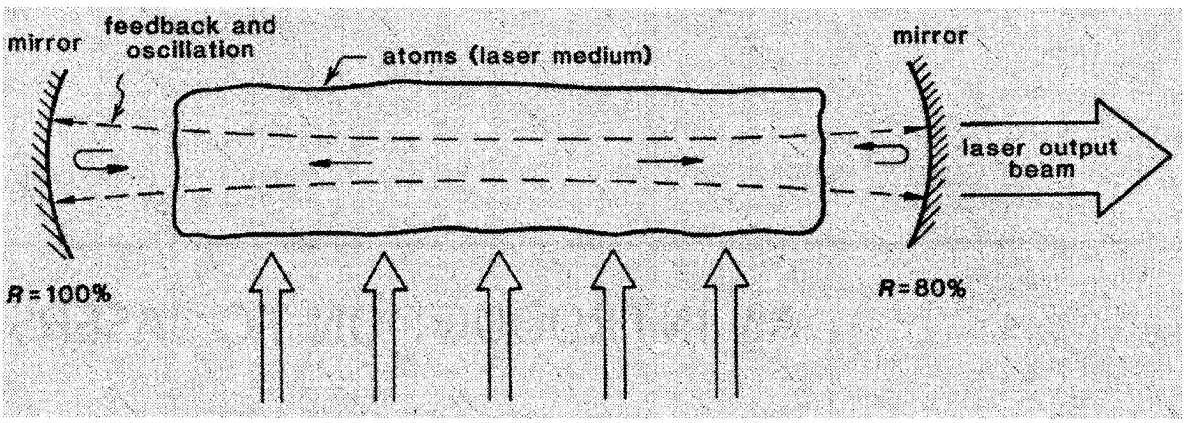

Figure 2.1: Elements of a typical laser oscillator (Lasers [1], pp2).

A fiber laser is essentially a fiber amplifier situated within a cavity that can provide optical feedback. There are many different possible cavity designs for a fiber laser, but the most common one is the Fabry-Perot. The Fabry-Perot cavity consists of a gain medium placed in a resonant cavity formed by two flat high-reflecting mirrors at either end of the

cavity. The cavity itself is made of optical fiber and the mirrors are usually butt-coupled to the fiber ends to avoid losses. Alignment is difficult with such a design since even a small change in the position of one of the mirrors leads to high cavity losses. Other designs avoid this alignment problem by using dielectric mirrors directly deposited on the fiber ends or by using a fiber Bragg grating.

The laser cavity used in this experiment is the ring cavity, which provides unidirectional operation. The basic advantages of the ring cavity are that it requires no mirrors and is an all-fiber cavity. Figure 2.2(a) shows a simple model of a ring cavity formed by a fiber coupler, a doped fiber gain medium, an isolator, and a polarization controller. The coupler has one port for the input pump, one port for the laser output and two ports which are connected together to close the loop of the ring cavity. The isolator is required to allow propagation in only one direction in the fiber cavity, and the polarization controller to adjust the polarization of the light.

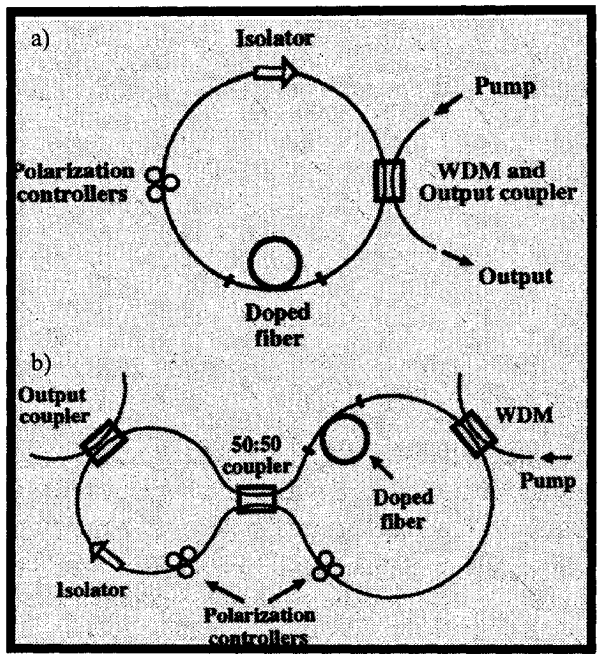

Figure 2.2: (a) Schematic of a unidirectional ring cavity used for fiber lasers (Applications of Nonlinear Fiber Optics [4], pp204); (b) Schematic of a figure-8 cavity useful for mode-locked fiber lasers (Applications of Nonlinear Fiber Optics [2], pp205).

Many other fiber laser designs are based on this simple ring cavity, such as the figure-8 cavity, as shown in Figure 2.2(b). The right-hand ring of the figure-8 cavity is composed of a gain medium whereas the left-hand ring is composed of an isolator and an output coupler. A polarization controller is needed on both sides of the figure-8 since the isolator requires polarized light and a coupler is used to link the two rings together.

Since there is no isolator in the right-hand ring, the light coming from the coupler will be split into two beams that will interfere with each other once back in the coupler. Depending on their phase difference, the interfered beams will either be reflected or transmitted into the left ring. The figure-8 model is then an interesting cavity design since it controls the phase of the light and allows passive mode locking (passive mode-locking will be explained in more detail in section 2.6).

2.3. Laser Cavity Modes

Even though lasers are called 'monochromatic', all lasers produce light over a small but finite range of frequencies. The bandwidth of the laser is determined by the bandwidth of the gain medium and, in the case of low cavity loss, is also related to the characteristics of the optical cavity. When molecules are excited in the gain medium, the light emanating from the process acts as a wave and is reflected between two mirrors at the cavity ends to interfere with itself. This phenomenon leads to the creation of standing waves with discrete frequencies inside the cavity, known as longitudinal modes.

In a Fabry-Perot cavity, a simple equation links the distance between the two mirrors at a distance L from each other and the wavelength λ of each longitudinal mode inside the cavity:

$$L = \frac{m\lambda}{2} \tag{2.1}$$

where m is an integer and is called the mode order. For a specific distance L, only certain longitudinal modes can oscillate, while all others are suppressed by destructive interference. Since L is usually much greater than the wavelength λ, the relevant mode orders are very large and many modes can oscillate inside the cavity within the laser gain bandwidth. The inter-mode frequency separation can be deduced using Equation 2.1 and the relation $f = c/\lambda$, where c is the speed of light inside the cavity, and is written as follows:

$$\Delta\nu = \frac{c}{2L} \tag{2.2}$$

The combination of the longitudinal modes inside the cavity and the gain bandwidth thus give the laser a real spectral bandwidth (see Figure 2.3). Since the inter-mode frequency spacing is relatively small compared to the gain bandwidth, the laser operates in a

multimode regime. Understanding the interaction of these oscillating modes with each other is critical for the development of the concept of mode locking.

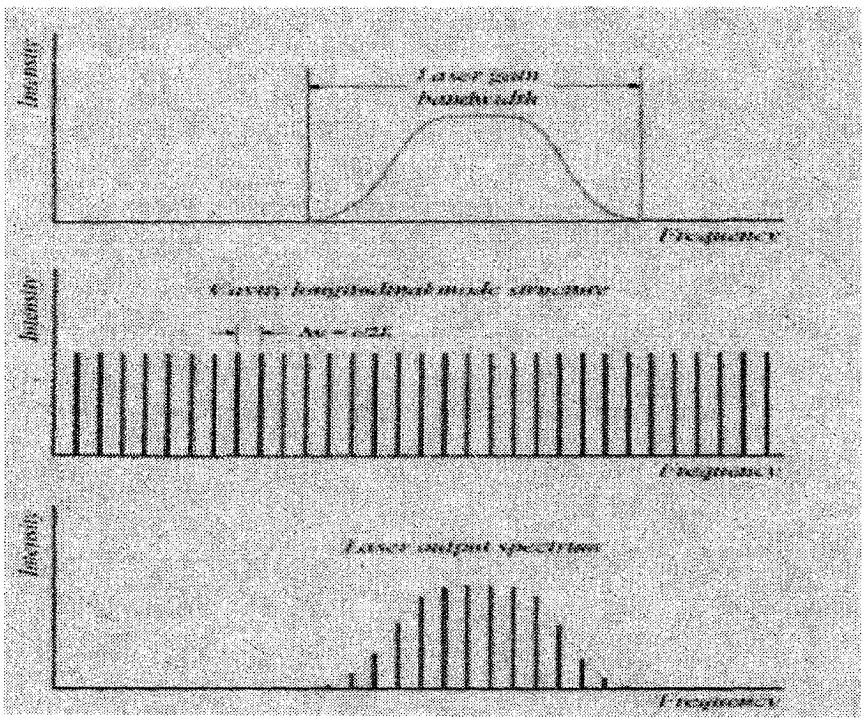

Figure 2.3: Combination of the longitudinal modes inside the cavity and the gain bandwidth [41].

2.4. Mode-Locking Principle

The cavity of the laser contains longitudinal modes that oscillate at discrete frequencies. Since these frequencies do not possess a direct relationship among themselves, each mode oscillates independently of the others. As a consequence, the modes do not necessarily have the same phase.

The total optical field *e(t)* inside the cavity can be written as follows:

$$e(t) = \sum_{n} E_n e^{(i\varphi_n - i\omega_n t)} \tag{2.3}$$

where E_n, φ_n, and ω_n are respectively the amplitude, phase and frequency of one mode, and n is an integer that signifies the number of modes oscillating inside the cavity. Since the phase has a random distribution among the modes, the laser will simply operate in a

multimode CW (Continuous Wave) regime as the interference between the modes tends to average out to zero in the intensity of the total optical field *e(t)*. In the time domain, this results in an incoherent pulse of light that gets repeated every round trip as seen in Figure 2.4 (a).

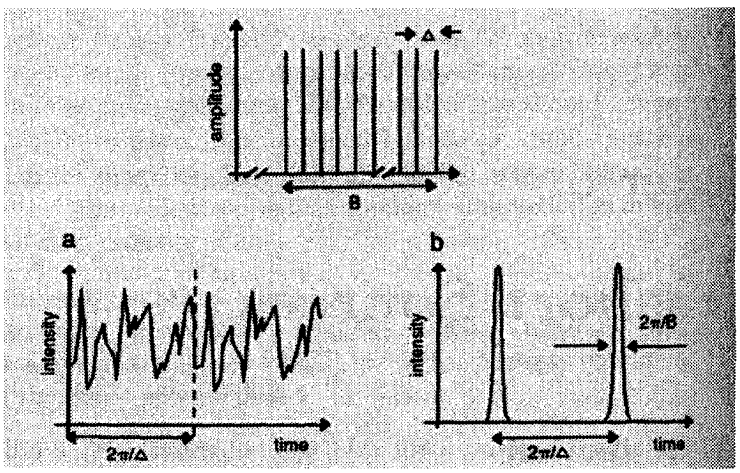

Figure 2.4: A set of equally spaced modes, and the inverse Fourier transform of that spectrum. In (a), the modes have a random phase distribution. In (b), all modes are "locked" to the same phase (Ultrashort Laser Pulse Phenomena[8], pp210).

If the phase of all the modes in Equation 2.3 could be fixed, for example, to a value of zero, then the total optical field would be:

$$e(t) = \sum_n E_n e^{(i\omega_n t)} \tag{2.4}$$

This sum can be performed analytically by noting that the amplitude E_n for all modes is the same and that the mode frequency $\omega_n = \omega_o + n\omega$. The result of the total intensity can then be written as follows:

$$|e(t)|^2 = \frac{\sin^2\left(\frac{N\omega t}{2}\right)}{\sin^2\left(\frac{\omega t}{2}\right)} E_o^2 \tag{2.5}$$

where N is the number of modes locked together. This results in a train of pulses with a repetition rate equal to the inter-mode frequency spacing of the cavity since the period,

$2\pi/\omega$, gives a repetition rate of $2l/c$ as seen in Figure 2.4 (b). The peak power of each pulse is exactly N times the average power.

To illustrate the phenomenon, the optical field and intensity for three modes is plotted in Figure 2.5 where the phases have been fixed at $t = 0$ seconds. When these three modes are added together, the combination of destructive and constructive interference leads to a train of pulses with a peak intensity three times the average intensity.

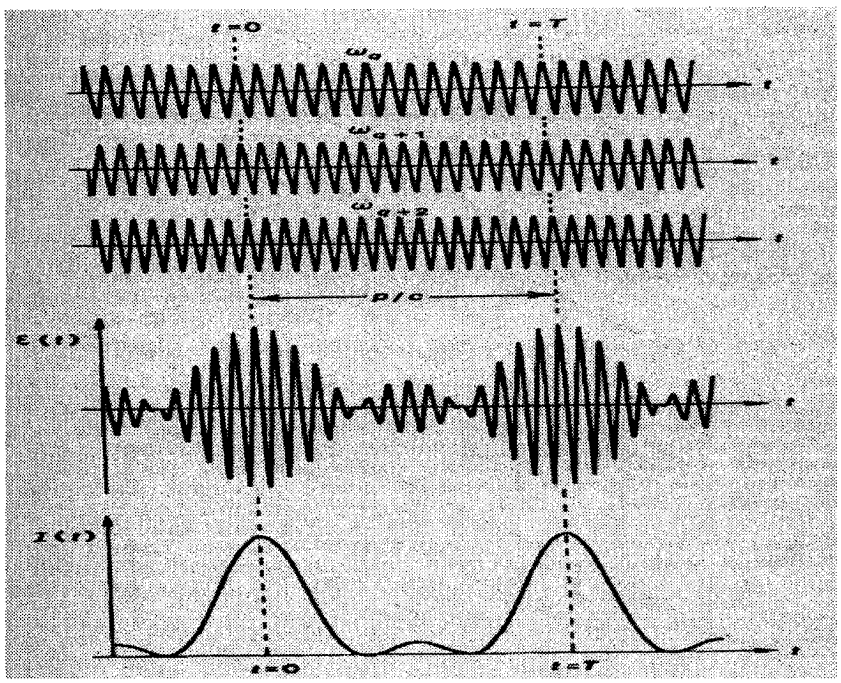

Figure 2.5: Superposition of three equally spaced frequency components which are all exactly in phase at $t = 0$ (Lasers [1], pp 1047).

The overall pulse width will change according to the number of modes that the laser can sustain. If more longitudinal modes inside the gain medium bandwidth, all in phase, could be added into Figure 2.5, the result would be a shorter pulse. In fact, if N modes are locked together inside the cavity with a frequency separation of Δv, the total spectral bandwidth will become $N\Delta v$. If the pulse width τ represents the time from the maximum peak pulse to its first zero and is written as $\tau = T/N$, it can be approximated to be $\tau \approx (N\Delta v)^{-1}$. Although an approximation, this equation adequately describes the relationship

between the pulse width and the spectral bandwidth. Nevertheless, in order to have an exact relationship between these two parameters, the nature of the gain bandwidth needs to be considered.

This characteristic of fixing the phase of multiple modes is called mode-locking and is frequently used in fiber laser systems to generate short pulse durations. The two most common techniques are called active mode-locking and passive mode-locking.

2.5. Active mode-locking

Active mode-locking requires an external signal to induce a modulation to the optical field inside the cavity and to force all the modes to be in phase. There are three techniques for active mode-locking: AM (amplitude modulation) mode-locking, FM (frequency modulation) mode-locking, and synchronous pumping.

AM mode-locking generally uses an acousto-optic or electro-optic modulator inside the cavity. This modulator is driven by an electrical signal and generates sinusoidal amplitude modulation of the optical field inside the cavity. In the frequency domain, the AM produces modulation sidebands separated by twice the modulation frequency f_m. Assuming that a mode is modulated by a high modulation frequency f_m, its frequency f_o will encounter a shift of (f_o-f_m) and (f_o+f_m).

In order to have mode-locking, the modulation frequency must be chosen in a way that these two sidebands overlap the two frequencies of the adjacent modes inside the cavity. The reason is that since the sidebands are driven in-phase, the mode and its two neighbouring modes can be phase-locked together; in fact, the energy will be distributed over all the sidebands. Therefore, the modulation frequency has to be equal to the inter-mode frequency spacing of the cavity laser. As a consequence, the process of modulation is

repeated for sidebands equal to an integer multiple of the cavity mode spacing and is complete when all the modes included in the gain bandwidth are locked together (see Figure 2.6).

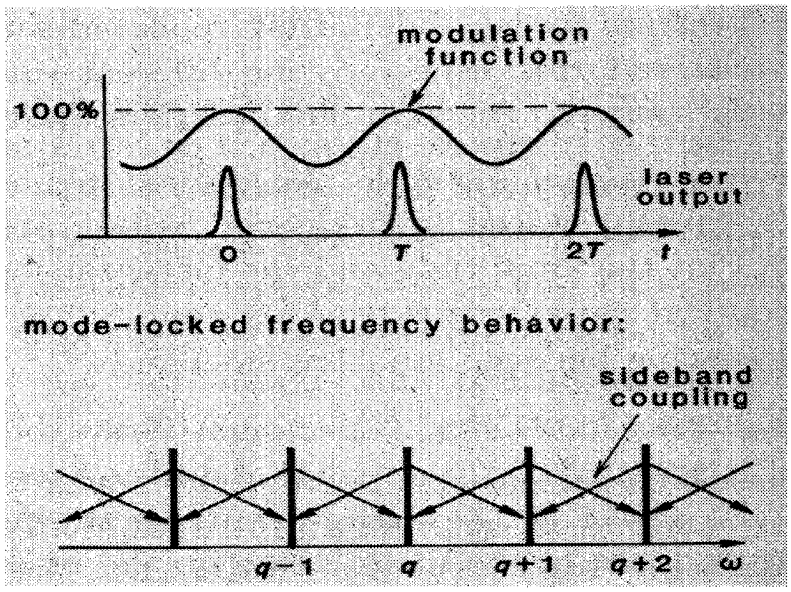

Figure 2.6: Active AM mode-locking of a standing-wave and its description in the time and frequency domains (Lasers [1], pp 1056).

In the time domain, the process of amplitude modulation can be understood as follows: the modulation can be represented as a thin shutter included inside the cavity that modulates the loss of the optical signal in a step-like manner. When the shutter is closed, no light passes through the modulator; when the shutter is opened for a short period of time, the light passes through the modulator. Since the shutter is open for such a short period of time, the high losses mean that no single mode can oscillate in the cavity. The only exception is if the modes are all in phase, creating a very narrow pulse with a time duration smaller than the shutter opening speed. This narrow pulse, arriving at the instant when the shutter is opened, is not affected by the shutter and will survive at each round-trip, allowing the mode-locking to build up over successive cycles in the cavity. The shutter opening at

the exact moment the pulse passes through is the equivalent of a modulation frequency that corresponds exactly to a multiple of the inter-mode frequency spacing.

FM mode-locking uses a frequency or a phase modulator, instead of the amplitude modulator, inside the cavity. This type of modulator uses an electro-optic effect that is driven by an electrical signal to induce a frequency shift to the light. If the modulation frequency is exactly equal to the intermode frequency spacing, some modes encounter an up-shift in frequency while others encounter a down-shift in frequency. The only mode that is not affected is the one that encounters no frequency shift by the modulator. These shifts will continue until the modes are either in phase with the non-shifted mode or are outside the gain bandwidth of the laser and hence suppressed. This frequency shifting mechanism eventually leads to mode-locking and produces a very narrow pulse.

Harmonic mode-locking is frequently used with AM or FM mode-locking. The modulation frequency is chosen as a multiple integer of the intermode frequency spacing to produce a short optical pulse with higher repetition rates. This method is very useful for applications in telecommunication where the repetition rate is an important criterion to consider. Harmonic mode-locking using an FM modulator is the approach used in this experiment.

The final form of active mode-locking is referred as synchronous pumping. In this case, the modulator is not placed inside the cavity but instead modulates the pump laser current at a frequency that matches an integer value of the inter-mode frequency spacing. This form of mode-locking also results in a short optical pulse.

2.6. Passive mode-locking

Passive mode-locking relies on the inherent characteristics of the laser itself and does not require any active components inside the cavity to produce a mode-locked pulse. One method uses a nonlinear element in the laser cavity that is intensity-dependent and changes the intracavity light to produce ultrashort pulses. Such devices are called saturable absorbers. A saturable element is a material that has constant optical absorption properties for low-intensity optical sources, but decreases in absorption capacity as the optical light increases in intensity. The saturation point is reached when the light has a sufficiently high intensity to overcome the nonlinear effect of the material and propagates without intensity changes.

When the saturable absorber is placed inside the laser cavity, the low-intensity light is attenuated or absorbed by the nonlinear effect. At this point, the absorption is larger than the gain of the laser and prevents the signal from building up inside the cavity. However, when the gain of the laser is high enough to overcome the absorption of the saturable absorber, small oscillations caused by noise are formed inside the cavity. Due to the somewhat random noise distribution, a noise spike that has a slightly larger intensity can propagate preferentially due to the nonlinear element. In fact, as the gain continues to sustain the oscillation level, the high-intensity spike will amplify and eventually overcome the loss of the saturable absorber.

The saturable absorber will then allow the noise spike to propagate and grow in intensity and will absorb all weaker noise spikes that have not reached the saturation point. The central spike experiences less loss than its less-intense sidebands such that the pulse width shrinks until its spectral bandwidth is equal to the gain bandwidth, which results in

the formation of a single, very short optical pulse that is repeated every round trip: a mode-locked pulse.

In most cases, passive mode locking leads to a shorter pulse than for active mode-locking. In fact, using a passive element inside the cavity leads to a perfect synchronism between the modulation and the pulse since the modulation process is induced by the pulse itself; the shorter the pulse, the greater the efficiency of modulation. Saturable absorbers also have very fast response times, which help the build-up process. In contrast, since the modulation frequency in active mode-locking is fixed at the round-trip time of one of its harmonics, some fluctuations or imperfections in the laser could cause the pulse to not be synchronised with the modulation signal and thus lead to pulse broadening, as shown in Figure 2.7 (b).

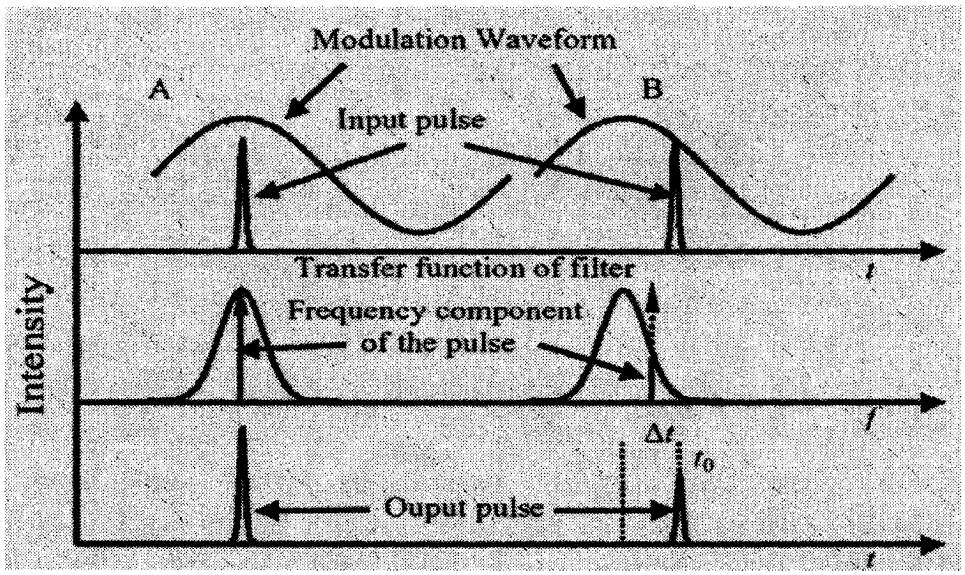

Figure 2.7: The principle of modulation loss variation in asynchronous mode locking: *A* is the synchronized modulation case and *B* is the asynchronous modulation case [20].

Passive mode-locking leads to low repetition rates, however. Since passive elements are based on random processes, they usually lead to the formation of only one ultrashort pulse per round trip. Increasing the pump power could lead to the formation of two or more

pulses in the same round trip but the pulses are not necessarily equally spaced since each pulse is independently formed from random distributed noise. Harmonic active mode-locking is therefore a better candidate for telecommunication applications, since high and fixed repetition rates can be achieved with a simple change in the modulation frequency.

2.7. Principle of Q-Switching

Q-switching is a widely used technique that, as with mode-locking, generates ultra-short optical pulses in fiber lasers. This approach plays on the quality factor Q of the laser optical resonator and differs from passive mode locking in its requirement of much higher loss in the cavity to create a massive population inversion. By definition ([1], pp.180), the Q-factor measures the ratio of the energy of the light stored to the power dissipated in a certain volume. In more concrete terms, Q is the amount of light in the gain medium that is not lost and therefore available to join the resonator feedback loop. A low Q-factor means high cavity losses per round trip while a high Q-factor signifies the opposite.

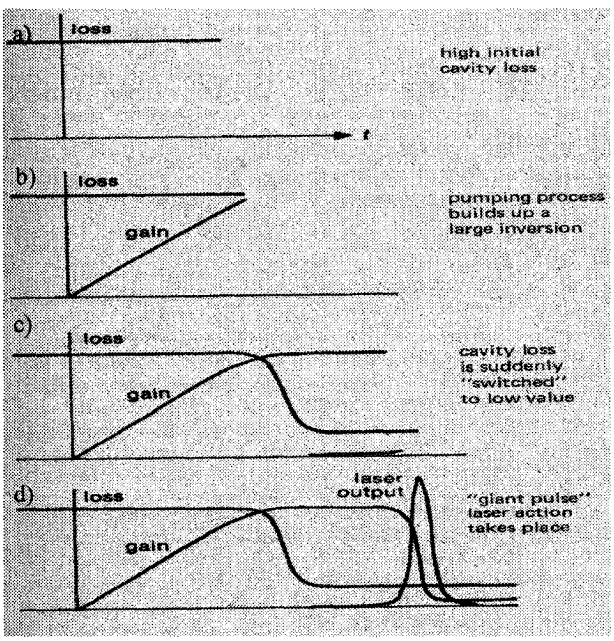

Figure 2.8: Laser Q-switching, step-by-step (Lasers [1], pp 1005).

In order to produce a pulse, the laser medium is first pumped with a low Q-factor to produce high cavity losses as shown in Figure 2.8(a). This allows the development of a population inversion in the cavity that is much larger than usual. As the population inversion increases, the energy stored eventually reaches a saturation level. This level is called gain saturation and is due to losses from different processes such as spontaneous emission inside the cavity (see Figure 2.8(b) and (c)). After this threshold has been reached, the Q-factor is restored abruptly to a high value and causes the gain to become much larger than the cavity loss. This unstable state precipitates oscillations that build up at an unusually rapid rate in the resonator and that initiate optical amplification by stimulated emissions, as shown in Figure 2.8(c).

This process allows a very quick transformation of the energy stored in the gain medium into photons, which oscillate in the optical resonator. The oscillation burst rapidly decreases the population inversion to a level well below the cavity loss level, which very quickly arrests further amplification of the pulse and leads to a very short pulse with a high peak intensity (see Figure 2.8(d)). This pulse is called a "giant pulse" and has a duration typically in the range of a few nanoseconds and a peak power three or four orders of magnitude higher than for the same fibre laser using the same pump power in CW regime.

There are two essential elements that determine the pulse shape as well as the performance of a Q-switched laser: the initial inversion ratio r and the cavity decay rate. The inversion ratio is the relation between the population inversion (gain) immediately after the switching process and the threshold inversion of the losses at the same time (see Figure 2.9). The cavity decay rate is sum of round trip cavity losses compared with the cavity round trip time.

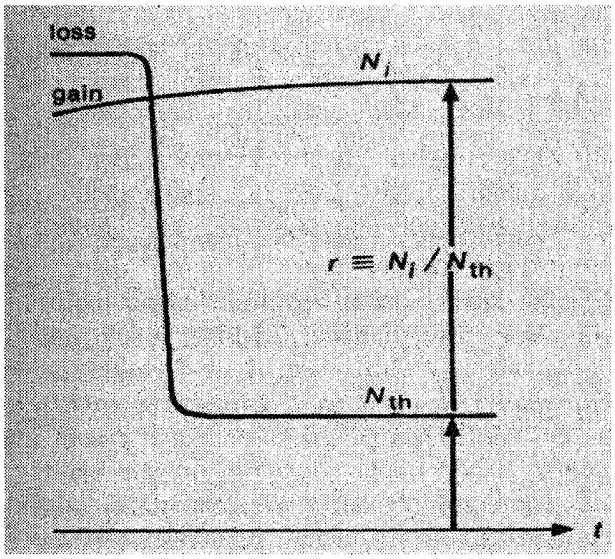

Figure 2.9: Inversion values and inversion ratio just after the Q-switch is opened (Lasers [1], pp 1011).

Figure 2.10 shows pulse shapes for Q-switching with different initial inversion ratios. The plots show that a Q-switched pulse is different from pulses produced in mode-locking processes. First, the pulse width of the Q-switched pulse appears to be broader. Since the mode-locking process is a balance between the modulation and the gain bandwidth, the pulse becomes shorter due to the wide available spectral bandwidth. In contrast, Q-switching doesn't give time to the system to find a balance before a pulse is launched, hence leading to a pulse with small spectral bandwidth and longer duration.

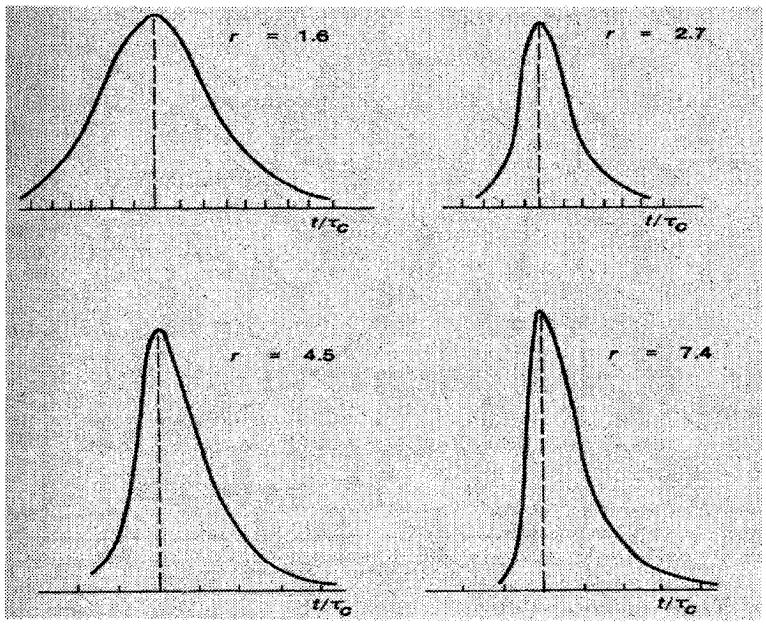

Figure 2.10: Exact Q-switched pulse shapes (Lasers [1], pp 1019).

In addition, the pulse shapes in Figure 2.10 are asymmetric. This asymmetry becomes much worse as the initial inversion ratio increases to a ratio much greater than one. This is because the initial inversion ratio gives the amount of energy that needs to be depleted after the Q-factor is restored. The growth rate of the leading edge of the pulse is then dependent on this ratio and increases in speed as the energy stored increases. The trailing edge of the pulse is dependent only on the cavity decay rate since the system has to drive the gain down to zero and hence is a slower process than for the leading edge.

There are two basic methods of Q-switching: active and passive Q-switching. Active Q-switching makes use of either externally controlled mechanical devices such as shutters and spinning mirrors or modulators to create the low and high Q-factor needed. The more widely used technique is passive Q-switching, which uses a saturable absorber with higher losses than similar absorbers used in passive mode-locking to allow the population inversion to reach the gain saturation level.

The explanation of the mode-locked fiber laser principles in this chapter is critical to understanding the design of such a laser. In fact, the choice of cavity components is important for the laser performance and hence must be carefully considered. The following chapter gives an overview of the cavity components chosen for the FM active harmonic mode-locked fiber laser at 40GHz as well as the laser performance.

3. Active FM Harmonic Mode-Locked Fiber Lasers: Components and Performance

3.1. Introduction

Each component of an active harmonic mode-locked fiber laser has a critical role to play in the generation of ultrashort pulses. Since the component parameters determine the performance of the fiber laser, they must be well defined and properly chosen. This chapter gives an overview of the characteristics of each element of the active FM harmonic mode-locked fiber laser used in this experiment, including the stability limitations.

3.2. Components of a Fiber Laser

The fiber laser used in this experiment makes use of harmonic active mode-locking with frequency (phase) modulation at a modulation frequency of 40GHz. The setup of the fiber laser is shown in Figure 3.1.

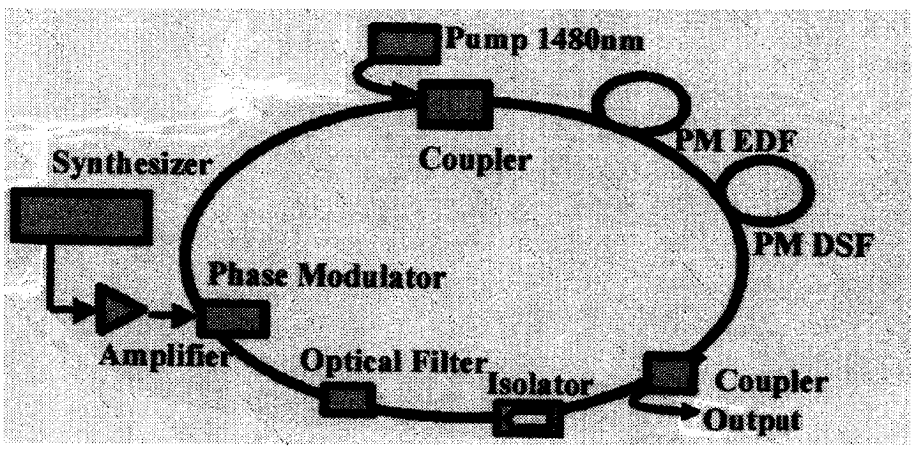

Figure 3.1: Setup of the fiber laser used in this experiment.

The cavity of the fiber laser is made of a ring since it is easier to integrate the components and avoids alignment problems. PM (polarization-maintaining) fiber is used to

control the polarization inside the cavity. The gain medium is composed of a pump laser feeding a section of erbium-doped fiber. The gain medium is followed by a section of dispersion-shifted fiber to compress the pulse into a soliton (further explained in section 3.2.2), a coupler to retrieve the output of the laser, an isolator to allow unidirectional propagation, an optical filter to maintain the bandwidth and the central wavelength at one specific value, and a phase modulator.

3.2.1. Erbium Doped Fiber Amplifier (EDFA)

The gain medium is the key element in the design of a laser. The optical gain determines the wavelength range of operation. Doped-fiber amplifiers, using rare-earth elements as the gain medium, are good candidates for use with fiber lasers since they can amplify and operate over a wide wavelength range from 0.5-3.5μm. The amplification characteristics of these amplifiers depend on the rare-earth element doped into the fiber. Erbium Doped Fiber Amplifiers (EDFAs) are the fiber amplifiers that have attracted the most attention for fiber lasers since they offer a wide gain bandwidth near 1.55μm, the principal fiber-optic communication wavelength.

When erbium is doped into silica fiber, it becomes triply ionized (Er^{3+}) resulting in the formation of new energy bands, as shown in Figure 3.2. These diverse energy bands offer many different possibilities for pumping the Erbium-doped fiber. Electrons can either absorb energy via the pumping and move up to a higher energy level or they can give off energy via stimulated or spontaneous emission and move back down to a lower energy level. The wavelength of the pump must be the same as one of the transition bands for the dopants to be excited. As a consequence, it is possible to pump the EDFA efficiently using a semiconductor laser at either 0.98μm or 1.48μm (see Figure 3.2).

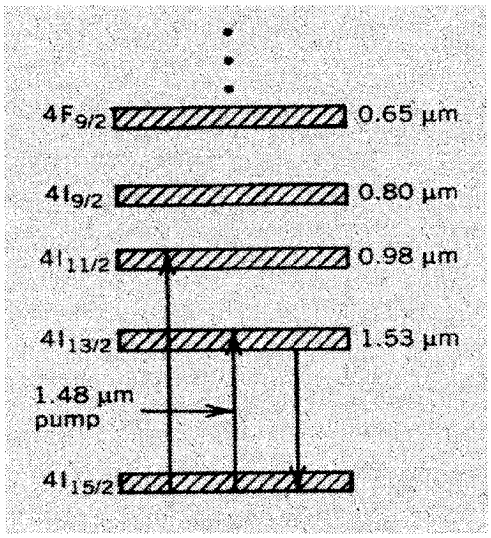

Figure 3.2: Energy levels of erbium ions in silica fibers (Applications of Nonlinear Fiber Optics [2], pp 158).

When the pump laser is turned on, the doped ions absorb the photons and are excited into one of the upper energy levels. Since this higher energy level is an unstable state however, the dopants encounter a rapid nonradiative relaxation to a lower energy in a metastable state. The EDFA is classified as a three-level amplifier, which means the dopants in the metastable energy level undergo no further relaxation process since the next lower energy level available is the ground state (see Figure 3.3). Since the electron pumping occurs at a rate that exceeds the rate of emission, excited ions accumulate in the higher energy state and form a population inversion.

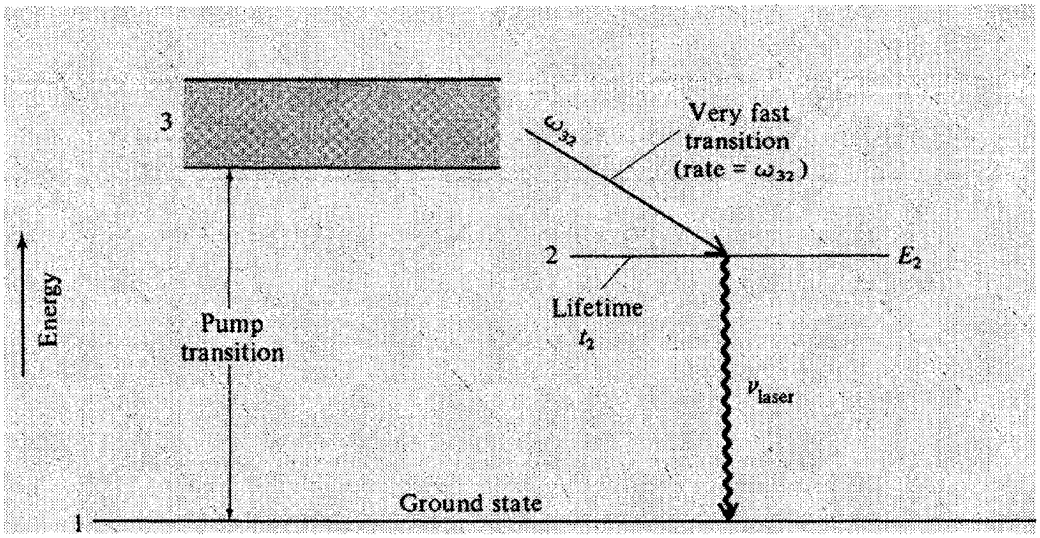

Figure 3.3: Energy-level diagram of an idealized three-level laser (Optical electronics in Modern Communications [3], pp 193).

The energy stored in the population inversion provides the gain medium for the incident signal. The input signal is injected into the EDFA and stimulates the dopants in the metastable (excited) state to give up their energy and fall back to the ground state. The energy released is converted into photons with the exact characteristics of the incident signal, which is thus amplified.

The net gain g depends on the characteristics of the population inversion and the strength of the incident signal. The ideal gain for a three-level pumping scheme with a homogeneous broadened gain medium is written as follows:

$$g = \frac{g_o}{1 + (\omega - \omega_a)^2 T^2 + \frac{P}{P_s}} \tag{3.1}$$

where ω and ω_a respectively represent the frequency of the pump signal and the atomic transition frequency (or the centre frequency of the gain medium), g_o is the peak gain value, T is the dipole relaxation time, P is the optical power of the incident signal and P_s is the saturation power.

If the gain remains in the unsaturated regime, the P/P_s ratio can be neglected and Equation 3.1 reduces to:

$$g = \frac{g_o}{1+(\omega-\omega_a)^2 T^2} \tag{3.2}$$

Equation 3.2 [2] is governed by a Lorentzian profile and is maximum when $\omega = \omega_a$, or when the frequency of the input signal equals the frequency of the atomic transition. However, due to the amorphous nature of the silica, the gain g changes slightly from the ideal case (see Figure 3.4).

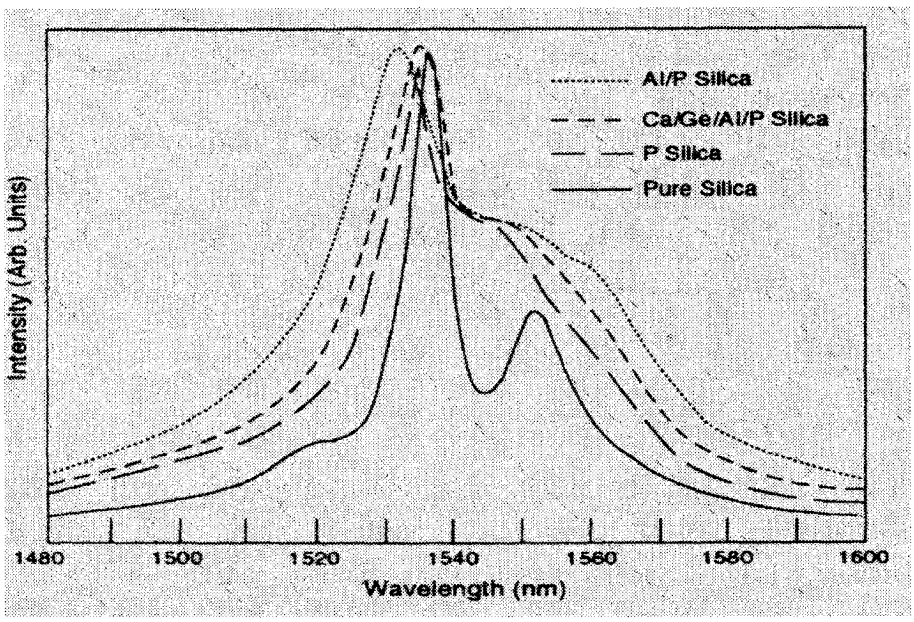

Figure 3.4: Gain spectra of four EDFAs with different core compositions. Codoping of silica core with aluminium or phosphorus broadens the emission spectrum considerably (Applications of Nonlinear Fiber Optics [2], pp 160).

The gain spectrum is strongly dependent on the composition of the core of the fiber and can be used to produce a broad gain bandwidth. Figure 3.4 represents the gain spectra of an EDFA for various core compositions. The gain profile is not uniform over the whole spectrum and changes considerably from a pure silica core to a silica core with codopants. The gain bandwidth for a pure silica core has two main peaks and a narrow bandwidth near

1.55μm. However, with a proper choice of codopants, the spectral bandwidth of the silica core at 1.55μm increases to a value exceeding 30nm (see Figure 3.4 with *Al/P*). Although the gain is not completely uniform over the entire bandwidth, the overall gain spectrum is useful for fiber laser applications.

3.2.2. Dispersion Shifted Fiber (DSF) and Solitons

Dispersion and nonlinear effects refer to a large variety of phenomena affecting the characteristics of an electromagnetic field in a specific medium. In optical fibers, dispersion and non-linear effects strongly affect the behaviour of the pulse and must be characterised and controlled in order to produce the least amount of distortion possible in the pulse.

The fiber laser cavity is made of single-mode polarization maintaining (PM) fiber. The fiber used in this experiment, called 'panda' fiber, has two rods sandwiching the core of the fiber to place a stress on the core. This effectively maintains the polarization of the incident signal along the length of the fibre. PM fiber has the property of keeping the state of polarization constant over the length of the fiber. Single-mode fiber is used to eliminate intermodal dispersion but intramodal dispersion can still cause the pulse to broaden. The most common form of intramodal dispersion is known as group velocity dispersion (GVD).

The group velocity v_g is related to the rate of propagation of the pulse envelope as follows:

$$v_g = \frac{c}{n} - \frac{kc}{n^2}\frac{dn}{dk} \tag{3.3}$$

where c is the speed of light, n is the refractive index and k is the average propagation number. The strong dependence of the refractive index on the group velocity leads to the definition of the group index of refraction n_g as:

$$n_g = \frac{c}{v_g} \tag{3.4}$$

In media such as optical fibres, the group index of refraction changes with frequency due to chromatic dispersion (see Figure 3.5). Since v_g is related to n_g, the various frequencies of the finite spectrum pulse launched into an optical fiber will then travel at slightly different group velocities and lead to the group velocity dispersion (GVD) effect.

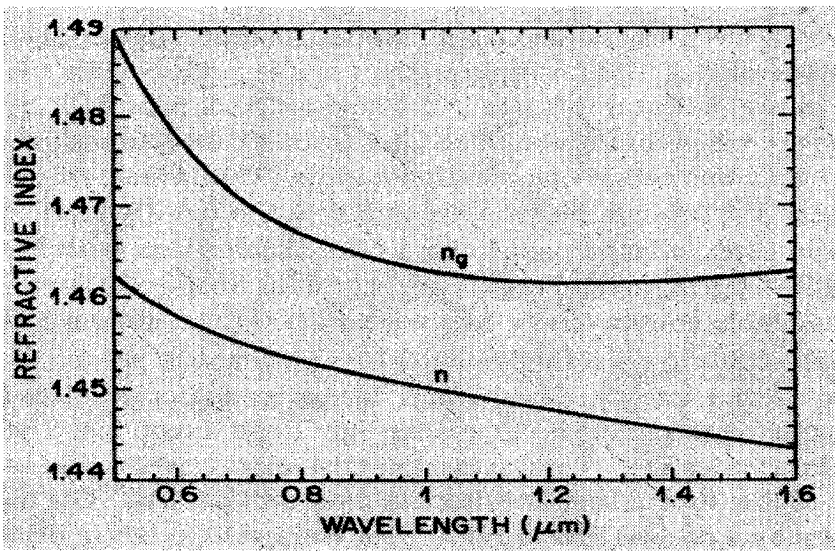

Figure 3.5: Variation of refractive index *n* and group index n_g with wavelength for fused silica (Nonlinear Fiber Optics [4], pp 8).

The GVD factor is written as β_2 and is derived from the expansion of the mode-propagation constant β using a Taylor series centred on the central frequency ω_o

$$\beta(\omega) = n(\omega)\frac{\omega}{c} = \beta_0 + \beta_1(\omega - \omega_0) + \frac{1}{2}\beta_2(\omega - \omega_0)^2 + \ldots \tag{3.5}$$

The parameters β_1 and β_2 are the first and second order dispersion parameters and are expressed as follows:

$$\beta_1 = \frac{1}{v_g} = \frac{n_g}{c} = \frac{1}{c}(n + \omega\frac{dn}{d\omega})$$

$$\beta_2 = \frac{1}{c}(2\frac{dn}{d\omega} + \omega\frac{d^2n}{d\omega^2}) \tag{3.6}$$

The factor β_2 is a function of the dispersion of the group velocity and represents the amount of expansion that a pulse encounters during its propagation through the fiber. Often, β_2 is expressed in terms of the dispersion parameter D as follows:

$$D = -\frac{2\pi c}{\lambda^2}\beta_2 \tag{3.7}$$

When the sign of D is negative, or in the normal dispersion regime, the high frequencies of the pulse exhibit a deceleration compared to the low frequencies, while a positive value of D represents anomalous dispersion and causes the opposite effect.

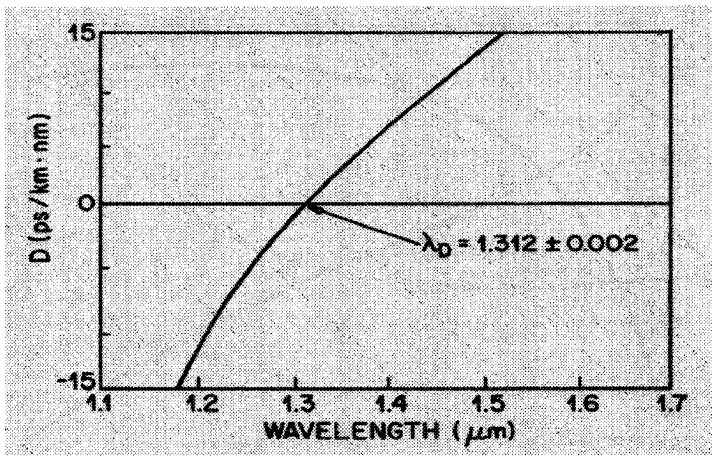

Figure 3.6: Measured variation of dispersion parameter D with wavelength for a single-mode fiber (Nonlinear Fiber Optics [4], pp 10).

Figure 3.6 shows the relationship between the dispersion parameter D and the wavelength in single-mode fiber. The most interesting characteristic of this curve is that the dispersion parameter changes from negative to positive as the wavelength increases; the zero crossing point is at a wavelength of 1.312μm. It should be noted that even though $D = 0$, the overall dispersion is not equal to zero, since higher-order dispersions still exist in the expansion of Equation 3.5. Nonetheless, when the dispersion parameter is at zero, it

signifies a decrease in the broadening of the pulse. Reproducing this property at the more desirable wavelength of 1.55μm would eliminate the second-order dispersion induced in the fiber laser. In order to achieve this, the application of nonlinear effects is required inside the cavity through a type of fiber called dispersion-shifted fiber (DSF).

Most nonlinear effects in the optical fiber come from the intensity dependence of the refractive index. The refractive index n, which is a function of frequency, also changes with the optical intensity and can be written as follows:

$$n(\omega, E^2) = n(\omega) + n_2|E|^2 \tag{3.8}$$

where $n(\omega)$ is given in Equation 3.5, $|E|^2$ represents the optical intensity, and n_2 is the nonlinear-index coefficient. This nonlinear index coefficient is related to the third-order susceptibility.

The most common nonlinear effect is self-phase modulation (SPM), which leads to spectral broadening of the pulse. During propagation through an optical fiber that is strongly dependent on the SPM effect, the optical field undergoes self-focusing. In fact, SPM induces a nonlinear phase shift $\Phi_{NL}(z, t)$, or frequency chirp, into the pulse. The relation existing between this phase shift and the intensity of the pulse is written as follows:

$$|\Phi_{NL}(z,t)| = n_2 k_o L|E(z,t)|^2 \tag{3.9}$$

where $k_o = 2\pi/\lambda$. As shown in Equation 3.9, $\Phi_{NL}(z, t)$ is proportional to the fiber length L, meaning that the frequency chirp increases with propagation distance. Since the pulse is forming new frequency components as it propagates through the fiber, the spectrum of the pulse broadens.

A combination of the effects of GVD and SPM can lead to the creation of an optical soliton, a pulse that propagates without distortion. In the normal dispersion regime ($D < 0$),

the combination of GVD and SPM leads to rapid broadening of the pulse since SPM exacerbates the rate of dispersion by increasing the propagation speed of high frequencies and decreasing the speed of low-frequencies.

In the anomalous-dispersion regime ($D > 0$) however, the effects of GVD and SPM counteract each other and actually narrow the pulse width. This narrowing occurs because the SPM-induced positive chirp cancels out the dispersion-induced negative chirp. The resulting pulse is called a soliton, which has a hyperbolic-secant shape, rather than Gaussian, that remains completely unchanged during its propagation. Soliton pulses are thus favoured in fiber laser applications.

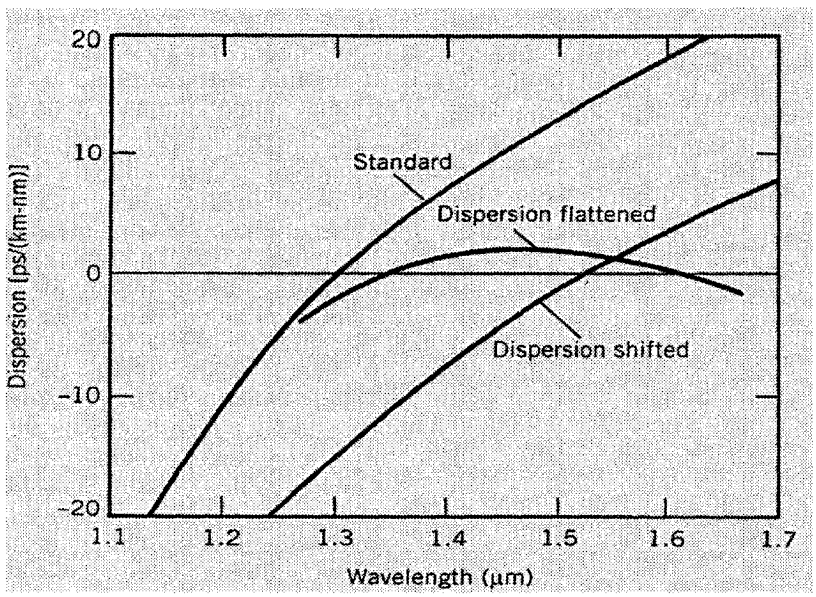

Figure 3.7: Typical wavelength dependence of the dispersion parameter *D* for standard, dispersion-shifted, and dispersion-flattened fibers (Fiber-Optic Communications Systems [6], pp45).

Therefore, dispersion-shifted fiber (DSF) is used inside the laser cavity to generate soliton pulses. DSF is single-mode fibre that has a modified core radius and core and cladding indices of refraction designed to shift the zero-dispersion point from 1.27μm to 1.5μm (see Figure 3.7). The SPM effect is stronger in dispersion-shifted fiber and can more

easily compensate the GVD effect. Once the properties of the laser cavity and pulse are known, the required length of dispersion shifted-fiber can be found through calculation.

3.2.3. Optical Couplers

Optical couplers transfer an optical signal from a designated input port to a designated output port. Depending on the application, the light launched into a single input can be distributed either equally or non-equally among the outputs. The physical principle of the coupler is based on the interaction of the modes between adjacent fiber cores. When two fibers are twisted together and heated, the distance between the cores is reduced and allows some transfer of light between the two fibers. The heating process is critical, since it determines the percentage of light that will be transferred from one fiber to the other. This kind of optical coupler is also reversible; a signal launched into the output of the coupler will be distributed either equally or non-equally among the inputs in exactly the same manner.

A two-input, two-output coupler is used in fiber lasers to collect the laser output from the cavity. The coupler is used to close the loop of the ring cavity with one input and one output, while collecting the laser output in the second output port. In order to inject the pump power into the cavity, a wavelength division multiplexer (WDM) is used. The WDM closes the loop of the ring cavity and allows the pump power to be combined with the signal from the cavity. For the laser output, the coupler used has a 90/10 ratio; i.e. 90% of the optical signal is kept inside the cavity to allow oscillations to build up, and the other 10% is used for measurement.

3.2.3.1. The Autocorrelator and the OSA

The two most common characteristics of the optical pulse are its shape and its spectral components. The Optical Spectrum Analyser (OSA) measures the spectrum of the pulse while the autocorrelator is used to measure the pulse duration, since fiber lasers produce pulses that are too fast for detection by the oscilloscope.

The autocorrelation function is the measurement of an input signal against itself using a technique called optical second harmonic generation. The input pulse entering the autocorrelator is first split by a beam splitter into two equal intensity pulses. One pulse encounters a retardation of τ seconds in comparison to the other pulse before the two pulses are recombined in a second harmonic generation crystal and detected by a second harmonic detector.

The second harmonic generation crystal is a nonlinear device that generates an output pulse at twice the frequency of any input pulse. Two pulses $E_1(t)e^{i\omega t}$ and $E_1(t-\tau)e^{i\omega(t-\tau)}$ are passed through the crystal and the resulting second harmonic field generated, $e_2(t)$, is sent to the detector. The output current $i_d(t)$ of the detector is proportional to the intensity of the second harmonic field and gives:

$$e_2(t) = \mathrm{Re}[E_2(t)\exp(i2\omega t)]$$

$$i_d(t) \propto E_2(t)E_2^*(t) = \left[E_1(t)E_1^*(t)\right]^2 + \left[E_1(t-\tau)E_1^*(t-\tau)\right]^2 + 4E_1(t)E_1^*(t)E_1(t-\tau)E_1^*(t-\tau) + s(\tau) \quad (3.10)$$

Since the optical detector is a slow device, only the first three terms of Equation 3.10 will remain, while the contribution of $s(\tau)$ is negligible [3]. The detector integrates the three currents and its output is then a function of the delay τ between the two pulses. The delay is then changed and integrated over the whole range of delay τ in order to reproduce

the optical pulse intensity. The electric signal from the detector is sent to an oscilloscope where the pulse shape and duration can be evaluated.

3.2.3.2. Photodetector (RF spectrum analyser)

The RF spectrum is a useful parameter for the mode-locking process. Since the RF spectrum is measured using electrical signals, a photodetector is required in order to convert the optical signal from the laser into an electric signal.

The RF spectrum shows the self-beat signal peaks and the mode beating peaks. The self-beat signals represent the difference in frequency between two modes oscillating inside the cavity. The photodetector has a bandwidth much lower than the signal frequency, but is able to detect the beating between two consecutive modes, or multiples of modes, because of the low frequency component of the beating. However, since the bandwidth of the photodetector used is 40GHz, only the first-order mode beating of 40GHz mode-locked pulses can be detected.

The self-beat signals are an important consideration in the choice of the modulation frequency since their frequencies give an exact value of a multiple integer of the inter-mode frequency spacing. For the fiber laser used in this experiment, the inter-mode frequency spacing was evaluated by taking the difference between two consecutive self-beat signals; it was estimated to be 0.75MHz.

Once the modulation frequency is turned on however, these self-beating peaks are considered to be noise, since all the modes should be locked in phase and only the mode beating signals should be seen. Therefore, the difference between the maximum intensity of the first-order mode beating and the self-beat peaks gives a good approximation of the signal-to-noise ratio (SNR) inside the cavity.

3.2.4. Optical Isolator

Optical isolators allow the transmission of light in only one direction. Since the fiber laser has a ring topology, the role of the optical isolator is to prevent any feedback from getting into the optical resonator and creating noise inside the cavity or the damaging the optical devices. The optical isolator is based on the Faraday effect, which uses a magnetic field to rotate the polarization of the light.

The optical isolator has three main parts: an input polarizer, a Faraday rotator, and an output polarizer. For the purpose of the discussion, the input polarizer is assumed to be vertical, and the output polarizer is assumed to be turned 45° to the right (see Figure 3.8). The Faraday rotator is an optical component that uses the Faraday effect to rotate the polarization of the light at a certain angle α, 45° to the right in this case.

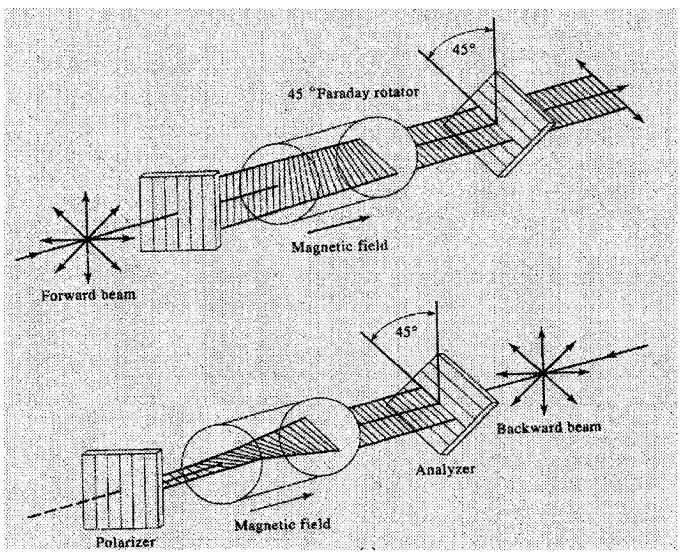

Figure 3.8: A Faraday isolator comprised of two polarizers rotated by 45° relative to each other on either side of a magnetic medium with $\theta_f = 45°$ (Optical Electronics in Modern Communications [3], pp29)

A wave propagating forward in the isolator is first polarized in the vertical position before entering the Faraday rotator. Since the linearly polarized light can always be

represented as a linear combination of right- and left-hand circularly polarized light, the wave is decomposed in the Faraday rotator and encounters a polarization rotation of 45° to the right. The wave thus has the same polarization as the output polarizer and propagates without attenuation. However, if a wave propagates backward into the isolator, it will first be polarized 45° to the right by the output polarizer, and rotated 45° further to the right by the Faraday rotator, which allows only non-reciprocal rotation. The polarization of the light when it arrives at the input of the rotator is then horizontal, which is blocked by the vertically polarized input polarizer.

Since the optical isolator requires the polarization to be consistent in order to work properly, the fiber laser is made of PM fiber.

3.2.5. Optical filter

The EDFA gain medium possesses a spectrum width of approximately 120nm, with a 30nm quasi-uniform gain band around 1550nm. It is difficult to mode-lock the fiber laser using only the gain medium since the non-uniform spectrum of the EDFA can create sufficient noise inside the cavity to produce unstable mode-locked pulses. An optical filter is thus required to restrict the bandwidth of the EDFA to the quasi-uniform gain band; a thin-film optical filter was used for this purpose.

The optical filter used in this experiment is tuneable, which allows the centre wavelength of the laser to be tuned over the whole uniform band of the EDFA. By scanning the wavelength, the best results for the optical spectrum of the laser for a certain modulation depth were obtained when the filter was centred at a wavelength of 1556.5nm; the filter was thus fixed at this wavelength for the duration of the experiment.

3.2.6. Phase Modulator and Synthesizer

The modulator is critical to the design of a fiber laser since it is the key component required to achieve active mode-locking. Frequency modulation, or more specifically phase modulation, of the modes inside the cavity was used to mode-lock the pulses in this experiment.

The phase modulator is based on the electrooptic effect present in certain types of crystal. Some crystals are highly sensitive in the presence of an electric field and their refractive index can change proportionally to an external applied field. These crystals must be birefringent; that is, an anisotropic structure with no symmetric inversion. An example of such a birefringent crystal is potassium dihydrogen phosphate, also known as KDP.

A birefringent crystal has two rays of propagation, ordinary and extraordinary, that could be characterized by different indices of refraction; that is, distinct velocities of propagation. By applying an electric field, the indices of refraction of the two rays of the crystal change proportionally to the field. Depending on the axis of propagation, an optical signal that enters the crystal will then encounter either a change in its state of polarization leading to amplitude modulation or a change in its output phase leading to phase modulation.

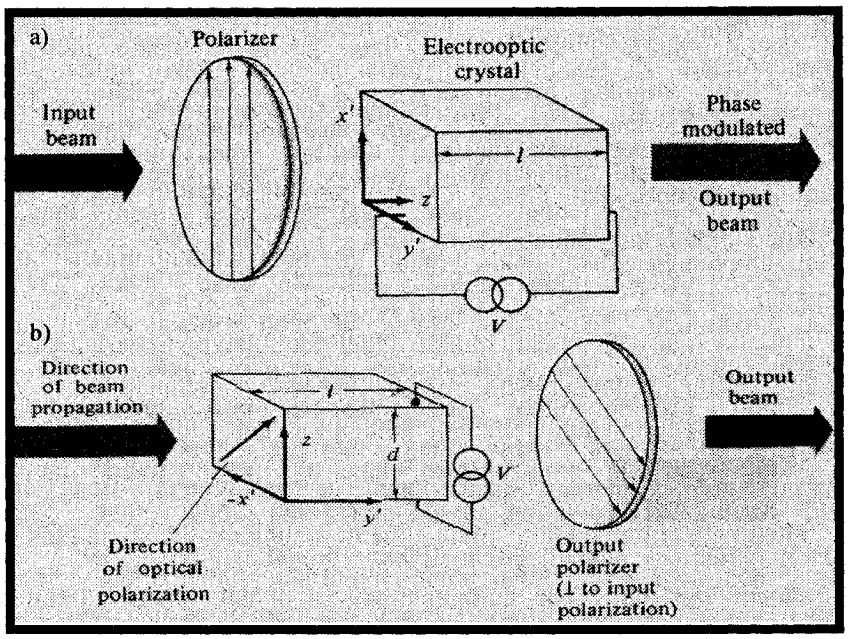

Figure 3.9: (a) An electrooptic phase modulator. The crystal orientation and applied directions are appropriate to KDP. The optical polarization is parallel to an electrically induced principal dielectric axis (x'); (b) A transverse electrooptic amplitude modulator using a KH_2PO_4 (KDP) crystal in which the field is applied normal to the direction of propagation (Optical Electronics in Modern Communications [3], pp348-9).

There are two ways of generating phase modulation, as shown in Figures 3.9(a) and 3.9(b) for a KDP crystal. The principle is to launch a pulse polarized along one of the two birefringent axes present in the crystal. If x' is the propagation axis shown in Figure 3.9(a), an optical field that enters the crystal will then propagate as:

$$e_1 = Ae^{i(\omega t - \frac{\omega}{c} n_{x'} z)} \tag{3.11}$$

where $n_{x'}$ is the index of refraction of the x' axis. After the electric field is applied, the index of refraction changes from $n_{x'}$ to $n_{x''}$ and the optical signal becomes

$$e_{1'} = Ae^{i(\omega t - \frac{\omega}{c} n_{x''} z)} \tag{3.12}$$

The change of the output phase of the signal, $\Delta\varphi$, can be written as follows:

$$\Delta\varphi = -\frac{\omega z}{c} \Delta n_{x'} \tag{3.13}$$

where $\Delta n_{x'} = n_{x''} - n_{x'}$. Since the electric field applied to the crystal is proportional to $\Delta n_{x'}$, it is then also proportional to the change in phase, $\Delta\varphi$.

The difference between Figures 3.9(a) and 3.9(b) depends on the axis of the applied electric field. In Figure 3.9(a), the field is parallel to the propagation axis while the field in Figure 3.9(b) is transverse to the axis of propagation. Transverse phase modulators are preferable since the field electrodes don't interfere with the optical signal. Similarly, the retardation can be increased simply by employing longer crystals, which obviously is not possible in the longitudinal case. The variation in the output phase for the transverse modulation is slightly different from Equation 3.13 since the optical signal is polarized at 45° between the x' and z axes and launched on the y' axis. Nevertheless, the principle remains the same since the refractive index of the z-axis is not affected by the applied field.

The phase modulator used in the fiber laser is based on a $LiNbO_3$ crystal. The applied electrical signal changes the refractive index n of the crystal in order to change the optical length and, as a result, changes the output phase of the light. The model of the modulator is very similar to that shown in Figure 3.9(a).

The electric field applied to the modulator is generated by a synthesizer that allows a tuning of the signal frequency and amplitude. The synthesizer used in the setup of the fiber laser can tune the frequency up to 40GHz with a maximum power level of 16dBm.

3.3. Stability of the Fiber Laser

The total cavity length of the fiber laser, including all components, is approximated to be 298m. A cavity of this length is more susceptible to problems of stability since optical fibers react to any changes in its environment. Therefore, external temperature variations –

such as those caused by an air conditioner – affect the internal properties of the optical fiber and cause instabilities.

A drift in temperature induces a stress in the fiber, leading to a change in its physical length l – usually expressed as a compression or an expansion of the fiber – as well as a change in its refractive index n. The relation between the two parameters is given by:

$$L = nl \tag{3.14}$$

where L represents the optical length of the fiber. From Equation 3.14 it is clear that a variation of either l or n results in a variation of the optical length of the fiber. For the fiber laser, this results in a change of the inter-mode frequency spacing Δv, as

$$\Delta \upsilon = \frac{c}{L} \tag{3.15}$$

where c is the speed of light. Since the modulation frequency is fixed at a multiple integer of the inter-mode frequency spacing, which varies with temperature, the fiber laser becomes unstable.

The change in the inter-mode frequency spacing due to temperature fluctuations can be roughly estimated with the help of the modulation frequency. As previously mentioned, the modulation frequency has to be kept at a multiple of the inter-mode frequency spacing to remain mode-locked. Therefore, the modulation frequency could be tuned to follow the variations of the inter-mode frequency spacing over time.

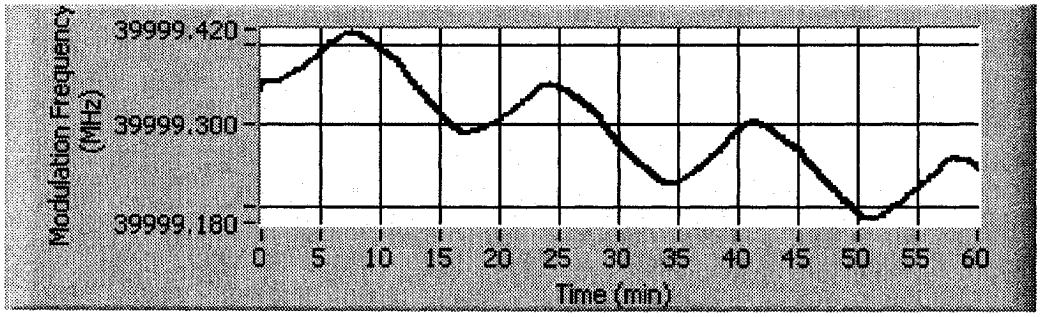

Figure 3.10: Evolution of the modulation frequency with time.

Figure 3.10 shows the variation of the modulation frequency over a period of 60 minutes. From the figure, it is clear that the main factor affecting the fiber laser cavity is the air conditioner. In fact, an air conditioner is controlled by a feedback system that keeps the temperature near a certain predetermined value. Depending on the parameters of the controller, the system oscillates slightly around the required temperature but remains stable on average. Since the cavity of the fiber laser is relatively long, it is more susceptible to change and follows these periodic fluctuations in temperature. Note that although there appears to be a linear decline over time in Figure 3.10, this was apparently a random process.

Figure 3.10 provides an approximation of the maximum change in the physical cavity length. The number of pulses in one round-trip N that are allowed to oscillate inside the cavity of the mode-locked fiber laser is related to the modulation frequency F_m and the inter-mode frequency spacing $\Delta\nu$ as follows:

$$N = \frac{F_m}{\Delta \upsilon} \tag{3.16}$$

At 40GHz, and with an inter-mode frequency spacing of 0.75MHz, the number of modes N inside the cavity of the fiber laser is approximately 53333. If a temperature fluctuation occurs, the equation becomes:

$$N = \frac{F_{m'}}{\Delta \upsilon'} \tag{3.17}$$

A variation of the modulation frequency and of the inter-mode frequency spacing will then result in:

$$\frac{\Delta(F_m)}{N} = \Delta(\Delta \upsilon) \tag{3.18}$$

From Figure 3.10, the maximum change in the modulation frequency over a single oscillation of the temperature is about 500kHz, which gives with the help of Equation 3.18 a $\Delta(\Delta v)$ of 9.375Hz. Using Equation 3.15, the variation of the optical length can be derived: a positive variation of Δv leads to a negative variation of the optical length.

$$\Delta \upsilon + \Delta(\Delta \upsilon) = \frac{c}{L - \Delta L} \tag{3.19}$$

$$\frac{\Delta \upsilon}{\Delta \upsilon + \Delta(\Delta \upsilon)} = \frac{L - \Delta L}{L} \tag{3.20}$$

$$\frac{\Delta(\Delta \upsilon)}{\Delta \upsilon} = \frac{\Delta L}{L} + \frac{\Delta(\Delta \upsilon)\Delta L}{L \Delta \upsilon} \tag{3.21}$$

where the second term of Equation 3.21 can be neglected. The maximum optical cavity length L can then be calculated from Equation 3.13; the optical length of the fiber was calculated to be 417m.

$$\Delta L = \frac{417m \times 9.375Hz}{0.75MHz} \tag{3.22}$$

Therefore, the maximum change in the optical cavity length, ΔL_{max} is 5.2×10^{-3} m or 0.52cm. Using Equation 3.14, the variation of the physical cavity length was calculated to be 3.6mm.

Even though temperature fluctuations can be reduced by isolating the fiber laser or making the cavity length shorter, they will always remain present to some extent. As a consequence, some method of stabilization is required to stabilize the fiber laser. The following chapter gives an overview of the three different stabilization approaches developed in this project: the computer-controlled method, the computer-controlled PZT method, and the circuit-controlled method.

4. Methods of stabilization

4.1. Introduction

Three different methods were developed to stabilize the active harmonic mode-locked fiber laser at 40GHz: computer control of the modulation frequency, circuit control of the optical cavity length using a piezo fiber stretcher, and computer control of the piezo fiber stretcher. This chapter provides an overview of each method from the concept to the design and the setup. The results and optimization of each method will be presented in Chapters 5 and 6.

4.2. Reference Level

Each stabilization approach requires a real-time reference to determine the quality of the mode-locking of the fiber laser in order to make the appropriate changes and keep the laser stable. Several different parameters were considered as a possible reference, including the maximum RF intensity or the maximum autocorrelation intensity near the resonance frequency. Neither was found to be useful; the RF intensity didn't have a significant enough change relative to the frequency detuning and the autocorrelation intensity fluctuated too much to be considered as a reference (see Figure 4.1(a) and 4.1(b)). However, the DC signal that results from mixing the laser output, measured with the photodiode, and the signal delayed from the phase modulator did change with frequency and was found convenient as a reference.

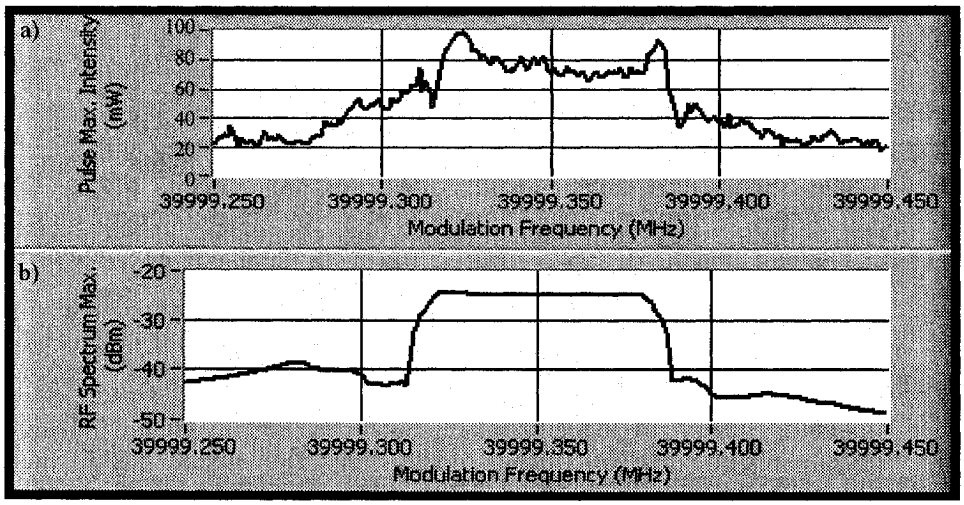

Figure 4.1: (a) The dependence of the maximum of the autocorrelation signal on the modulation frequency near the resonance. (b) The dependence of the maximum of the RF spectrum on the modulation frequency near the resonance [14].

In order to obtain the DC level, two electrical components are added at the output of the photodetector: a mixer and a phase shifter. The mixer is a nonlinear device made of semiconductor diodes that provides as output signals the sum and the difference of two electrical input signals with distinct frequencies. If two signals having similar high frequencies are sent into the mixer, their difference gives a DC level while their sum is outside the detectable frequency range. Since a high modulation frequency is used for the fiber laser, the choice of a mixer is useful to get a reference signal. The mathematical calculation that leads to this result is explained as follows:

Two distinct signals v_1 and v_2 are considered:

$$v_1 = A_1 \cos(\omega_1 t) \text{ and } v_2 = A_2 \cos(\omega_2 t + \varphi) \tag{4.1}$$

Mixing these two signals gives:

$$v_1 v_2 = \frac{A_1 A_2 [\cos(\omega_1 t - \omega_2 t + \varphi) + \cos(\omega_1 t + \omega_2 t - \varphi)]}{2} \tag{4.2}$$

If the two high frequencies ω_1 and ω_2 are the same, then:

$$v_1 v_2 = \frac{A_1 A_2 [\cos(\varphi) + \cos(2\omega_1 t - \varphi)]}{2} \tag{4.3}$$

The only component that remains is the DC signal, since the frequency at $2\omega_1$ is too high for the electronics used to be considered.

The intensity of the output DC signal depends on the power of each input signal and the phase difference between the two signals, which is very sensitive to the quality of the fiber laser near resonance frequency. This phase delay between the two signals can be controlled using a phase shifter that induces an electrical retardation to the signal to change its phase. The phase shifter used in the fiber laser setup can retard the signal from 0 to125ps. With specific phase delays applied to the signal coming from the synthesizer, the change of the DC signal near the resonance frequency was found to be roughly linearly dependent on the modulation frequency (see Figure 4.2 for a delay of 12ps). This characteristic was found to be a useful reference and was used in all three stabilization methods.

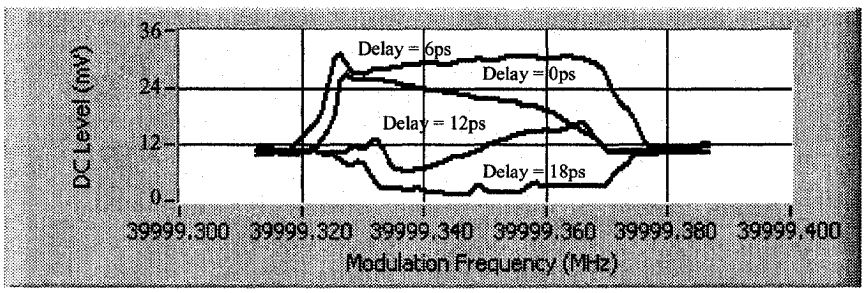

Figure 4.2: The dependence of the DC signal form the mixer as a function of the relative time delay between the signals from the synthesizer and the laser output near the resonance. The choice of zero time delay is arbitrary [14].

4.3. Computer-Controlled Method

4.3.1. Concept

The computer-controlled stabilization method was developed in [14]. The idea was to build a simple, cheap method of stabilization entirely controlled by a computer and

hence easy to use in laboratory experiments. The goal was not to counteract the effect of temperature drift but to follow the drift by adjusting some of the laser's parameters. The most practical parameter for adjustment was the modulation frequency, since it is critical for mode-locking but its adjustment leaves the laser cavity intact. Given that the inter-mode frequency spacing changes with temperature variations, a change in the modulation frequency could lead to a readjustment of the mode-locking and therefore a way to stabilize the laser.

4.3.2. Design

Only one design was created for the computer-controlled method using a LabView™ program. This allows an easy way of programming with visual block diagrams and an interface where real-time results can be seen, and allows interaction between the computer and the fiber laser's devices through GPIB cables. Since one objective of the stabilization method was to be simple, LabView™ was the best alternative.

The program makes use of programming loops, case statements, and timing in order to execute different tasks at specific time and in chronological order. It interacts with the synthesizer, the RF spectrum analyser, the OSA and the oscilloscope for the autocorrelation to either send or to retrieve data. Since the program needs a reference to the system in order to make changes, the computer has to get the DC level coming from the mixer and the phase shifter that control the behaviour of the DC curve at resonance frequency. The output of the mixer was then connected to the oscilloscope from which the DC level could be sent to the LabView™ program; the phase shifter was directly connected to the computer via a GPIB cable.

4.3.3. Setup

The setup of the fiber laser with the computer-controlled method is shown in Figure 4.3.

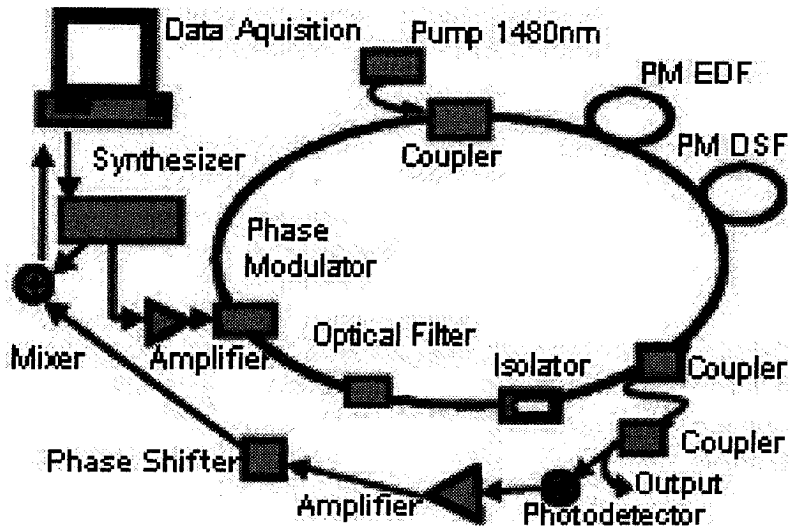

Figure 4.3: Setup of the fiber laser using the computer-controlled method.

The main task of the LabView™ program is to adjust the modulation frequency of the synthesizer to maintain the DC signal at a constant pre-set value. This pre-set value is determined by finding the relationship between the change in modulation frequencies near resonance and the DC level from the mixer. Thus, the program requires the output of the mixer, the synthesizer, and the RF spectrum analyzer.

The first step is to find a harmonic of the inter-mode frequency spacing near the modulation frequency required, which is 40GHz in this case. This task is executed by evaluating the self-beating signals in the RF spectrum window, choosing the peak that is closest to the centre of the span of the RF spectrum and tuning the synthesizer to this peak frequency. Since the inter-mode frequency spacing was 0.75MHz, the span was set at 3MHz and the centre frequency at 39,999.5MHz as a trade-off between the processing time of the RF spectrum and the resolution of the peaks.

Once the modulation frequency is fixed at the position of a single self-beating signal, the program measures the value of the DC signal from the mixer, within a modulation frequency window of stability, and keeps this curve as a reference. For certain frequencies at a specific phase delay, a linear relationship exists between the DC signal and the modulation frequency. For optimal accuracy, the phase delay that produces the highest monotonically increasing slope is chosen and the DC signal pre-set value is set at the mid-point of the slope as shown in Figure 4.4.

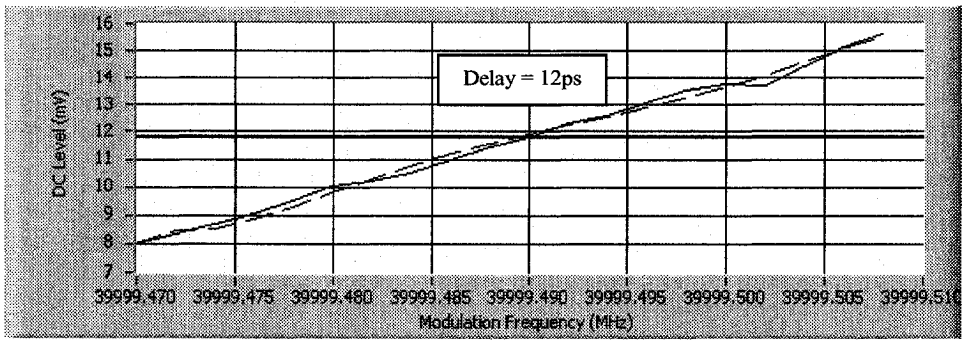

Figure 4.4: Fit of the DC level curve with the highest monotonically increasing slope (dashed) and the mid-point of the range in a 40kHz frequency modulation window.

When a fluctuation in temperature subsequently changes the optical cavity length of the laser, the program is able to recognize the shift in the self-beating signal position from the RF spectrum and to adjust the modulation frequency in consequence with the help of the DC curve. The program takes the difference between the modulation frequency that corresponds to the reference level and the modulation frequency that corresponds to the DC level measured and consequently adjusts the modulation frequency of the synthesizer to return to a mode-locked regime. This loop perpetuates forever or until the program is asked to stop.

As the loop is being executed, the LabView™ program also takes measurements from the fiber laser, including the maximum intensity peak of the RF spectrum, the signal-

to-noise ratio, the maximum pulse intensity and duration, the bandwidth of the optical spectrum, and the DC level and modulation frequency over time. These measurements are used to evaluate the performance of the computer-controlled method and to compare it with the circuit-controlled stabilization method.

4.4. Circuit-Controlled Method

4.4.1. Idea

The circuit-controlled method is based on Shan [15] and Nakazawa [17]. As opposed to the computer-controlled method, this method directly counteracts the effect of temperature variations in order to eliminate them. Since temperature variations either increase or decrease the physical cavity length, a device had to be found that could also change the physical cavity length to counteract the change due to temperature fluctuations. The device also had to be controllable via an independent circuit with a rapid execution speed. The device chosen for the application was a piezo fiber stretcher composed of a piezo crystal and 10m of optical fibre wound around an ellipsoid base, as shown in Figure 4.5.

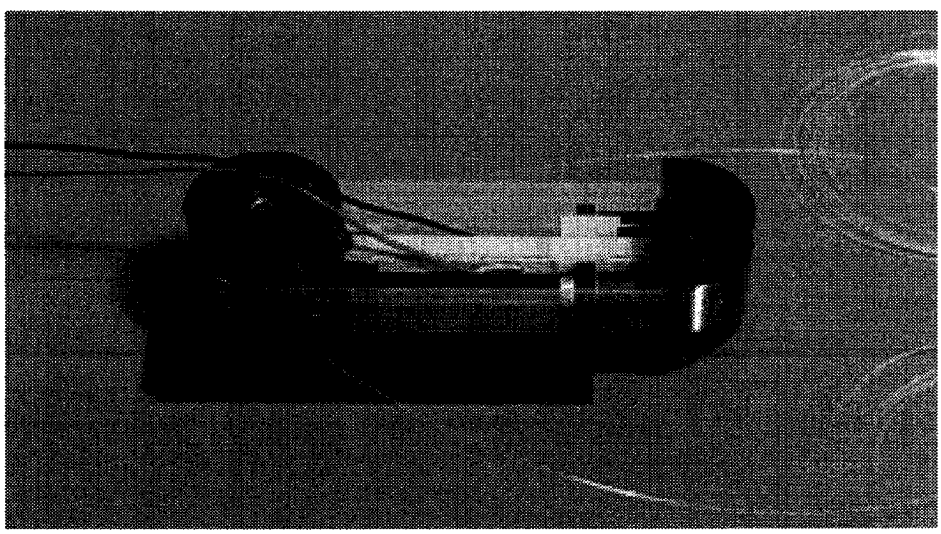

Figure 4.5: Piezo fiber stretcher.

A piezoelectric device is a crystal that can either generate a voltage in response to a mechanical stress applied to it or conversely it can reversibly change in shape – on the order of nanometres – in response to an applied voltage. The piezo fiber stretcher uses the latter characteristic of the piezo crystal to stretch or compress the optical fiber wound around it. An electronic circuit controls the piezo crystal and therefore determines the amount of stretching by adjusting the voltage applied. The relation between the voltage applied and the stretch can be considered quasi-linear.

The stress induced in the optical fiber of the piezo fiber stretcher causes an increase or a decrease in the fiber length. Placing this fiber inside the fiber laser cavity therefore results in a change of the optical cavity length. Since the piezoelectric effect can be controlled using a circuit, the piezo fiber stretcher is a good candidate for counteracting fluctuations in temperature.

An external controller to the circuit of the piezo fiber stretcher had to be designed so that it could use, as with the computer-controlled method, the DC level from the mixer to change the voltage applied to the piezo when temperature fluctuations occur. This controller requires a feedback loop for a real-time reference to the system and a time response comparable to the time response of the temperature fluctuations.

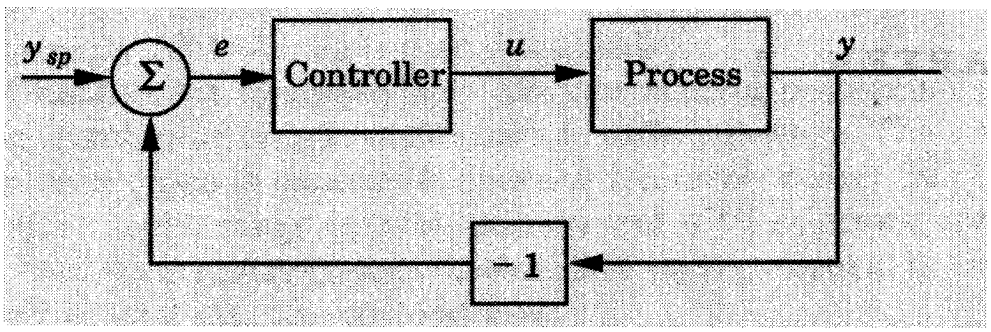

Figure 4.6: Block diagram of a simple feedback system (PID Controllers: Theory, Design, and Tuning [5], pp 6).

Figure 4.6 shows a block diagram of a system using a feedback loop to control external disturbances. The controller makes a decision based on the real-time reference e coming from the feedback loop and sends its response u to the process, which basically represents the action taken to the control response received. The process variable y coming from the output of the process gives a response from the system to the action at the input of the control. The real-time reference sent to the control is in fact the difference between two elements: the process variable y and a setpoint that represents the value required for the system to remain stable. As a consequence, the controller attempts to maintain this difference at zero.

In order to use the fiber laser as a feedback control system, a process, a real-time reference value, and a controller needed to be determined. In this case, the piezo fiber stretcher represented the process since it could modify the fiber laser cavity length, the DC level from the mixer was the real-time reference, and the controller for the application was chosen to be the *PID* controller.

PID controllers are widely used in industry since they are efficient for many different applications. *PID* stands for Proportional response, Integral response, and Derivative response. Their main characteristics are to provide feedback, to get rid of steady-state offsets and to anticipate the future, respectively. The derivative parameter was found unnecessary for the fiber laser application since the disturbances, which in this case is temperature fluctuations, is not a fast process. Therefore, the derivative part was removed for the controller design and a simple *PI* controller was used instead.

4.4.2. Design

The piezo fiber stretcher was chosen based on the calculation of the maximum change in the optical cavity length, as undertaken in Chapter 3. Since 3.6mm of stretch was required of the physical cavity length, the piezo fiber stretcher chosen had a maximum stretch of 4mm and a frequency response limited to 10Hz for big steps in voltage, i.e. 0V to 5V, and 1kHz for small steps, i.e. 0V to 0.01V.

The circuit-controlled method was designed according to two different models. The first model was simple and used a chip called an HTC-1500, which is a temperature controller that makes use of a *PI* circuit. The other model was designed specifically for the fiber laser and was more flexible and useful. A full explanation of both models will clarify the choice made.

The two models possess some similarities. The *PI* controller circuit is basically the same for both models and makes use of amplifiers. An electrical amplifier is made of transistors and can be used, among others, as a gain amplifier, an integrator, a low-pass filter or a combiner, as shown in Figure 4.7 (a), (b), (c), and (d). Here the *P* can be represented as a gain amplifier and the *I* as an integral amplifier. These four amplifier designs are found in the circuits of both models. Although their respective circuits are similar, the difference between the two models remains in the choice of the resistances, capacitances, and the type of amplifiers.

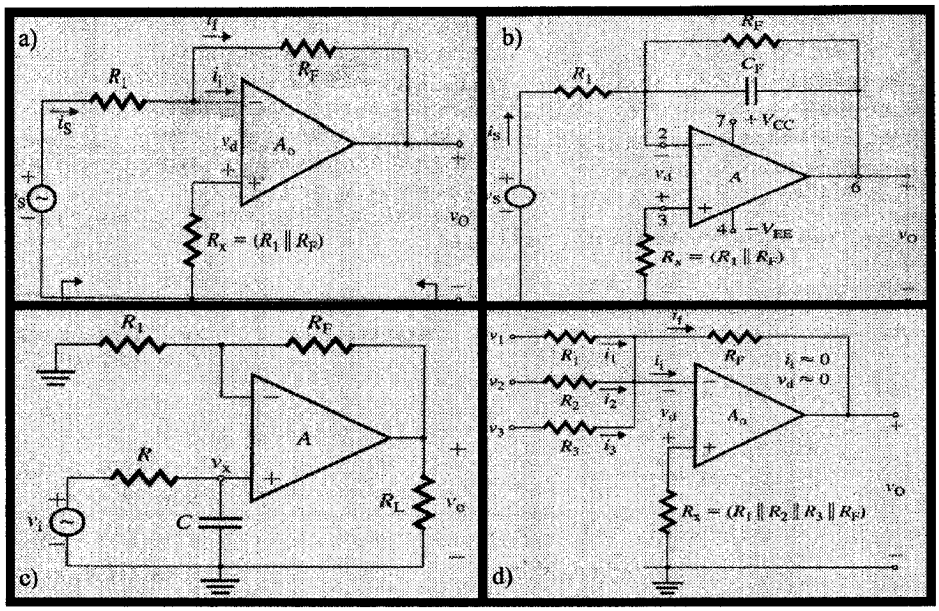

Figure 4.7: (a) Gain amplifier circuit; (b) Integrator circuit; (c) Low-pass filter circuit; (d) Inverting summing amplifier circuit (Microelectronic Circuits, Analysis and Design [7], pp277, 282, 427, 292).

Another similarity is related to the reference level as well as to the voltage applied to the piezo fiber stretcher. Since both models require a DC level, the signal from the mixer and the signal going to the piezo fiber stretcher needed to be filtered. Two low-pass filters with cut-off frequencies of 1kHz and 1MHz were then added to both models to avoid damage due to electrical overload. The program of the computer-controlled method is also very helpful for the two designs as an initiator, since it starts the process of mode-locking of the laser and determines the value of the DC level used as the reference level to signify when the laser is mode-locked, which a *PI* controller cannot do. The LabView™ program was then modified so that its role wasn't to control the *PI* circuit but to assist it.

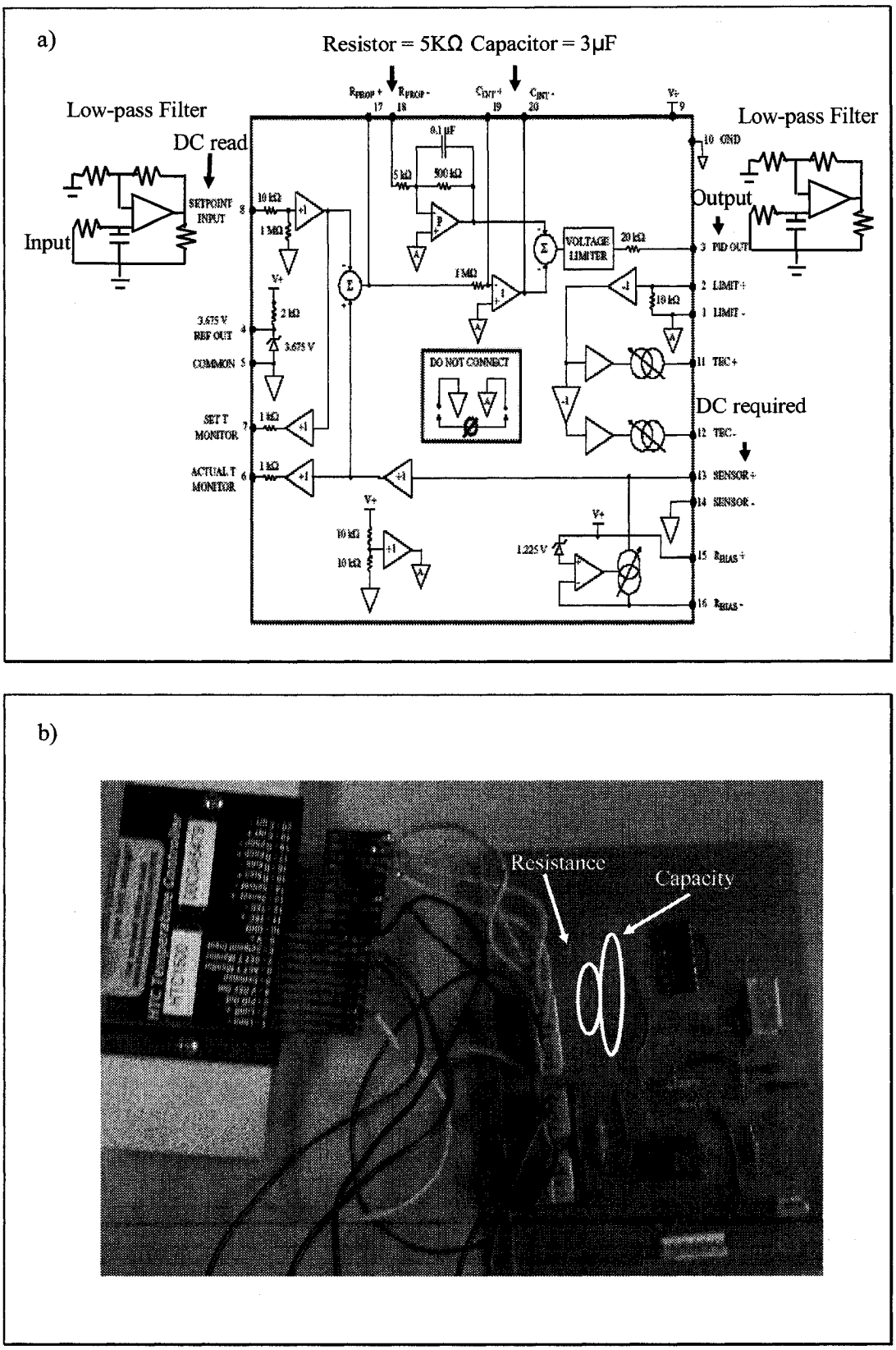

Figure 4.8: (a) Schematic of the first model of the controller circuit; (b) Photograph of controller circuit.

The first model is shown in Figure 4.8 (a) and 4.8 (b). In Figure 4.8 (a), the DC read is the process variable and the DC required is the setpoint. Although the HTC-1500 is effective for the stabilisation of the fiber laser, it encounters many problems. The chip is designed to control currents, but the piezo fiber stretcher is controlled by voltages. Since the chip is used in a way that it was not designed for, there were some limitations in the performance of the controller. The second problem is in the design of the chip itself. Since the chip is integrated, the *P* and *I* functions cannot be separated from the chip, limiting their individual optimization. A possible solution would be to use the optimal values of the resistance of the *P* and capacitance of the *I* given in the chip's data sheet and shown in Figure 4.8 (a), however these don't necessarily give good results for all systems and weren't found optimal for use with the fiber laser. The main problem was that the gain of the *P* was very high, reacting too quickly to temperature fluctuations. Therefore, the optimisation of the circuit had to be done by hand.

The final problem with the first model of the control circuit was the voltage controller at the output of the chip, which limited the value to be between 0.5 and 4.1V. Since the piezo fiber stretcher accepts voltages between 0 and 5V, the chip cannot operate over the whole range, limiting once again the performance of the controller. All these problems led to the creation of a new model for the control circuit that was more adapted to the needs of the fiber laser.

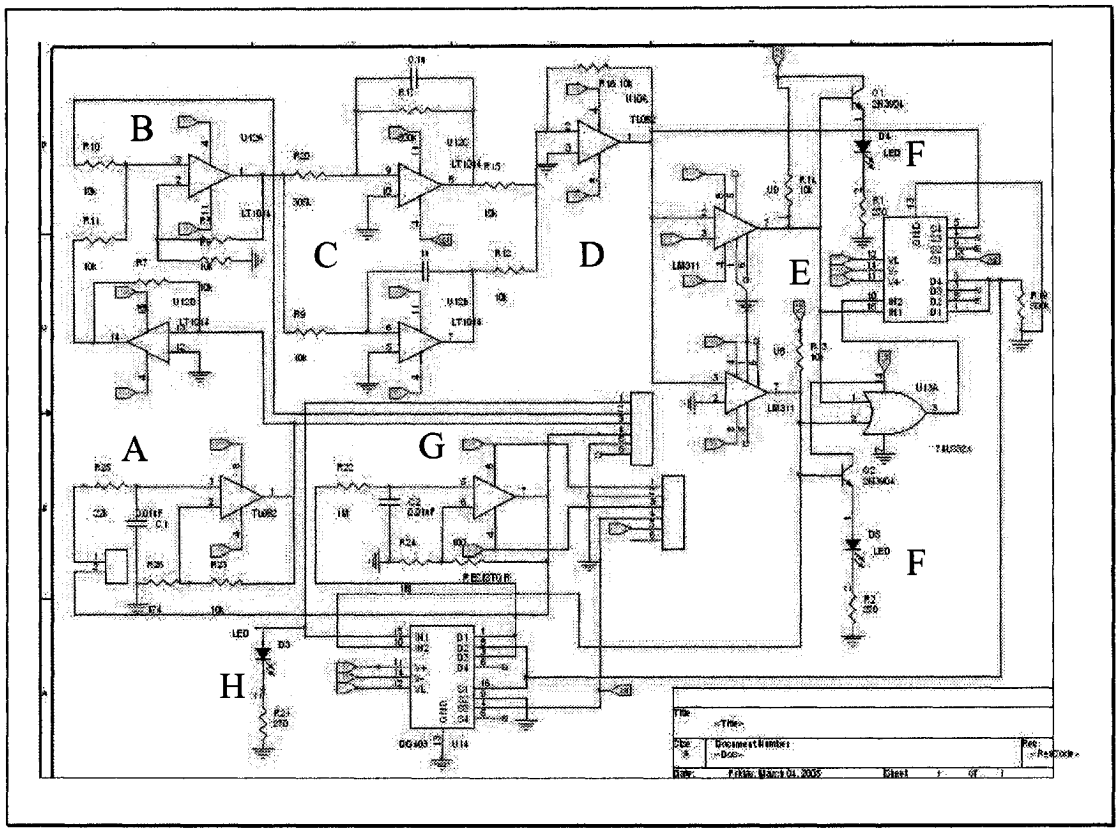

Figure 4.9: Schematic of the second model of the controller circuit, designed and built in the laboratory using amplifiers with a wide-gain bandwidth of 4MHz.

The schematic of the circuit of the second model is shown in Figure 4.9. It comprises the *PI* circuit, the error control and a few other complementary components. Starting from the left side of Figure 4.9 in region A, the DC level from the mixer is filtered and then sent to an inverting amplifier. In region B, a summing amplifier adds this signal to the setpoint. Since one signal is negative and the other positive, the output gives the error control for the *PI*. The signal is then equally divided in two, one part going to the *P* and the other part to the *I*, as seen in region C. In region D, the two signals are recombined with the help of another summing amplifier to give the value of the voltage required for the piezo fiber stretcher. The output voltage is then checked in region E before it is sent to the piezo fiber stretcher.

The voltage check works as a voltage controller. It makes sure that the output voltage from the control circuit is between 0-5V, which is the limitation of the piezo fiber stretcher. The original idea was to use a Zener diode at 5V with a regular diode in cascade in order to limit the voltage. The main problems with this design were the cut-off voltage of -0.7V of the regular diode and the difficulty of getting a Zener diode that had exactly the 5V requirement. Therefore, the idea was rejected in favour of one that used comparators, switches, and an OR logic gate.

The principle is the following: the output signal from the *PI* controller is first sent to two comparators that compare the signal with both 0V and 5V. If the voltage is lower than 0V, the comparator automatically tells the switch to keep the signal at ground level or 5V if the signal is higher than 5V. The OR gate simply tells the switch to block the output voltage of the *PI* controller if the voltage is out of range. Two indicators, made using light-emitting diodes and transistors, were added to the design simply to indicate whether or not the system had reached either of the two voltage limits, as seen in region F of Figure 4.9.

A further design characteristic is that the piezo fiber stretcher has to be effective at both lengthening and shortening the optical cavity length, since temperature variations are random and can be either positive to negative. The piezo fiber stretcher therefore needs to be stretched to the middle point of its stretching range, which corresponds to an input of 3.1V, to be able to compensate equally for positive and negative variations; the calculation of the middle point is further explained in section 4.5.2. The pre-stretched voltage has to be applied before taking the measurement of the setpoint and then has to be removed once the *PI* controller is turned on. Therefore, the switch shown in region G of Figure 4.9 is used to send the pre-stretched voltage to the piezo fiber stretcher first and then to switch to the output voltage of the *PI* controller once the setpoint has been given. A further LED

indicator is included in region H to indicate whether or not the *PI* is controlling the system or not. Finally, the low-pass filter in region G ensures that the signal sent to the piezo fiber stretcher is DC level.

Given the need of the computer to exchange signals with other instruments, two analog input and output cards of 16 ports each were added to the computer. The DC level from the mixer was transferred from the oscilloscope to one port of the receiver. With these two I/O cards, the computer was able to get data from the circuit and evaluate its performance as well as to control the switches. The role of the computer in the circuit-controlled method is explained in the following section.

4.4.3. Set-up

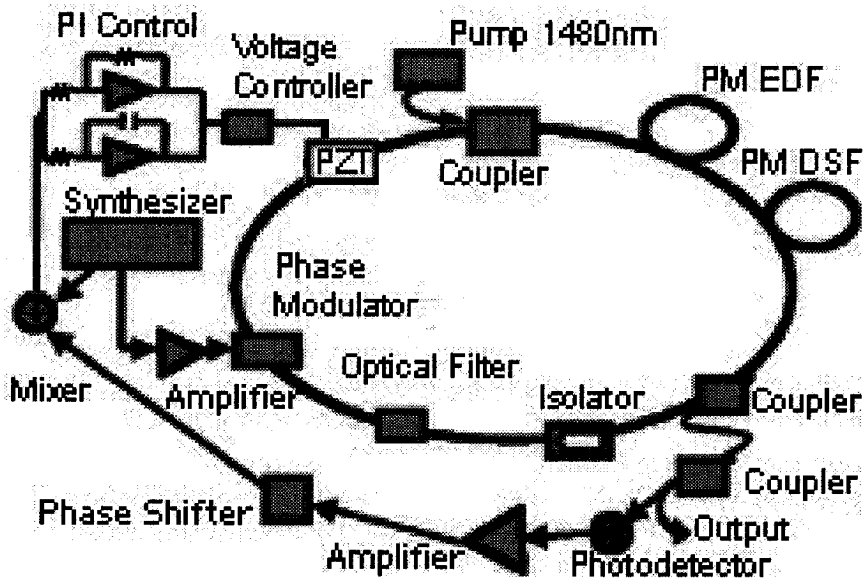

Figure 4.10: Set-up of the fiber laser using the circuit-controlled method.

The set-up of the fiber laser with the circuit-controlled method is shown in Figure 4.10. In the circuit-controlled approach, the *PI* control system is used to track and eliminate the difference between the DC signal required and the DC signal read from the mixer. Multiple tasks must be executed in chronological order. The first step is to find the reference level, or set point. With the piezo fiber stretcher already pre-stretched, the

computer turns on the synthesizer frequency at the frequency self-beat signal from the RF spectrum closest to 40GHz. At that point, the fiber laser is mode-locked and the DC level from the mixer can be sent to the computer and saved as the setpoint. For a higher degree of accuracy, many measurements of the setpoint are averaged before sending the final result back to the circuit.

The computer then instructs the switch in region G to let the *PI* controller stabilize the fiber laser. Consequently, the pre-stretched signal is replaced by the DC level from the mixer for comparison with the set point. The *P* part of the circuit gives a proportional response to the difference, as shown in Figure 4.11 (a), while the *I* part of the circuit smoothly corrects the offset between the *P* response and the required DC signal, as shown in Figure 4.11 (b). The signal from the *PI* controller thus drives the piezo fiber stretcher to restore the original fiber laser optical cavity length.

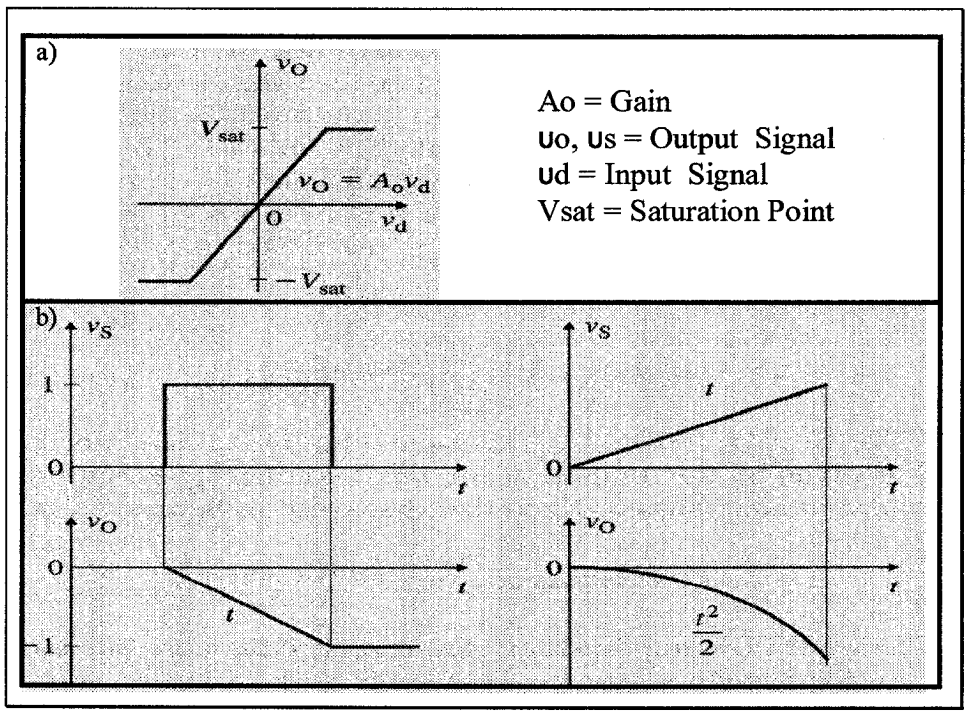

Figure 4.11: (a) Transfer characteristics of a *P* controller; (b) Typical input and output signals of an *I* controller (Microelectronic Circuits, Analysis and Design [7], pp269, 282).

The computer is used only for determining the setpoint and does not contribute to the stabilization process once the signal is applied to the switch in G. While the *PI* controller is operating, the computer only measures the various parameters of the laser pulse. Nevertheless, the computer can stop the *PI* controller at any time by instructing the switch to send the pre-stretched value to the piezo fiber stretcher.

4.5. Computer-Controlled Method with a Piezo Device

4.5.1. Idea

A hybrid approach of stabilization was implemented only as a transition between the computer-controlled and circuit-controlled methods. This hybrid method is not presented in either Chapter 6 or Chapter 7 on the comparison and generalization of the experiment since it was a transition experiment between the two main approaches and exhibits almost the exact performance characteristics as the computer-controlled approach. This hybrid method does provide another way of stabilizing the laser, however.

As with the circuit-controlled method, the piezo fiber stretcher was placed inside the cavity, but the program built for the computer-controlled method was used to directly control the piezo itself instead of the *PI* controller. The piezo fiber stretcher had to be characterized in order to find the reference curve between the voltage applied to the piezo fiber stretcher and the change in the DC level at the mixer. Similarly, it was necessary to determine a pre-stretched voltage to compensate for both increases and decreases of the temperature.

A further advantage of the hybrid method was the possibility of eliminating the 0-5V limitation of the piezo fiber stretcher, which limited to total stabilization time in the circuit-controlled method, to make use of the modulation frequency to keep the fiber laser

stable over an essentially infinite time period. The same LabView™ program used in the computer-controlled method was used to run the system since it was already effective, optimized and simple to update to control the piezo fiber stretcher.

4.5.2. Design

Only one design was built for this stabilization method. The first stage was the characterisation of the piezo fiber stretcher. A LabView™ program was designed to obtain a relationship between the voltage applied to the piezo fiber stretcher and the DC level at the mixer. With the modulation frequency turned off, the program first gets the frequency of the self-beat signals contained in the RF spectrum window. The program then applies a voltage to the piezo fiber stretcher and takes measurements of the frequency change for each peak. For a 3MHz span, four or five peaks can usually be seen on the RF spectrum and the program takes an average that is kept in memory. The voltage applied is tuned over the whole 0-5V range and a curve is drawn, as shown in see Figure 4.12.

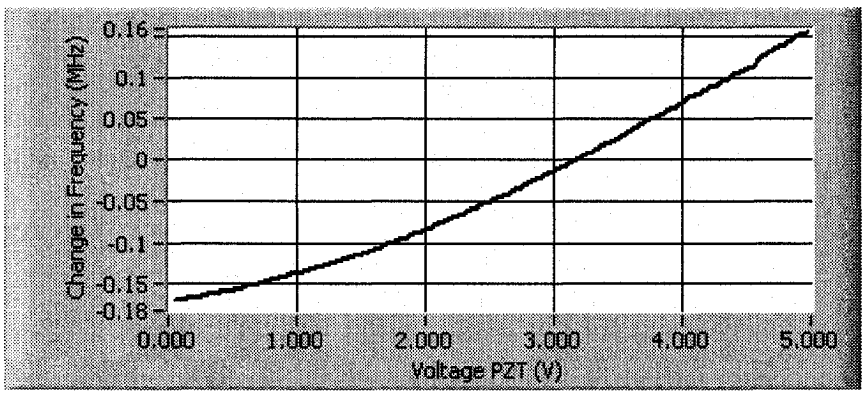

Figure 4.12: Frequency change vs. voltage applied to the piezo fiber stretcher.

The principal problem is to find a relationship between the variations in frequency and the DC level from the mixer when the modulation frequency is turned on. The solution is to use the curve that associates the shift in modulation frequency with the DC level from the mixer – a relationship already measured for the computer-controlled method. In fact, a

shift in the modulation frequency related to the self-beat signal is equivalent to a shift in the position of the self-beat peak related to the modulation frequency.

Once the program has found the best phase delay and built the linear curve, the voltage applied to the piezo fiber stretcher can be linked to the DC level from the mixer and used as a reference curve. An important parameter that needs to be taken from the curve is the pre-stretched value of the piezo fiber stretcher. Since the curve is nonlinear, the middle point is not exactly at the nominal middle point of the voltage range, which corresponds to 2.5V, but appears to be at 3.1V, as shown in Figure 4.12. This value is then chosen as the pre-stretched value of the piezo fiber stretcher for this method, as well as for the circuit-controlled method.

The LabView™ program was operated in a similar manner as for the computer-controlled method, with the exception of some modifications. Instead of the modulation frequency, the stabilisation parameter was chosen to be the voltage applied to the piezo fiber stretcher. A new routine also had to be included inside the LabView™ program to indicate the piezo fiber stretcher voltage limits. It works as follows: if the voltage limits of the piezo fiber stretcher were reached, the modulation frequency was automatically shifted to the setpoint value and the value of the voltage applied was set to the pre-stretched value of 3.1V to perpetuate the stabilisation. In order to change the modulation frequency however, the computer requires the same reference curve as used in the computer-controlled method.

4.5.3. Setup

In the hybrid computer-controlled method with PZT, the computer is used to control the voltage applied to a piezo fiber stretcher in order to stabilise the fiber laser. Starting

exactly like the circuit-controlled method with a pre-stretched value of 3.1V, the computer finds a self-beat signal and turns on the modulation frequency at the center peak. At that point, the setpoint is sent to the computer and saved as a reference. When a temperature variation changes the optical cavity length, the program is able to use the reference curve and the DC level to get the voltage required and to apply it to the piezo fiber stretcher. The process is repeated until the voltage limits of the piezo fiber stretcher are reached, in which case the modulation frequency is changed and the voltage applied is reset to 3.1V to continue the stabilization process.

5. Experiments, Results and Optimization

5.1. Introduction

Once the design of each stabilization method was completed, each was tested with the fiber laser system. Many different parameters are taken into account in the evaluation of the performance of each method, including the modulation frequency for the computer-controlled method, the voltage applied to the piezo fiber stretcher for the circuit-controlled method and the computer-controlled with PZT method, the optical spectrum, the autocorrelation, the RF spectrum, and the DC level at the mixer.

Once functional, each stabilization method was then optimized. This chapter gives an overview of the results obtained with the computer-controlled method, the computer-controlled PZT method and the circuit-controlled method as well as the optimization for each. The two principal approaches are compared in Chapter 6.

5.2. Computer-Controlled Method

5.2.1. First Experiments and Problems Encountered

The performance of the computer-controlled method depends principally on the design of the LabView™ program itself. The efficiency of the coding process, which constitutes the heart of the stabilization method, determines whether or not the method is efficient. Despite many possible ways to code the same functionality, there are very few algorithms that are able to greatly reduce the time of execution for any specific task. The algorithm that best manages operation time with thus give the best results.

Although not very accurate, the first prototype of the program that succeeded in stabilizing the laser provided a good starting point because the time response of the computer was fast enough for the modulation frequency to keep track of the changes in

temperature. An example of the performance of the first prototype is shown in Figure 5.1 for 60 minutes of stabilization.

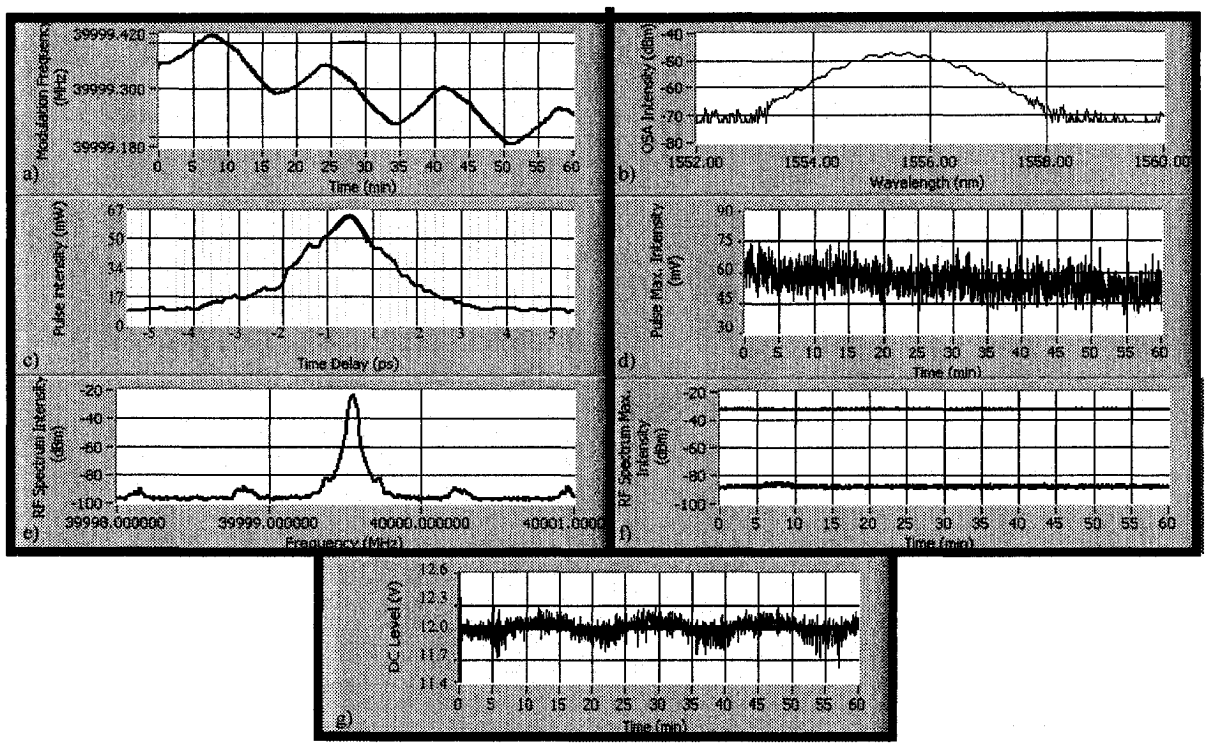

Figure 5.1: Results of the first 60-minute experiment using the computer-controlled method for the (a) modulation frequency, (b) the optical spectrum, (c) and (d) the pulse characteristics, (e) and (f) the RF spectrum characteristics, and (g) the DC level.

The modulation frequency in Figure 5.1(a) closely follows the variations in temperature where the oscillations from the air conditioner can be seen. The optical spectrum in (b) has small modulation depths with peaks separated by 40 GHz, as expected. The autocorrelation maximum intensity in (d) fluctuates with time but maintains the same average value; although a general downward trend in the average value can be seen in (d), this is due to the autocorrelator itself and not to the pulse and is thus not considered. The RF spectrum in (e) gives low noise peaks while in (f) a stable maximum RF intensity peak remains over the whole period of stabilisation. Finally, the DC level in (g) gives a kind of square oscillation; that is, when the change in the modulation frequency increases, the DC level value is lower than the reference value and vice-versa. This phenomenon is regrettable

since it never allows the DC level to actually reach the setpoint, but only to oscillate around it. From these results, it appeared that the first thing to improve with the program would be its time response.

The small modulation depth of the optical spectrum had to be characterized. Usually, this problem is due either to a mismatch between the modulation frequency and the intermode frequency spacing or to the optical filter. In order to find out if it was a problem with the LabView™ program, a test was done where the modulation depth was evaluated while the setpoint on the DC curve was changed slightly from its middle point in the stabilized regime. The modulation depth essentially did not change from one setpoint to another. Next, the modulation frequency was adjusted manually, without any stabilization process, to try to mode-lock the laser while looking the modulation depth on the OSA. The poor response indicated that the optical filter was at fault, not the LabView™ program.

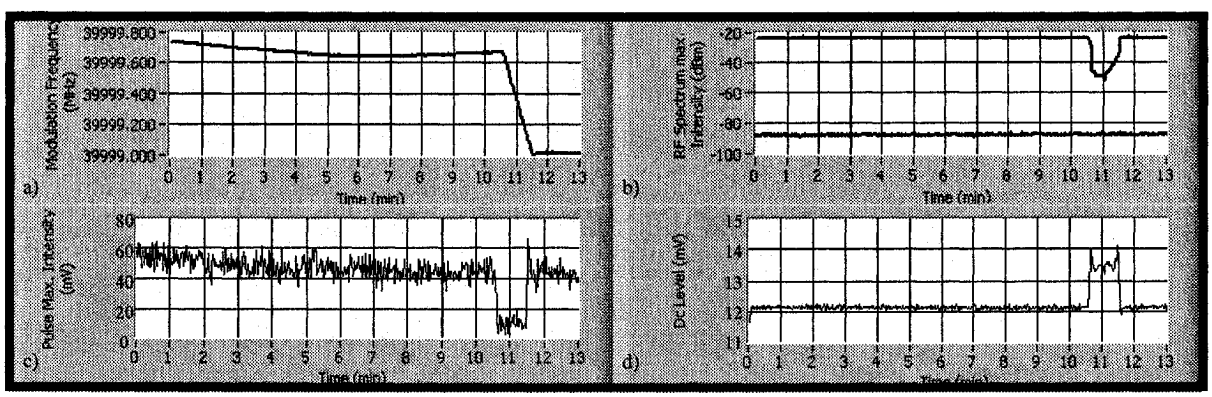

Figure 5.2: Instabilities encountered using the computer-controlled method in (a) the modulation frequency, (b) the RF spectrum, (c) the pulse intensity, and (d) the DC level.

The first use of this prototype also produced some unpredictable problems that needed to be fixed. Figure 5.2 shows some examples of unexplained results in the modulation frequency, the RF maximum intensity, the autocorrelation and the DC level

with time for one specific experiment. After 10 minutes, the fiber laser became unstable for one minute before suddenly returning to mode-locked regime.

Several scenarios were proposed to find the origin of the problems. Two possible causes of the instability were found, both related to the DC reference curve. The reference curve is the heart of the stabilization process for the computer-controlled method and the laser will remain unstable if the program cannot get a good representation of the system from the reference curve.

When the computer has taken all the measurements of the DC level from the mixer in a specific modulation frequency window, it does a fit of all the points to find the setpoint as shown in Figures 5.3(a) and (b). If the curve is not completely linear, the program may encounter problems.

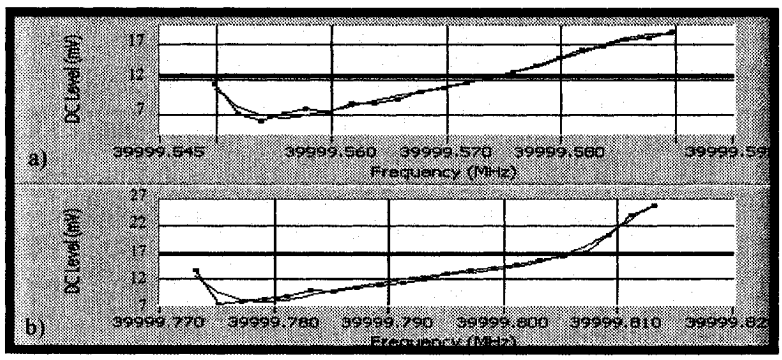

Figure 5.3: Two cases showing the non-linear regions of the DC level that cause instability.

In the scenario represented in Figure 5.3 (a), the program's fit of the data curves upward at lower frequencies instead of maintaining the nominally linear relationship; the midpoint is thus underestimated. A related problem is that a single DC level represents two different changes in modulation frequency; since the program will change the modulation frequency to match the closest DC level in the reference curve, the wrong DC level is chosen from time to time.

In the case of Figure 5.3 (b), the DC level fit curve has more difficulty representing all the data and the midpoint is closer to the edge of the mode-locking area, which is only 40 kHz wide. This scenario can also lead to instability, since the DC level decreases drastically at the outer limits of the range.

If the DC level decreases too much, the program is not able to find the change in modulation frequency required for that specific low DC level from the reference curve. The program therefore takes a default value, assigned to be the first data point of the curve, which can further decrease the DC level. The instability will remain until the modulation frequency reaches the next self-beat signal. At that point, the DC level will increase and allow the program to re-establish the mode-locking process at the new peak.

5.2.2. Optimization

In order to optimize the first prototype, the two problems discovered with the DC reference curve had to be resolved; the curving data fit line and a midpoint that is near the outer limits of the range. For the case of the curving data fit line, given the low number of data points in the curving part of the fit of Figure 5.3, this data was simply removed from the fit curve. A case statement basically evaluates each data point in reference to its neighbor and ensures that the changes in the DC level are sequential. This method allows an evaluation of each edge and guarantees that the curve is linear with a positive slope. If too many data points are removed from the curve, the program simply stops operating, meaning that the choice of the phase delay is not accurate.

For the case when the midpoint is near the limits of the range, a simple way to avoid the edge of the mode-locking range is to use a reference level that can be changed dynamically. In other words, once the middle point has been chosen by the program and is

found to be too close to the edge of the stabilization window, it can be changed manually to the center while the program is running.

Once these two problems had been solved, further optimization was undertaken at the level of the execution speed of the program. The only way to decrease the time response is to increase the speed of the program's loops by getting rid of all extraneous operations. For example, originally the program used to obtain the pulse width and the optical spectrum bandwidth while it was running, but fitting the two parameters required a long processing time. In order to avoid this waste of the program's time, the program was modified to save the data from the autocorrelation and the OSA into files so that another independent program can evaluate the parameters without interfering with the stabilization process.

To improve the modulation depth of the OSA, a different optical filter was tested inside the cavity. This filter was numerical, which means that its shape, its bandwidth and its central wavelength could be adjusted by the computer. After attempting many different combinations, the program was found to give the best results with a square-shape filter of 4nm bandwidth at a central wavelength of 1570nm.

The only disadvantage of this filter is that it operates with single-mode fiber instead of PM fiber. Since the isolator is polarization dependent, the new optical filter required a polarization controller to maintain the state of polarization. The polarization controller was not that effective however because it had to be operated manually; a polarization stabilizer is needed. Even with the polarization controller, the single-mode fiber sometimes modified the state of polarization in such a way that the modes inside the cavity were no longer seen on the RF spectrum and caused problems for the control program. These fluctuations did not occur too quickly however, so the numerical filter was still found to be a reasonable alternative for the fiber laser.

5.2.3. Final Results

Once the first version of the LabView™ program was optimized, the program was found to be very effective and did not encounter any further problems. Figure 5.4 shows the results for 80 minutes of laser operation using the optimized computer-controlled method. The optical spectrum in (b) shows a strong modulation depth and the DC level in (g) is able to follow the reference level more closely than before.

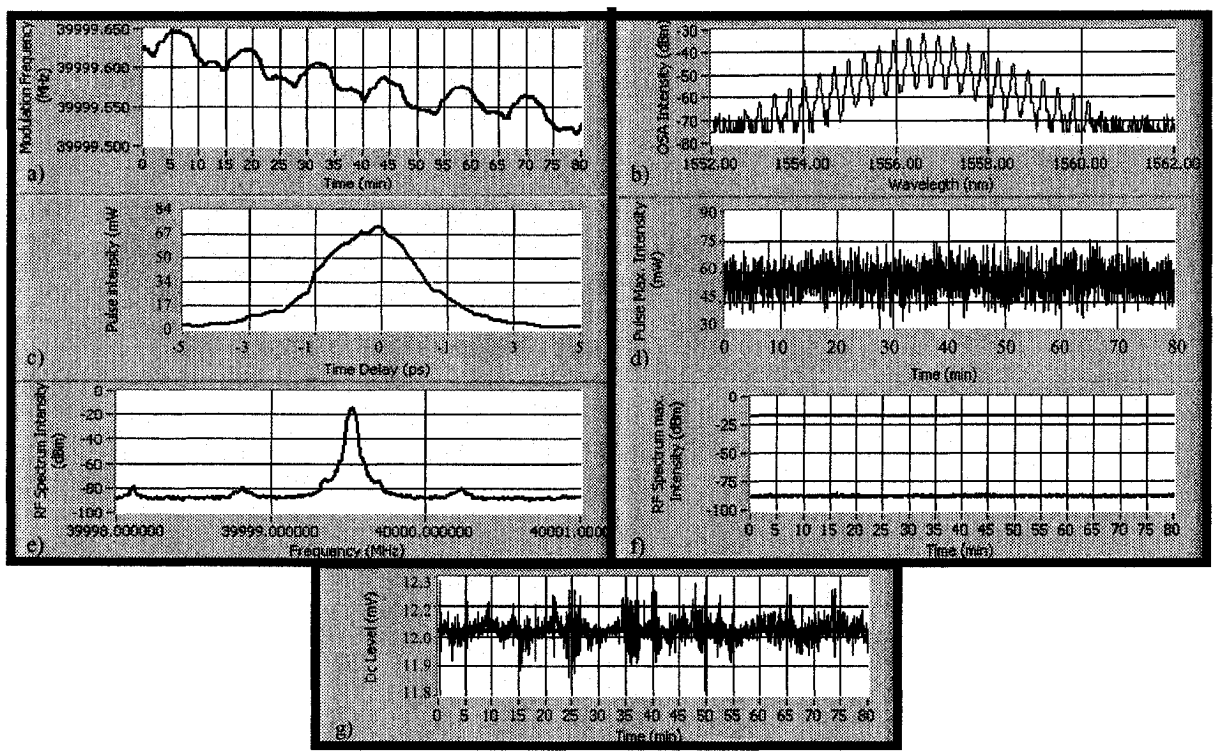

Figure 5.4: Results of the optimized 80-minute experiment using the computer-controlled method for (a) the modulation frequency, (b) the optical spectrum, (c) and (d) the pulse characteristics, (e) and (f) the RF spectrum characteristics, and (g) the DC level.

5.3. Computer-Controlled Method with the PZT

5.3.1. First Experiments and Problems Encountered

The hybrid stabilization method is based on the computer-controlled method and has the same LabView™ program structure. The only difference in the two programs is the reference parameter; the computer-controlled method uses the modulation frequency, while the hybrid method uses the voltage applied to the piezo fiber stretcher. Figure 5.5 shows the first results using the hybrid stabilization method for 100 minutes of stabilization.

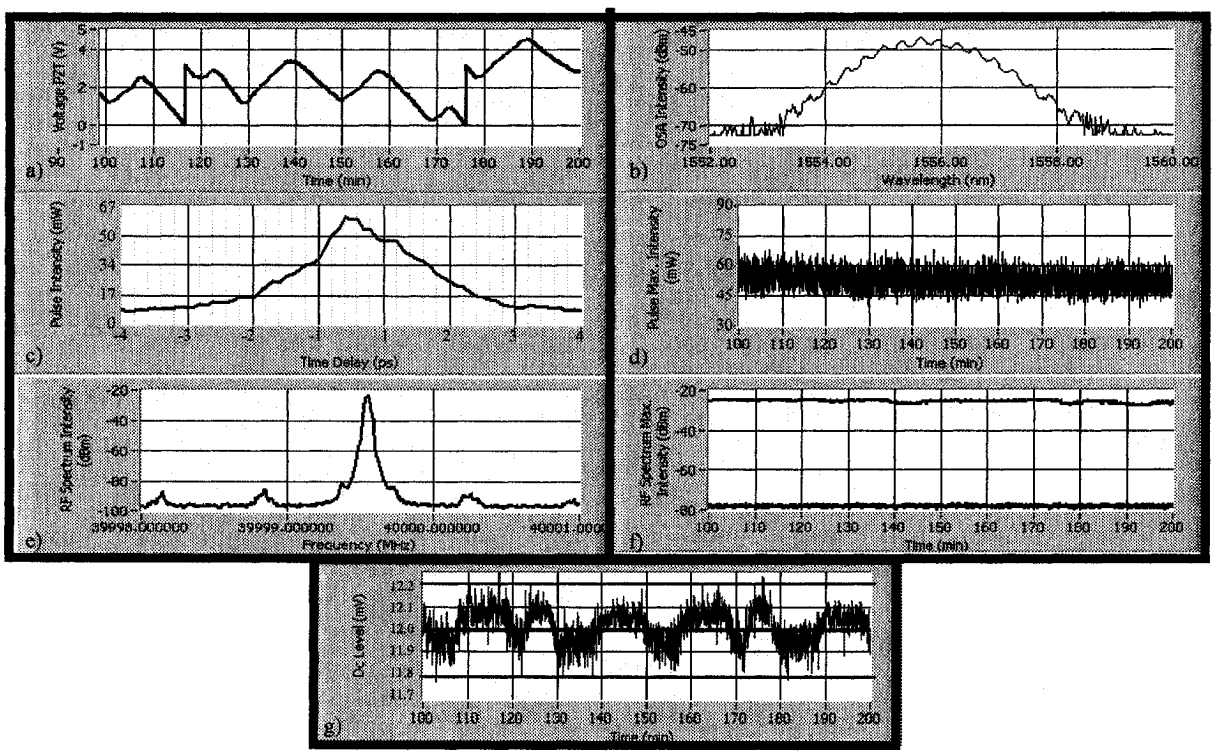

Figure 5.5: Results of the first 100-minute experiment using the computer-controlled method with the PZT for (a) the voltage applied to the PZT, (b) the optical spectrum, (c) and (d) the pulse characteristics, (e) and (f) the RF spectrum characteristics, and (g) the DC level.

Since the first version of the computer-controlled PZT method was built before the full optimisation of the computer-controlled method, it encountered the same problems in

the initial experiments as described in section 5.2.1. As expected, the modulation depth and the DC level were found to be the same as for the computer-controlled method.

As with the computer-controlled method, the stabilization of the computer-controlled PZT is strongly dependent on the reference curve of the program. Therefore, both stabilization methods encounter problems of instability related to the reference curve. As shown in Figure 5.6, the instabilities of the hybrid method are not the same as with the computer-controlled method but can be explained by the same scenario shown in Figure 5.3 (a) and (b). In fact, Figure 5.6 shows oscillation between a low value and a high value of the DC level. Since the voltage applied to the piezo fiber stretcher doesn't appear to be affected by variations in the DC level as shown in Figure 5.6 (a), it may be possible that the setpoint is either at one edge of the DC level curve, as in Figure 5.3 (b), or that the DC level keeps oscillating between the two values, as in Figure 5.3 (a). Indeed, it was in the testing of this hybrid method that the solutions to the instabilities of the computer-controlled approach were found.

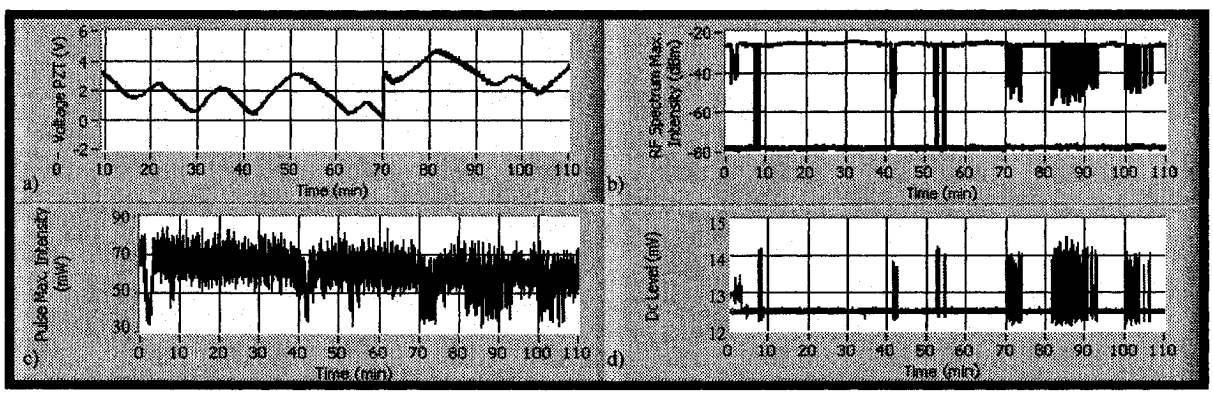

Figure 5.6: Instabilities encountered using the hybrid computer-controlled method with the PZT in (a) the voltage applied to the PZT, (b) the RF spectrum, (c) the pulse intensity, and (d) the DC level.

5.3.2. Optimization

The problems encountered with the hybrid computer-controlled PZT method are essentially the same as for the computer-controlled method, so the optimization followed the same steps as for the computer-controlled method.

5.3.3. Final Results

Once the LabView™ program had been optimized, the hybrid computer-controlled PZT method was as effective as the computer-controlled method. Figure 5.7 shows the results for the optimized hybrid computer-controlled PZT method over 225 minutes. When the lower limit is reached in Figure 5.7 (a), the change in the modulation frequency can be seen at many different places by a big step of the voltage from 0 to 3.1V.

Even when optimized, the oscillations of the DC level shown in Figure 5.7 (g) are found to be a bit worse than for the computer-controlled method. The reason is that the voltage applied to the piezo fiber stretcher is given by the power supply of the acquisition card, which encounters small fluctuations in voltage. These fluctuations are sent to the piezo fiber stretcher, which reacts by increasing or decreasing the length of the fiber and consequently affecting the DC level from the mixer.

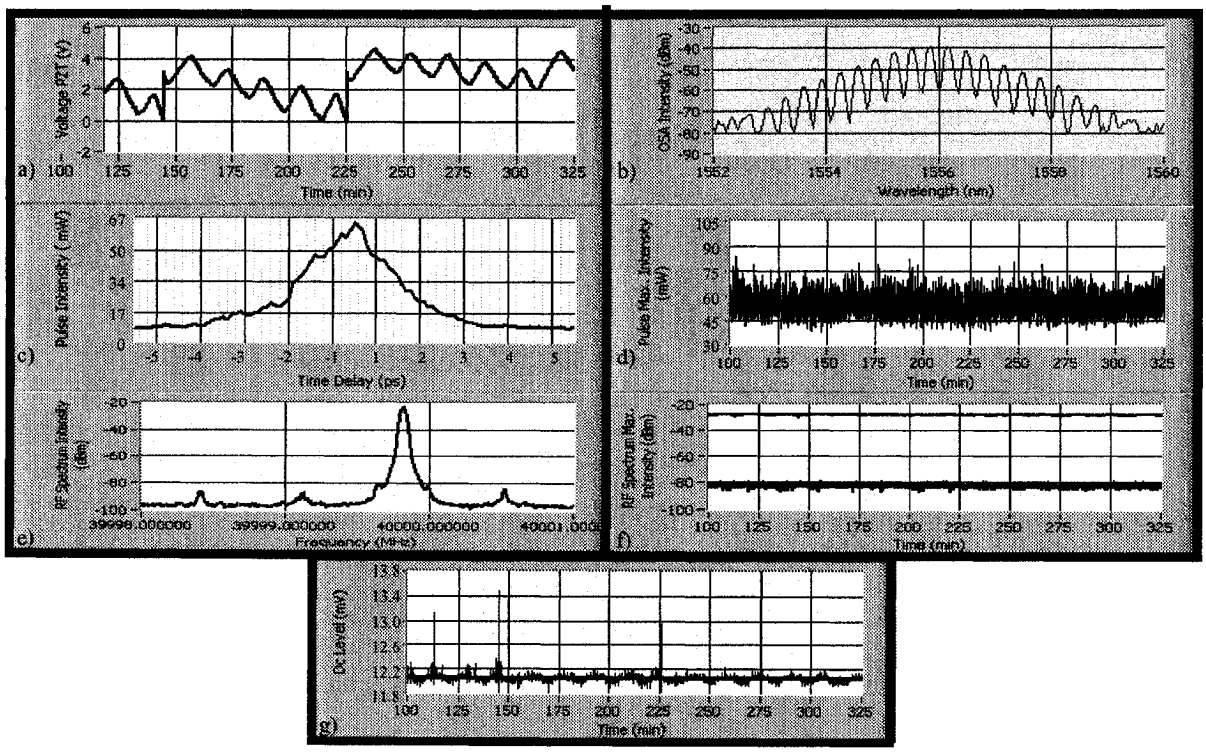

Figure 5.7: Optimized results of a 225-minute experiment using the computer-controlled method with the PZT for (a) the voltage applied to the PZT, (b) the optical spectrum, (c) and (d) the pulse characteristics, (e) and (f) the RF spectrum characteristics, and (g) the DC level.

5.4. Circuit-controlled Method

5.4.1. First Experiments and Problems Encountered

The performance of the circuit-controlled method is a function of the design of the *PI* controller. Specifically, the choice of the resistance and the capacitance that determine the gain of the *P* and the gain of the *I*, respectively, is critical. The two gains are related, and only certain combinations of the two gains can successfully stabilize a system. Their choice is then limited to an area of stabilization as shown in Figure 5.8; note that the values in Figure 5.8 depend on the parameters of the system because each system reacts differently to an external disturbance and possesses its own stabilization area.

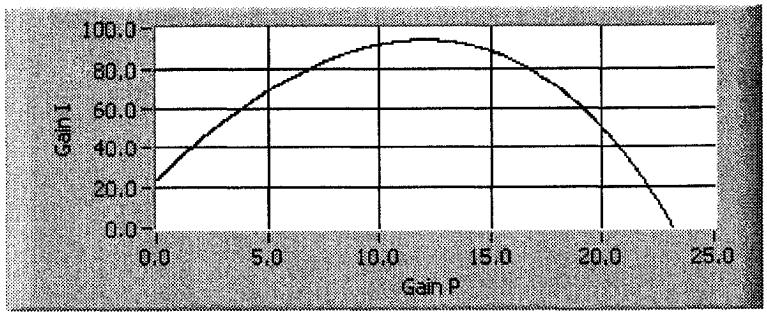

Figure 5.8: Stability zone for a specific *PI* controller.

On a *PI* chip, the values of the resistance and capacitance can be chosen to obtain the best possible combination of *P* and *I* for a specific application. As an initial test, the capacity of the *I* and the resistance of the *P* were chosen to be the standard values of the first circuit-controlled model that used the HTC-1500 prefabricated circuit. The specific values were 5kΩ for the resistance and 5μF for the capacity, giving a *P* gain of 100.

In contrast with the two previous methods, the first experiments with the circuit-controlled method gave no sign of stabilization at first. To give an example of the performances of the first version of the method, some results are shown in Figure 5.9 for 4 minutes of attempted stabilization.

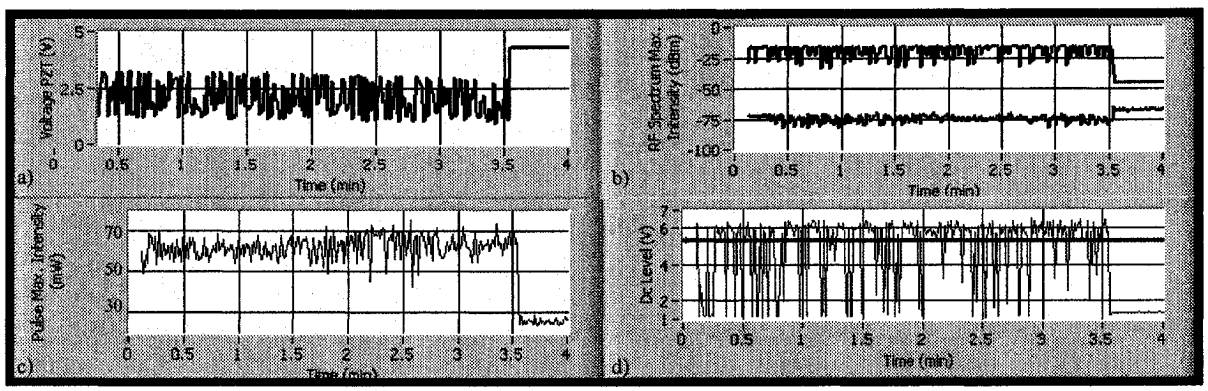

Figure 5.9: Instabilities encountered using the circuit-controlled method with the PZT in (a) the voltage applied to the PZT, (b) the RF spectrum, (c) the pulse intensity, and (d) the DC level.

It is clear from Figure 5.9 that the principal problem was related to the design of either the *P* or the *I* since the voltage kept oscillating between the two extremes values. If

the gain of the *P* is too high, then the DC level is adjusted by increments that are too large for the laser to be stabilized at a stationary value. Given that this is what is observed in Figure 5.9 (a), and since the gain of the *I* was not very high, it was determined that the instabilities were most likely caused by the *P* characteristics.

The *PI* circuit also had two other problems related to the DC level and the phase delay between the synthesizer and the output of the laser. From the oscilloscope, it appeared that the DC signal coming from the mixer encountered some fluctuations (see Figure 5.10), meaning that the circuit was introducing noise in the fiber laser system. The problem was found to be related to the structure of the circuit itself, since the circuit had been built on a breadboard using long wire, power supplies, and sockets for the chips. All these components introduced noise into the circuit and increased the likelihood of instabilities.

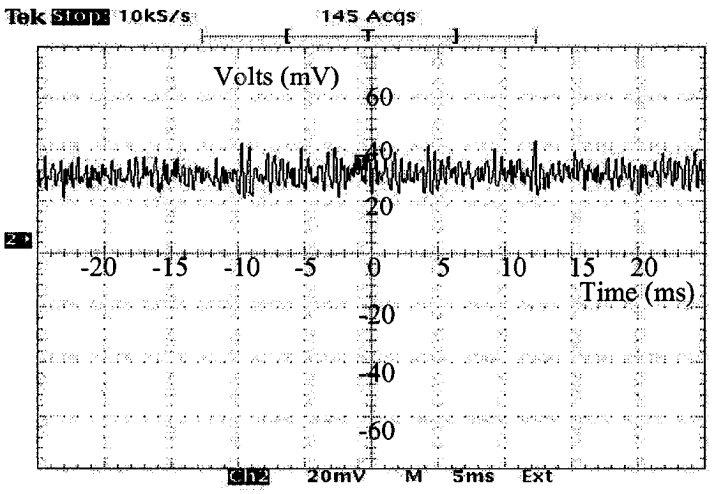

Figure 5.10: Fluctuations of the DC level from the mixer with the first experiment of the circuit-controlled method.

The second problem caused by the *PI* circuit was that the phase delay between the synthesizer and the output of the laser was not linear. The *PI* controller requires a signal

level that is affected linearly by a disturbance in order to stabilize a system and the non-linearity of the relationship chosen meant that instabilities could still occur.

5.4.2. Optimization

To find the optimal parameters for the *P* and *I* components, the step response method of Ziegler-Nichols [5] was used, since it is both simple and provides a good approximation of the optimum values. The step response of an open loop system is used to determine the loop's behaviour, which gives the parameters needed for the controller (the resistance of the *P* and the capacity of the *I*).

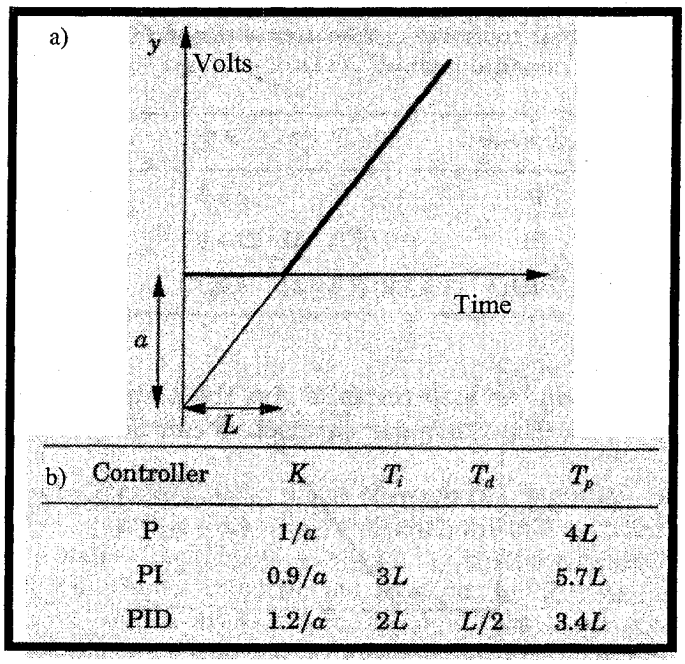

b)

Controller	K	T_i	T_d	T_p
P	$1/a$			$4L$
PI	$0.9/a$	$3L$		$5.7L$
PID	$1.2/a$	$2L$	$L/2$	$3.4L$

Figure 5.11: (a) Characterization of a step response using the Ziegler-Nichols method; (b) PID controller parameters obtained from the Ziegler-Nichols method (PID Controllers: Theory, Design, and Tuning [5], pp135-6).

Figure 5.11 (a) shows a typical curve of an open loop system reacting to a step response. From this open loop response curve, the point that represents the maximum value of the slope is taken and a tangent from that point to the starting point of the step response is drawn. The parameters a is related to *P* since it is a gain, and the parameter L is related to

I, since *I* relates to a time constant. For a *PI* controller, the value for the gain and the value of the time constant are given in Figure 5.11(b).

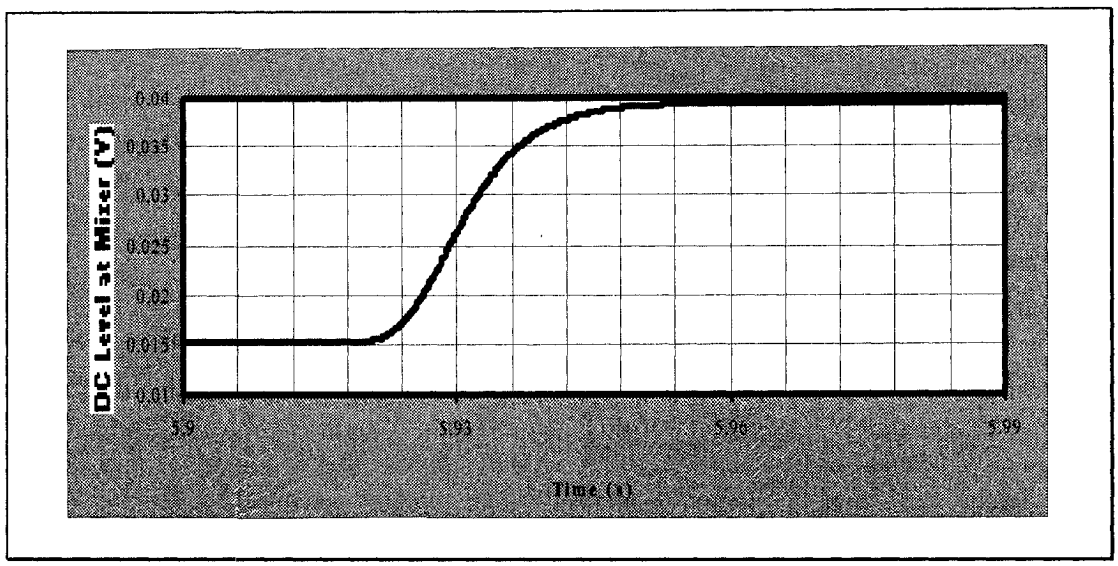

Figure 5.12: The open loop step response of the fiber laser.

The open loop step response of the fiber laser was taken by sending 1V to the piezo fiber stretcher and getting the DC level from the mixer (see Figure 5.12). From this curve, the parameters *a* and *L* were found. The gain of the *P* was evaluated at 45 and the time delay of the *I* was evaluated at 0.033s. The two results were then converted into the corresponding resistance for the *P* and capacitance for the *I*; the two values were found to be 11kΩ and 0.33μF, respectively. Upon attempting stabilization with these two values in the closed-loop system, the system still suffered oscillations, as shown in Figure 5.12. The problem stems from the fact that the real system never steps up by 1V when a temperature fluctuation occurs so the values of the gains were overestimated using the step-response method.

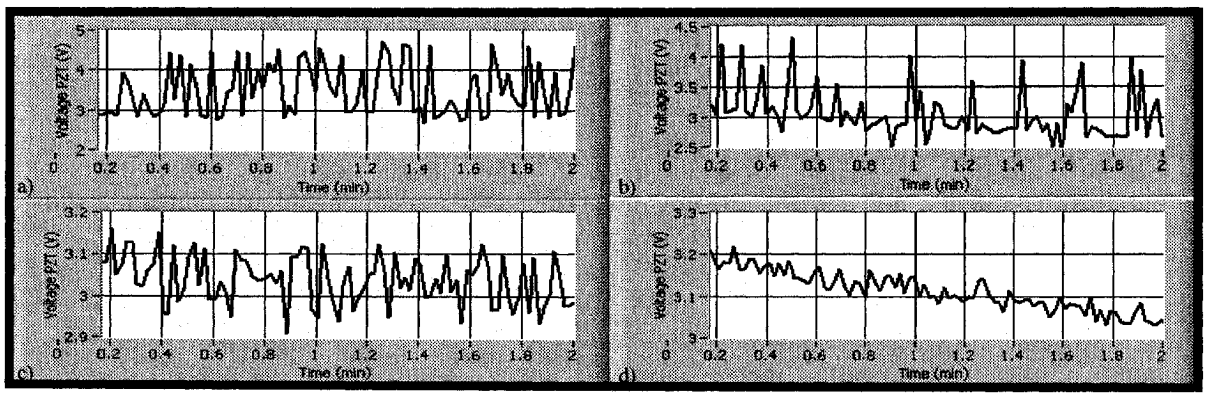

Figure 5.13: PZT voltage measured against various resistance / capacitance combinations: (a)10kΩ/0.3μF; (b) 20kΩ/0.3μF; (c) 20kΩ /0.44μF; and (d) 40kΩ/0.44μF.

The values of the *P* and *I* were then manually adjusted near the values given by the Ziegler-Nichols method to attempt to find the values that would properly stabilize the laser. Figure 5.13 (a), (b), (c), and (d) show experiments using different combinations of resistance and capacitance; the system was finally stabilized with a resistance of 50kΩ and a capacitance of 0.44μF.

Finally, the reaction curve of the *PI* controller was evaluated in order to get the system settling time and overshoot to make sure that the values of the gain were both accurate and optimized. The settling time is the time that the *PI* controller takes to stabilize within 2% of the steady state value of the setpoint (see Figure 5.14 for the definition of t_s). The overshoot is the difference between the first gain of the curve and the steady state value (see Figure 5.14 for the definition of the *o*).

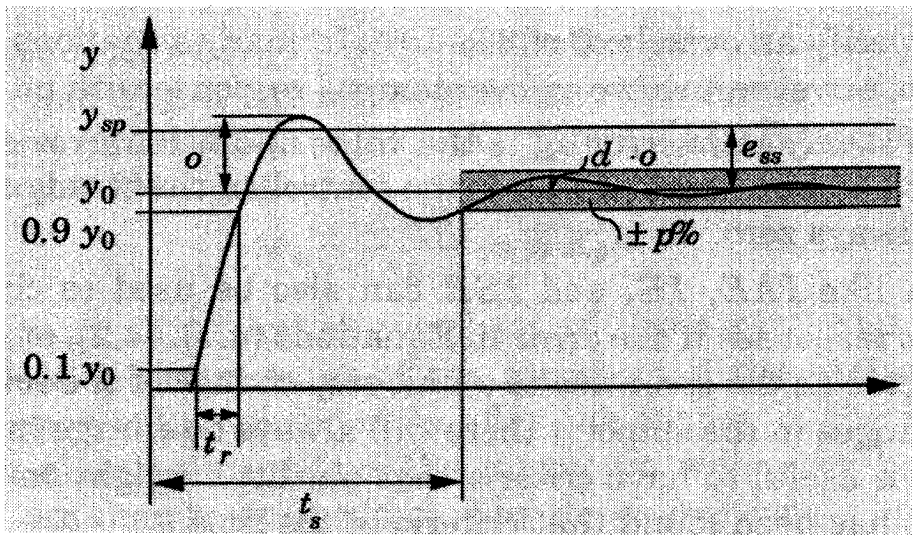

Figure 5.14: Definition of the overshoot and settling time parameters (PID Controllers, Theory, Design, and Tuning [5], pp 127).

The reaction curve obtained using the initial stabilizing resistance and capacitance values of 50kΩ and 0.44μF had a poor overshoot value of 1V and a settling time of 0.2s, as shown in see Figure 5.14(a). Following further adjustment of the capacitance and resistance, the overshoot was less than 0.1V. The optimal combination was found to be 250kΩ for the resistance and 1μF for the capacitance, giving an overshoot of only 0.03V and a settling time of 0.12s (see Figure 5.15b).

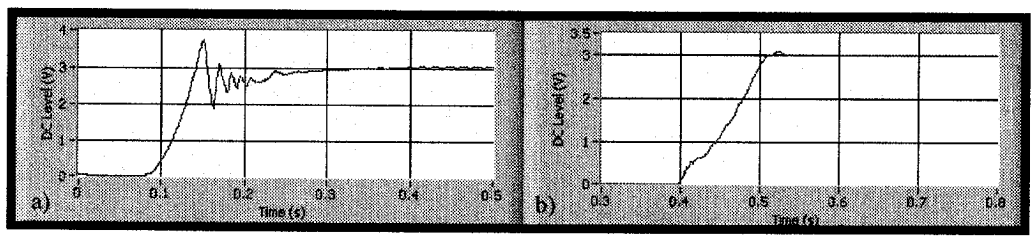

Figure 5.15: (a) Reaction curve of the *PI* controller with 50kΩ and 0.44μF; (b) Reaction curve of the *PI* controller with 250kΩ and 1μF.

In order to reduce the noise as much as possible, the *PI* circuit structure was soldered onto an integrated circuit. This allowed the elimination of the sockets and wires, with the exception of the jumpers, and a unique ground level distributed across the entire circuit board. The only two parameters of the entire circuit that were kept floating were the

capacity of the *I* and the resistance of the *P*. The number of power supplies required was reduced from seven to four, and even these were eventually replaced by batteries. The photograph of the soldered circuit is shown in Figure 5.16. Following these changes to the circuit, the DC level from the mixer was found to be stable.

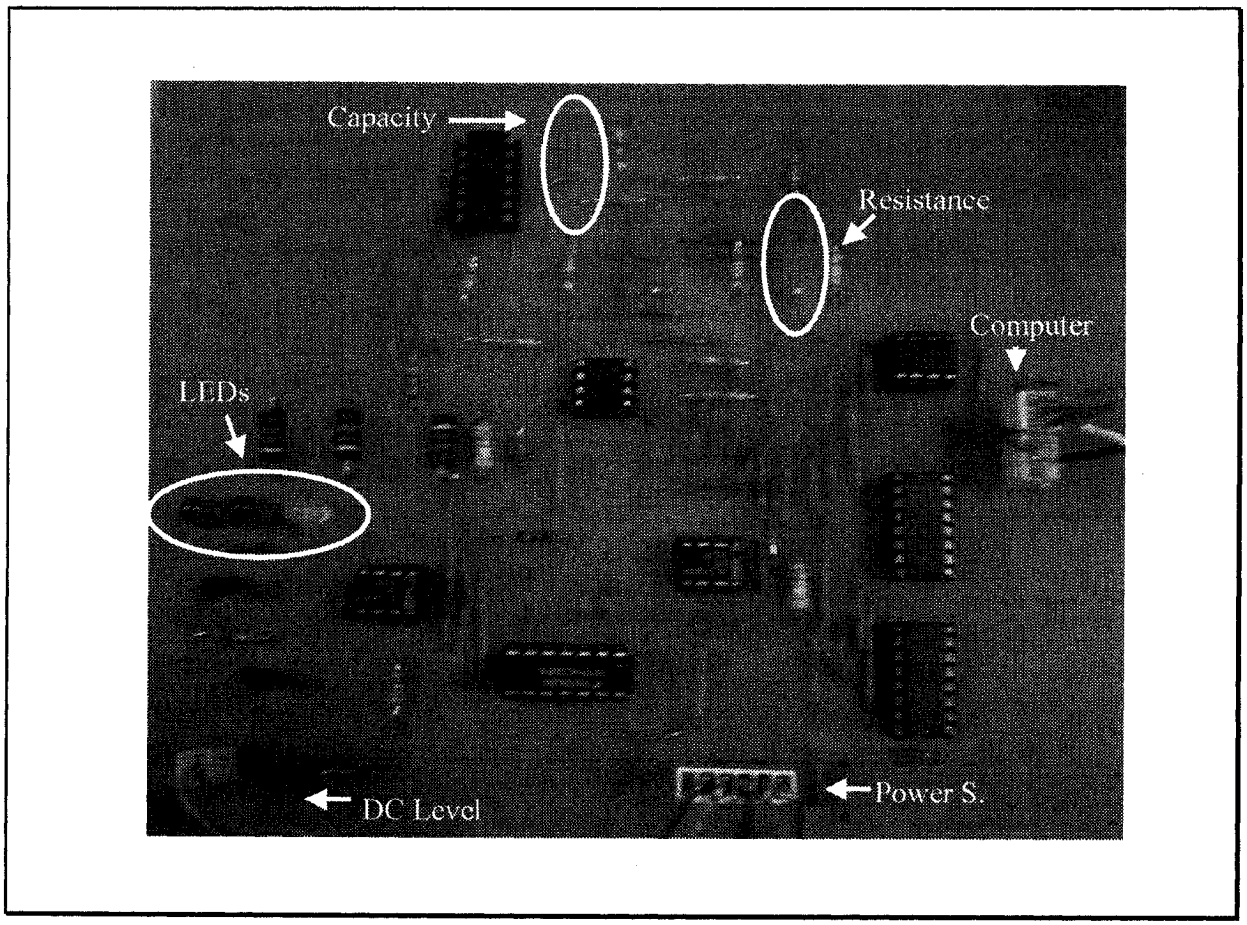

Figure 5.16: Photograph of the soldered circuit designed and fabricated in the laboratory.

5.4.3. Final Results

The circuit-controlled method required more effort to optimize than the computer-controlled and the hybrid computer-controlled PZT methods of stabilization. However, the final setup was found to be very effective at controlling the signals and stabilizing the laser. Figure 5.15 shows the results for the optimized circuit-controlled method. As with the

modulation frequency for the computer-controlled method, the voltage applied to the PZT in Figure 5.17 (a) allows the system to follow the variations in temperature. The DC level in Figure 5.17 (g) appears to maintain its value at the setpoint without any large visible oscillations, meaning that the *PI* controller is very effective at stabilizing the laser.

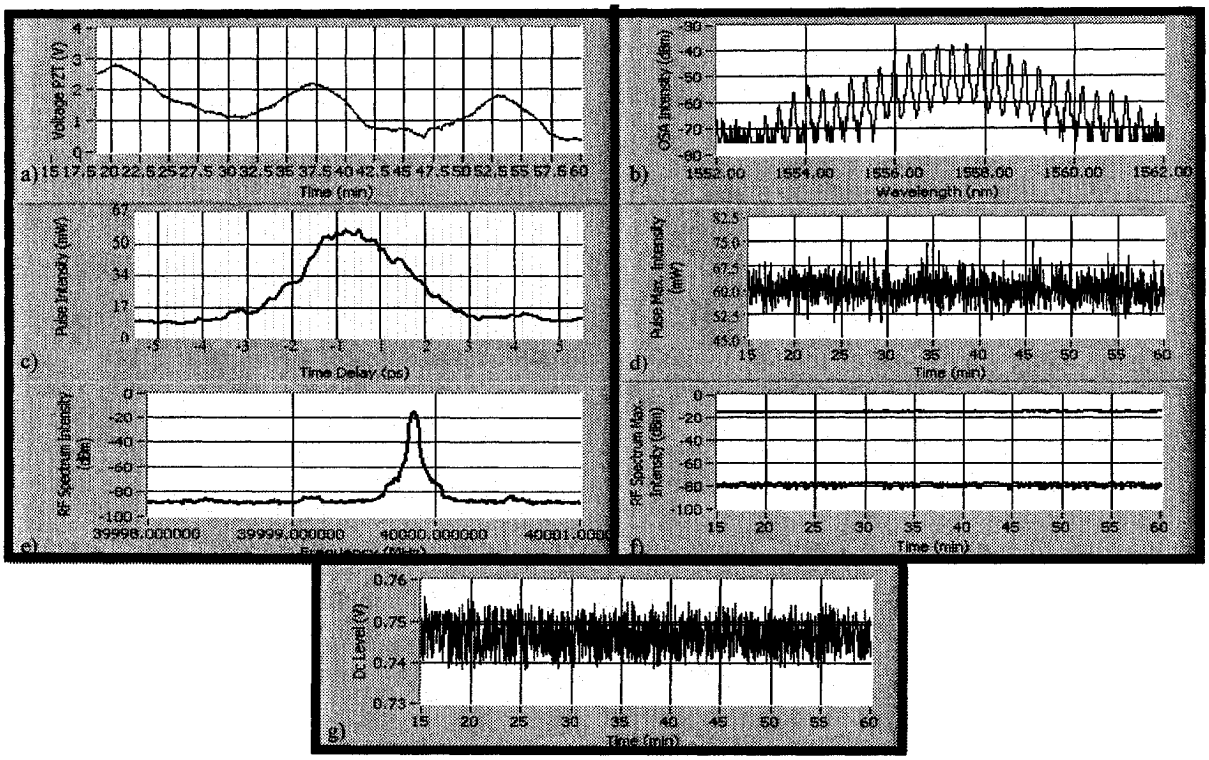

Figure 5.17: Optimized results of a 45-minute experiment using the circuit-controlled method for (a) the voltage applied to the PZT, (b) the optical spectrum, (c) and (d) the pulse characteristics, (e) and (f) the RF spectrum characteristics, and (g) the DC level.

6. Comparison of the computer-controlled method and the circuit-controlled method

6.1. Introduction

Given that the results of stabilization with the computer-controlled method and the circuit-controlled method after optimization are found to be very accurate, the two methods are compared in order to draw conclusions on their respective performance and utility. As previously mentioned, the hybrid approach using the computer to control the PZT was not compared with the other two methods simply because it was a transition method to aid development of the circuit-controlled method and its performance mirrors closely that of the computer-controlled method.

Several parameters were used to compare the computer- and circuit-controlled approaches including the pulse train, the length of the stabilization period, the RF (Radio Frequency) spectrum of the laser output, the time response, the DC signal from the mixer, the time jitter of the pulses, the pulse width, the optical spectrum bandwidth, and the amplitude of the pulse. The results show that both approaches are efficient methods of stabilizing a harmonic FM mode-locked fiber laser.

6.2. Stability of the Repetition Rate

Figure 6.1 shows the evolution of the modulation frequency over time for both approaches; the variation in modulation frequency caused by temperature fluctuations is easily observed for the computer-controlled approach, since the change in modulation frequency is used to track the temperature fluctuations, while there is no variation with the circuit-controlled approach, which changes the optical length specifically to maintain the same modulation frequency.

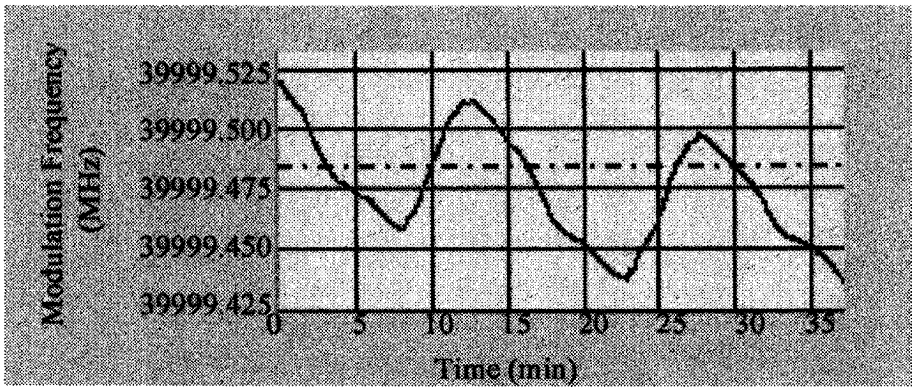

Figure 6.1: Evolution of the modulation frequency over time for the computer-controlled approach (solid line) and the circuit-controlled approach (dashed line).

The clear disadvantage of the computer-controlled approach is that the synthesizer frequency must be modified for every round trip in the laser cavity. This means that optical pulses are sent through the fiber with differing time lags. For very small modulation frequency changes the pulses would be recoverable at the receiver, but when frequency changes are larger than the bandwidth of the receiver the pulses are not recoverable. In fact, the modulation frequencies that can be detected are limited by the receiver's narrow bandwidth. For telecommunications applications then, the circuit-controlled approach enjoys the advantage that the modulation frequency does not fluctuate.

6.3. Period of Stability

A clear disadvantage for the circuit-controlled approach is the length of time over which the laser remains stabilized. The voltage applied to the piezo-fiber stretcher is fixed and must be kept in the range of 0-5V. When the voltage reaches one of the two boundary voltages, usually within a couple of hours, the fiber laser becomes unstable. In contrast, the computer-controlled approach does not have such a limit. In principle, it could remain stable until the modulation frequency has reached the bandwidth limitation of the RF amplifier. Given that the bandwidth limitation of the amplifier is 10GHz and that the

fluctuations affecting the laser are in a 100kHz band, it would take an extremely long time for the computer-controlled method to become unstable.

In addition to this practically limitless stability, the computer-controlled approach is simple to integrate and less expensive, given that it requires no extra components such as a *PI* controller, a piezo-fiber-stretcher or a high voltage controller.

6.4. Signal-to-Noise Ratio

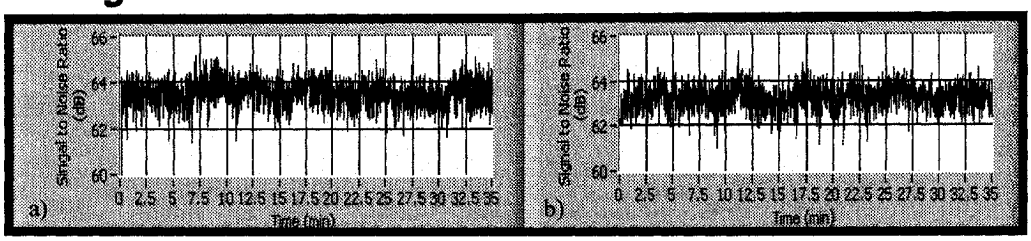

Figure 6.2: (a) Signal-to-noise ratio over time for the computer-controlled method; (b) Signal-to-noise ratio over time for the circuit-controlled method.

The side mode suppression ratio was measured for both approaches and was found to be roughly the same in both cases, with a value around 62dB (see Figure 6.2). Suppression of the side modes depends more on the characteristics of the fiber laser itself and not on the stabilization approach chosen. This criterion thus is not a determining factor as to which of the two approaches is more efficient.

6.5. Time Response

In regard to the time response, each approach was analyzed independently. The computer-controlled approach stabilizes the fiber laser using a LabView™ program that operates in a loop, evaluating the modulation frequency and making appropriate changes to follow the fluctuations. The time required to execute all tasks for a single loop is considered to be the time response for the computer-controlled approach; using the clock option of the LabView™ program's loop evaluation mechanism, it was approximated to be

1.2s. In contrast, the circuit-controlled approach operates independently of the computer, using instead a loop that is driven by amplifiers and a piezo fiber stretcher. Since the responses of the amplifiers are measured in microseconds, the time response is limited only by the millisecond response of the piezo fiber stretcher. The time response for the circuit-controlled approach was measured to be approximately 1ms when the circuit was operating in permanent regime.

Since the time response of the circuit-controlled approach is roughly three orders of magnitude faster than that of the computer-controlled approach, the former approach is clearly better for stabilizing the fiber laser. One caveat should be made regarding this comparison, however: it would be possible to significantly reduce the time response of the computer-controlled approach by controlling the fiber laser with a higher-performance micro-controller that could have a time response comparable to the circuit-controlled method, meaning that the computer-controlled approach could theoretically be made as fast as the circuit-controlled approach.

6.6. DC Level from the Mixer

The DC signal from the mixer was also measured in order to confirm the previous result regarding the time response of each method. Given that the computer-controlled method has a slower response time, the DC signal can change slightly even before a new modulation frequency is applied – never actually allowing the DC signal to remain at exactly the desired value, but rather to oscillate around it. Experiment showed that this was in fact the case. The standard deviation of the DC signal for the computer-controlled approach was measured to be 1.6 times the value measured for the circuit-controlled

approach (see Figure 6.3). This indicates that, in the absence of a dedicated micro-controller, the computer-controlled approach fluctuates more due to its slow response time.

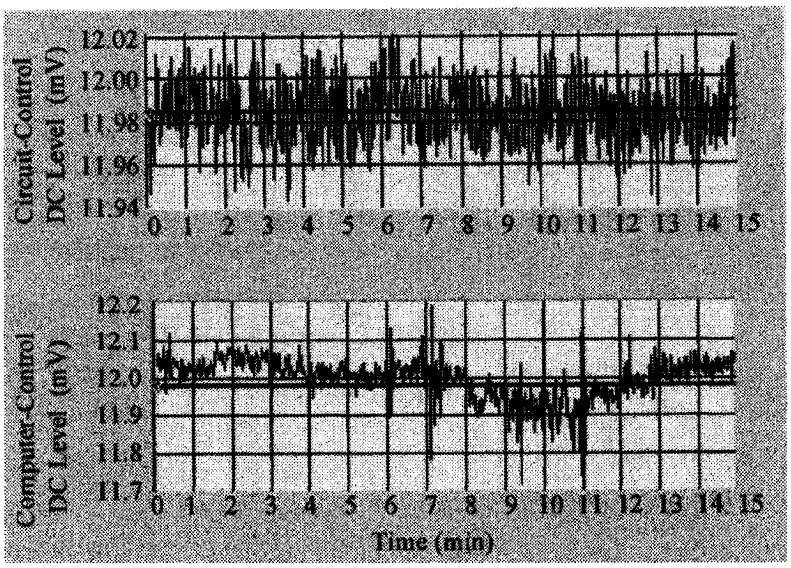

Figure 6.3: DC level vs. time for the computer-controlled approach and the circuit-controlled approach.

6.7. Timing Jitter

In order to measure the time jitter, a method based on Von Der Linde [18] and Yoshida [19] was employed. This method uses the RF spectrum to measure the integral of the SSB (single-sideband) phase noise of the fundamental frequency or harmonics for an approximation of the time jitter. There are usually three main factors that contribute to the phase noise: the variation of the pulse amplitude, the timing of the pulse, and the noise of the electronics, which are primarily due to the synthesizer. Figure 6.4 shows the relation between the three noises at different harmonics of the modulation frequency, which is represented by a delta function. The AM fluctuations are not affected by an increase in frequency and have the same form over all harmonics. The time jitter has no contribution to the DC level and becomes bigger as the number of harmonics increases. The electronic

noise from the synthesizer is basically a kind of jitter and can be included in the time jitter contribution.

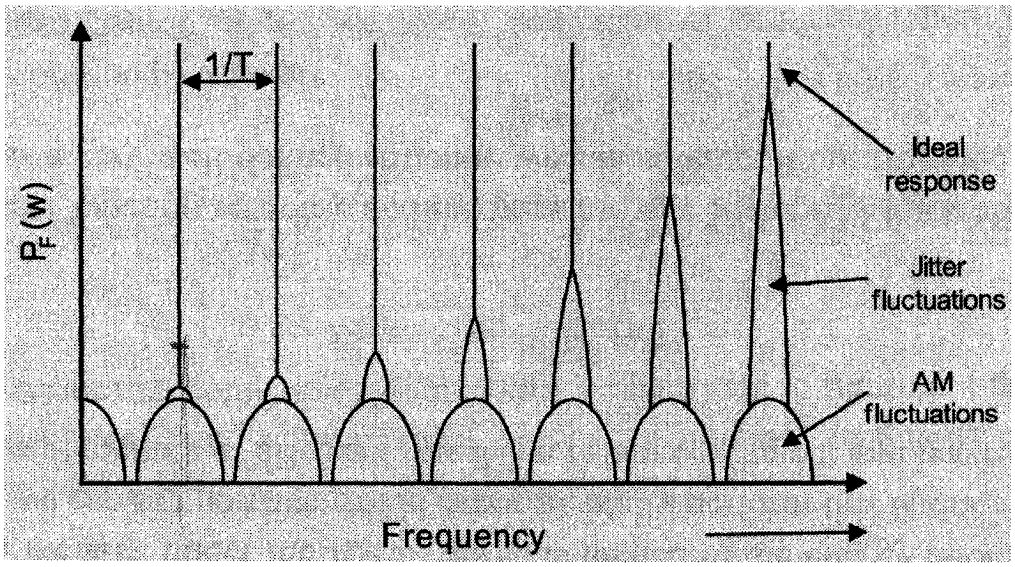

Figure 6.4: Behavior of the higher harmonics of the pulse train power spectrum [36].

In order to get only the contribution of the time jitter, the combined time jitter and synthesizer jitter must be isolated from the amplitude noise spectrum. The AM noise can be found by measuring the integral of the SSB phase noise at the spectrum origin since the amplitude noise is the only contribution at the DC level. In order to eliminate the AM noise, it must be subtracted from the SSB noise from a higher harmonic. Given that the time jitter is larger at higher harmonics, the best results are thus obtained by using the highest harmonic possible. Once the contribution of the AM noise is removed, the synthesizer jitter must be found. By injecting the signal from the synthesizer directly into the RF analyzer, the phase noise of the synthesizer can be evaluated. Assuming that the time jitter from the laser and the jitter from the synthesizer are uncorrelated, the former can be isolated.

In the case of the fiber laser, the only harmonic that can be seen on the RF spectrum is at 40GHz, since 80GHz is too high a frequency to be detected by the photodetector.

Therefore, the 40GHz phase noise is used to find the time jitter for both methods of stabilization. Although not entirely accurate, the time jitter found by using this first harmonic can still be a good approximation for the purpose of comparing the two stabilization methods.

A major problem related to the computer-controlled method occurs when trying to obtain the phase noise of the RF spectrum. The resolution bandwidth of the RF spectrum cannot be chosen to be too small over a large span since it takes too long for the RF spectrum analyzer to process the graph. As previously explained, the computer-controlled method uses the RF spectrum in order to stabilize the laser. While the program is running, there is no way to get the RF spectrum using another program or computer since the RF spectrum analyzer is already under command. Therefore, the RF spectrum must be taken as part of the program loop, complicating the analysis.

Since the jitter from the computer-controlled method is around 1Hz, the resolution bandwidth of the RF spectrum has to be very small in order to see the contribution of the jitter from the computer in the phase noise. With the RF spectrum inside the program, a decrease in the resolution bandwidth without a corresponding decrease in the span will cause the RF spectrum to be too slow – at least 30 seconds – and, as a consequence, destabilize the laser. Furthermore, too large a decrease in the span will lead the RF spectrum to lose the modulation frequency peak and therefore block the program from calculating the time jitter.

In addition, as part of the program's routine, the RF spectrum cannot be taken while the modulation frequency is actually changing in real time since two commands cannot be executed at the same time. As a consequence, it leads to a decrease in the accuracy of the method. This is a limit of the laboratory equipment; with two independent RF spectrum

analyzers and two computers this problem could be overcome. These problems don't exist with the circuit-controlled method since the computer doesn't affect the stabilization process once it is running and hence the RF spectrum can be taken at any time without affecting the *PI* controller.

To compare the two methods, these problems needed to be resolved. One solution was to obtain the RF spectrum for the computer-controlled method as soon as possible after the modulation frequency is adjusted by modifying the command in the LabView™ program. Another solution was to separate the phase noise from 0-1MHz in different ranges and with different resolution bandwidths and then to fit each section of the curve, including the peak jitter and relaxation oscillation frequency, for higher accuracy. The resolution bandwidth and the span were optimized such that they would not affect the computer-controlled program but still gave a good approximation of the phase noise plateau.

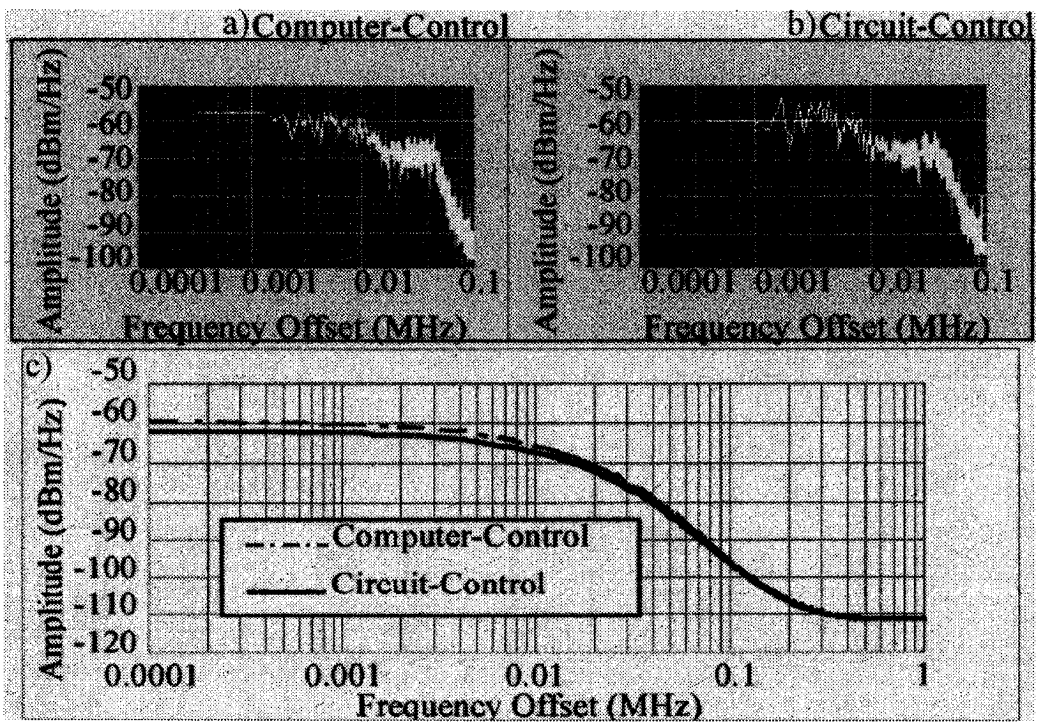

Figure 6.5: Real data and fit curve of the SSB noise of the RF spectrum vs. the frequency offset of the fundamental frequency (40 GHz) using the computer-controlled and circuit-controlled approaches for calculating the timing jitter.

Figure 6.5 (a) and (b) show the SSB phase noise of the fundamental frequency for both the computer-controlled and the circuit-controlled approaches, respectively. Both phase noises appear to have a peak noise at around 34kHz, exactly at the relaxation oscillation frequency of the laser. This peak noise is indeed very weak since the optical filter and the DSF fiber providing self-phase modulation help to eliminate this relaxation frequency. A further peak near 1kHz can be seen on the phase noise of the circuit-controlled method and not on the computer-controlled method. This peak represents the jitter due to the frequency response of the piezo fiber stretcher. As mentioned, the low-frequency peak jitter for the computer-controlled method cannot be seen in Figure 6.5(a) because the RF spectrum analyzer takes too long to process the program loop when the resolution bandwidth gets too small.

Figure 6.5(c) shows the fit curve for the phase noise floor of both methods. The RF spectrum span and the resolution bandwidth were set high enough to have a wide area of phase noise integration and to not destabilize the laser, respectively. The area under the fit curve for the circuit-controlled approach appears to be smaller. Overall, the time jitter for the circuit-controlled approach was found to be 120fs, while for the computer-controlled approach it was 197fs. Since the time response of the computer-controlled approach is longer, the frequency fluctuations are likely to be higher. In fact, the DC signal fluctuations allow the modulation frequency to never be locked at one self-beat signal but to oscillate around it. Another factor that could increase the time jitter is the small frequency fluctuations that are introduced to the modulator when there is a change in the modulation frequency. All these fluctuations increase the low frequency phase noise under the RF spectrum, as seen in Figure 6.5, which increases the time jitter, and hence diminishes the performance of the laser. Since the circuit-controlled approach has a faster time response

and a fixed modulation frequency, its induced noise is smaller, which in turn reduces the timing jitter.

6.8. The Time-Bandwidth Product

The optical spectrum bandwidth, the pulse width, and the intensity of the pulse were also considered in comparing the two approaches. The results using these three parameters did not clearly indicate on average that one method was better than the other. As with the side mode suppression, these parameters depend less on the method of stabilization than on the characteristics of the fiber laser itself. The optical spectrum bandwidth was found to be approximately 1.4nm for both methods. Using a hyperbolic-secant fit, the pulse width was approximated at 2.2ps.

The bandwidth-pulsewidth parameter $\Delta v \Delta \tau$ is defined as the product of the optical spectrum bandwidth with the pulse width. Its value depends on the shape and the amount of chirp in the pulse. It is a useful parameter since it characterizes the pulse and the performance of the fiber laser at the same time. The parameter has a lower limit which corresponds to an ideal value; that is, an unchirped pulse. For example, a Gaussian-shaped pulse is expected to have an ideal value at 0.44 while for the hyperbolic-secant shape the value is 0.315. Since the fiber laser is built in order to create a soliton, the value of $\Delta v \Delta \tau$ was expected to be 0.315; the experimental value was found to be 0.38, which is close to a transform-limited pulse as seen in Figure 6.6. A Gaussian fit was attempted but was not found to give as close a fit of the data as the hyperbolic-secant.

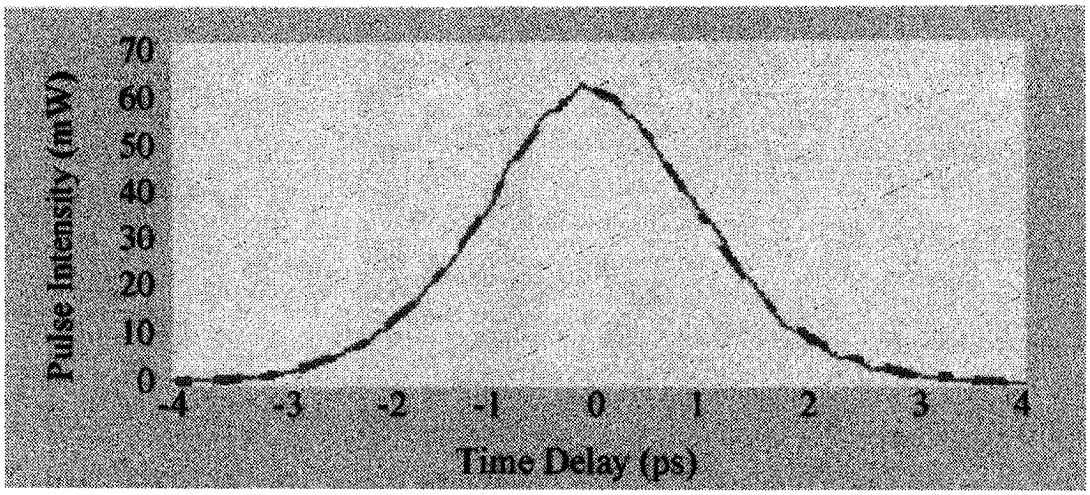

Figure 6.6: Output pulse shape of the fiber laser (solid line) fit using a hyperbolic secant shape (dashed line).

The peak-to-peak amplitude of the pulse was also compared for both approaches. On average the results are similar, but the dynamic results of the pulse amplitude are slightly more stable using the circuit-controlled approach (see Figure 6.7). The standard deviation for the computer-controlled approach was measured to be approximately 1.05 times the size of that for the circuit-controlled approach. The standard deviation of the pulse width and the optical spectrum bandwidth also showed that the circuit-controlled approach was slightly more stable. Due to the slower response time of the computer-controlled approach, all three of these parameters are more susceptible to change and hence produce poorer dynamic results than for the circuit-controlled approach.

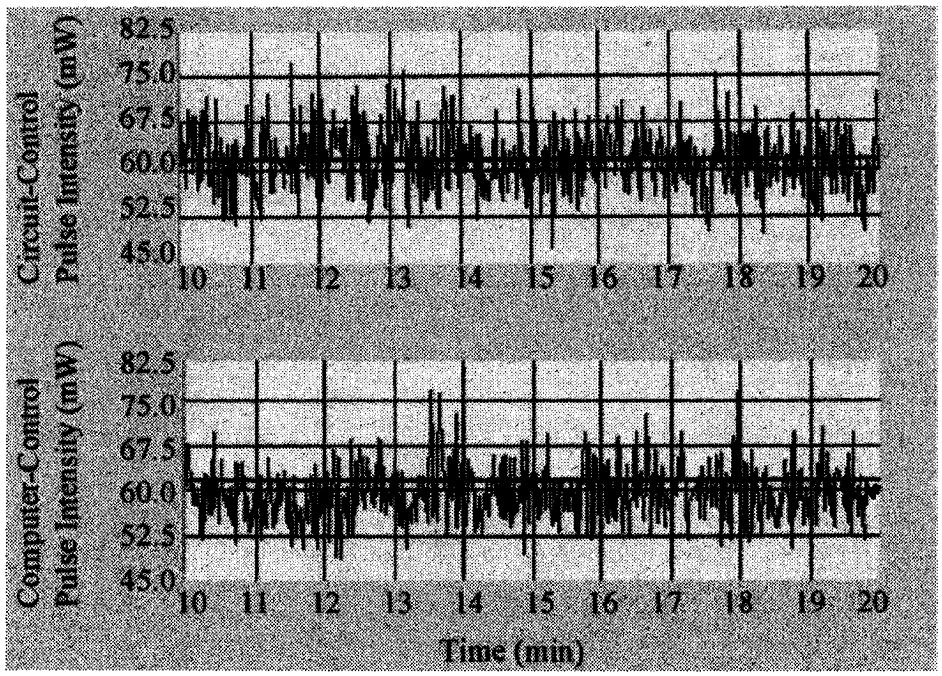

Figure 6.7: Pulse intensity over time for the computer-controlled approach and the circuit-controlled approach.

6.9. Conclusion

From the comparison of various parameters, both approaches possess strengths and weakness but are effective in stabilizing the fiber laser. Despite the variations in its repetition rate and the slow frequency response, the computer-controlled method is simple, gives an unlimited period of stabilization and has a low cost of fabrication. The circuit-controlled method, in contrast, possesses a high speed of execution and a fixed repetition rate but a shorter period of stabilization.

Although both the computer-controlled method and the circuit-controlled method were optimized to operate the fiber laser at 40GHz, the frequency range of stability was increased to see if the methods could stabilize the laser at other modulation frequencies. The final chapter provides an overview and some preliminary results of experiments at other modulation frequencies.

7. Generalization of the Methods of Stabilization at Different Repetition Rates

7.1. Introduction

The computer-controlled method and the circuit-controlled method were both optimized and found to be effective at stabilizing the fiber laser at 40GHz. In addition, their flexible design allowed them to be versatile enough to be generalized, with minor changes, so that they could also work at lower modulation frequencies. This chapter presents some results of stabilization using both methods for the active harmonic mode-locked fiber laser at 10GHz, 5GHz and 2.5GHz.

7.2. Experimental Considerations before Generalization

The LabView^{TM} program had to be modified in order that both the computer- and circuit-controlled methods could be generalized to work at the new modulation frequencies. These minor changes involved seeing if the stabilization parameters at 40GHz would exhibit the same behaviour at other modulation frequencies. The choice of possible modulation frequencies was also limited by the original choice of the fiber laser's components, optimized for operation at 40GHz. The photodetector, the synthesizer, the amplifiers and the dispersion-shifted fiber all caused some problems in the process of frequency generalization.

7.2.1. Photodetector – Synthesizer

The highest possible frequency that the synthesizer can generate is 40GHz and the bandwidth limitation of the photodetector is 40GHz. These two constraints thus give an upper limit to the range of modulation frequencies that can be applied to the fiber laser; the modulation frequencies must be lower than 40GHz.

7.2.2. Amplifiers

Since the amplifiers were originally chosen for operation at 40GHz, their operation at lower frequencies had to be ensured. The bandwidths of these amplifiers are limited to between 30GHz and 40GHz however, which was too restrictive for the frequency generalization. The amplifiers were thus replaced by new amplifiers that could operate at 10GHz with a bandwidth of 8GHz. These amplifiers could also operate at the three standard modulation frequencies, 10GHz, 5GHz and 2.5GHz, so these three frequencies were chosen for use in the generalization process.

7.2.3. Stability Parameters and Dispersion Shifted Fiber

Once the amplifiers were replaced, the stability parameters, including the maximum pulse intensity, the maximum RF spectrum peak intensity and the DC level from the mixer, were verified to ensure they behaved the same way at the three lower frequencies as at 40GHz. The pump laser was turned on and the synthesizer was set at one inter-mode frequency spacing near 10GHz. Next, the modulation frequency was adjusted in a window of 200kHz near the resonance frequency and the curves of the three stability parameters were taken.

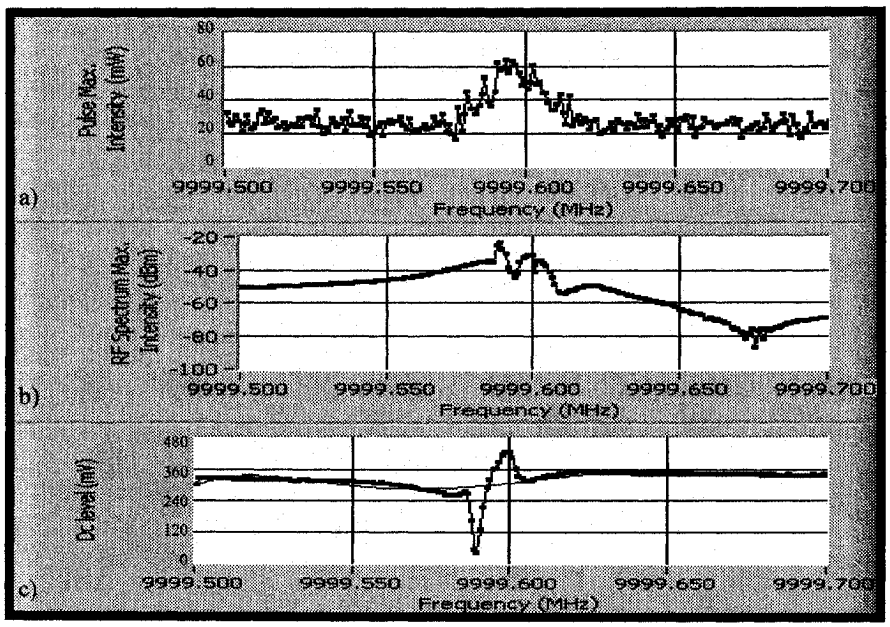

Figure 7.1: Three stability parameters at a resonance frequency near 10GHz, (a) the pulse, (b) the RF spectrum and (c) the DC level.

Figures 7.1(a), (b) and (c) show the optimal curves for the three stability parameters found by using the phase delay that gave the best possible DC level linear fit. Unfortunately, it appeared from Figure 7.1(a) and (b) that neither the RF maximum intensity nor the pulse maximum intensity was stable near resonance. Moreover, the DC curve in Figure 7.1(c) did not appear to be linear over a reasonable range. It was immediately suspected that noise inside the cavity caused these aberrations. In fact, the amplitude of the noise peaks in mode-locked regime of the RF spectrum increased significantly compared with the 40GHz set-up, as shown in Figures 7.2(a) and (b). From these figures, the first-order beating mode at 10GHz also appeared to be lower than at 40GHz, leading to a very poor signal-to-noise ratio.

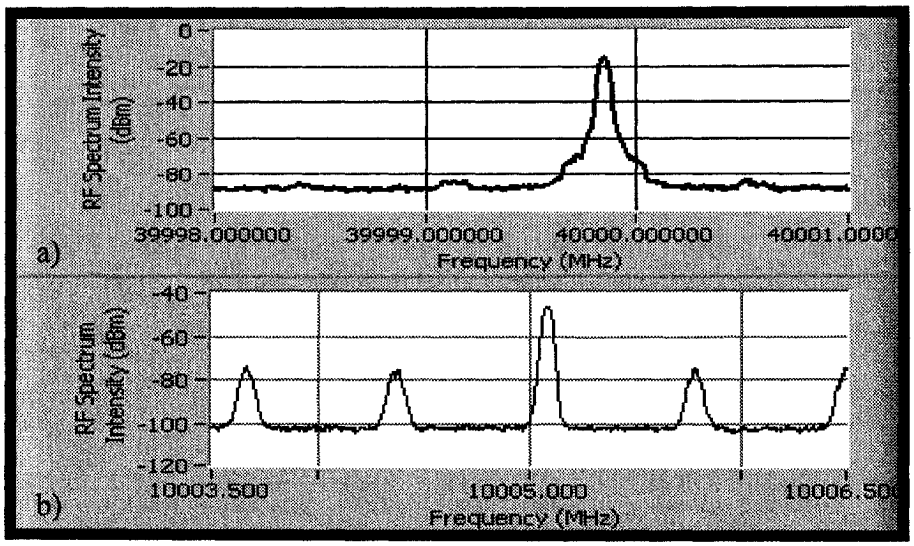

Figure 7.2: Mode-locked fiber laser with DSF on the RF spectrum at (a) 40GHz; (b) 10GHz;

In order to find the element(s) that had increased the noise, two hypotheses were proposed. The first hypothesis was related to the numerical optical filter, since the parameters of the filter were perhaps not optimized for 10GHz. Adjustment of the bandwidth and the central wavelength of the filter did not reduce the noise.

The second hypothesis was that these fluctuations were related to the dispersion inside the cavity. A soliton should provide the lowest induced noise possible, but from Figure 7.2 (b), it appeared that the pulse no longer had the properties of a soliton. To test the hypothesis, the dispersion inside the cavity at 10GHz was characterized.

Since the SPM effect is intensity-dependent, the peak power of the pulse strongly affects the total dispersion inside the cavity. A specific peak power is then required in order to compensate the GVD and SPM effects and support the fundamental soliton. The relation between the peak power and the dispersion is given by,

$$P_{peak} = \frac{3.11|\beta_2|}{\gamma T_{FWHM}^2} \quad \text{or} \quad |\beta_2| = \frac{P_{peak} T_{FWHM}^2 \gamma}{3.11} \tag{7.1}$$

where γ is the nonlinear parameter responsible for the SPM effect and is given in W^{-1}/km; T_{FWHM} is the pulse width given in picoseconds, and $|\beta_2|$ is the GVD parameter, given in ps^2/km.

The pulse width T_{FWHM} was evaluated at 7.7ps when the laser was mode-locked at 10GHz. The SPM effect occurs in both dispersion shifted fiber and in PM fiber; the value of γ for these two components is $3W^{-1}$/km and $2W^{-1}$/km, respectively. Since the fiber laser was a mix of both types of fiber, the approximate value chosen for use in the experiment was $2.5W^{-1}$/km.

The peak power P_{peak} can be deduced directly from the average power distributed inside the cavity when the pump power is turned on. The equation is given as follows:

$$P_{peak} T_{FWHM} = P_{average} T_R \tag{7.2}$$

where T_R represents the time spacing between adjacent pulses. From Equation 7.2 it is clear that the dispersion depends on the modulation frequency via the repetition rate, which means that the second hypothesis for the noise generation was likely correct.

The average power $P_{average}$ at the output of the 90/10 coupler was found to be 5.3mW with 1000mA injected into the pump and a repetition rate of 100ps. The peak power P_{peak} was then calculated to be 68.8mW. Since the dispersion is produced only inside the cavity, and only the 10% portion of the signal coming from the output of the coupler was measured, the final value of P_{peak} was 688mW. From Equation 7.1, the dispersion parameter $|\beta_2|$ was then evaluated to be $\pm 32.79 ps^2$/km, or ± 0.03279 ps^2/m.

The main components from the cavity that contribute to the dispersion parameter β_2 are the Erbium-doped fiber (EDF) ($0.020394 ps^2$/m), the dispersion-shifted fiber (DSF) ($-0.00306 ps^2$/m), and the pigtails of other remaining components such as the optical filter, the

phase modulator, the isolator, and the piezo fiber stretcher, which are all made of PM fiber (-0.001958ps^2/m). The negative dispersion values mean that the SPM effect is present in that specific section of fiber. The fiber length for each section is 6.2m for the EDF, 277m for the DSF, and around 25m for all the other remaining pigtails. Summing the contribution of each section of fiber gives the dispersion from the components B_{tc} inside the cavity.

$$B_{tc} = 6.2\text{m} \times 0.020394\text{ps}^2/\text{m} - 277\text{m} \times 0.00306\text{ps}^2/\text{m} - 25\text{m} \times 0.001958\text{ps}^2/\text{m} \quad (7.3)$$

The dispersion from the components B_{tc} was thus calculated to be -0.770 ps^2. The total length of the cavity is approximately 308.2m, so the value of $|\beta_2|$ in ps^2/m can then be converted to units of ps^2 in order to give the dispersion B_{ts} required for the fiber laser to create a soliton pulse.

$$B_{ts} = \pm 308.2\text{m} \times 0.03279\text{ps}^2/\text{m} \quad (7.4)$$

The above result for β_2 of $\pm$0.03279 ps^2/m then becomes $B_{ts} = \pm 10.1$ ps^2.

As hypothesized, the pulse was not a soliton. The large difference between B_{tc} and B_{ts} confirmed the problem of the noise seen on the RF spectrum. An element of Equation 7.1 therefore had to be changed to re-establish the soliton. Two parameters were considered: the peak power P_{peak}, and the dispersive components in the cavity. There was no way to change P_{peak} in a way that would allow the cancellation of the SPM and the GDV effects because the pump current could not be increased beyond the pump limiting value of 1000mA. As a result, the dispersion of the cavity itself had to be changed.

The only component that could be changed without affecting the performance of the fibre laser was the DSF. Using Equations 7.1 to 7.4 above from the first calculation of the total dispersion, the DSF length (x, in metres) required to ensure the formation of a soliton

was calculated. The values of P_{peak} and the pulse width are maintained, and the parameter $|\beta_2|$ from Equation 7.1 does not change. Equations 7.3 and 7.4 can be equated as follows:

$$-0.03279\text{ps}^2/\text{m}\times(6.2\text{m}+25\text{m}+\text{x})=6.2\text{m}\times(0.0561\,\text{ps}^2/\text{m})-25\text{m}\times(0.01958\text{ps}^2/\text{m})+\text{x}\times(0.00306\text{ps}^2/\text{m}) \quad (7.5)$$

$$1.0230\,\text{ps}^2+\text{x}\times0.03279\,\text{ps}^2=0.14168\,\text{ps}^2+\text{x}\times0.00306\,\text{ps}^2 \quad (7.6)$$

$$0.881\,\text{ps}^2=-\text{x}\times0.02973\text{ps}^2 \quad (7.7)$$

It is clear from the negative sign in Equation 7.7 that the SPM effect is much stronger than the GVD effect. This means that the DSF length chosen for the 40GHz mode-locked regime was too long for the cavity when a lower modulation frequency was used.

The DSF was taken out of the cavity and the same calculations were carried out once more. The current of the pump was also reduced from 1000mA to 800mA to accommodate the input power limitation of the numerical filter. In fact, removing 277m of DSF from the cavity increases the peak power since the cavity loss is reduced. The current was then adjusted to provide a P_{peak} of 1W. The pulse width had changed from 7.7ps to 12ps.

The dispersion B_{ts} required for the formation of a soliton was calculated and found to be 4.33389 ps^2 and the dispersion from the cavity B_{tc} was -0.14168 ps^2. The difference calculated to be 4.47557 ps^2 indicated that once again, the SPM effect was larger than the GVD effect. From Equation (3.7), the dispersion parameter D representing this difference was -3.47ps/nm. Given that no other components could be removed from the cavity to compensate the SPM effect, the final possibility was to artificially increase the GVD effect through a tuneable dispersion compensator.

The dispersion compensator is a circulator followed by a fiber Bragg grating. The circulator sends an input signal to the fiber Bragg grating, which reflects the wavelengths of

the input signal at different positions in the grating depending on the wavelength. It thus induces a chirp in the signal by giving different time delays to each wavelength. As a result, the short wavelengths encounter higher time delays than the longer wavelengths, creating the same effect as with GVD.

The tunable dispersion compensator that was available for this experiment could be tuned from -300 to -700ps/nm; it could not be used to compensate for only -3.47ps/nm. Therefore, it was decided to use no DSF in the laser cavity and to try the methods of stabilization at lower frequencies anyway. The fiber laser was then mode-locked again at 10GHz without DSF in the cavity in the hope that the noise from the RF spectrum would be comparable to the noise found at the original 40GHz modulation frequency.

The three stability parameters – the pulse intensity, the RF spectrum and the DC level – were measured again with the new cavity length. The best DC linear curve, the maximum RF spectrum and the pulse intensity are shown in Figures 7.3 (a), (b) and (c), respectively, for a phase delay of 80ps.

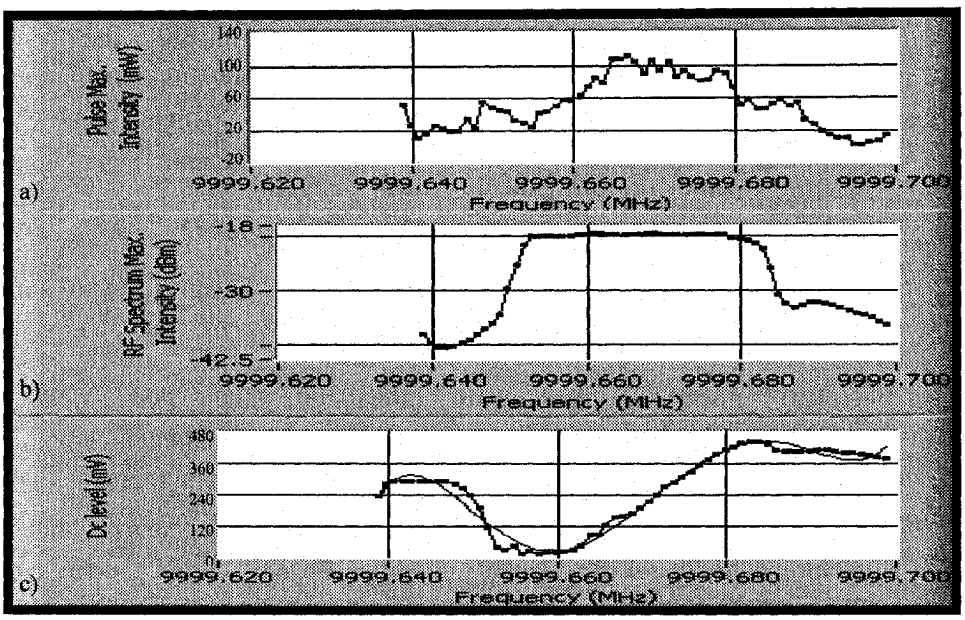

Figure 7.3: The three stability parameters at a resonance frequency near 10GHz with no DSF, (a) the pulse, (b) the RF spectrum and (c) the DC level.

All three stability parameters were stable, which indicates that generalization of the stabilization of the fiber laser to lower frequencies should indeed be possible.

7.2.4. Modifications to the LabView™ Program

Three minor changes had to be made to the LabView™ computer program, all related to the RF spectrum analyser. The first change was that the central wavelength on the RF spectrum needed to be tuneable to the three new modulation frequencies. The two other changes to the LabView™ program were the span and the resolution bandwidth of the RF spectrum, which were originally at 3MHz and 30kHz respectively. The removal of the DSF from the cavity resulted in a change of the optical cavity length as well as a change in the inter-mode frequency spacing. The inter-mode frequency spacing increased from 0.75MHz to 4.31MHz, as shown in Figure 7.3. With a span of 3MHz and an inter-mode frequency spacing of 4.31MHz, the program often could not get a single peak. The span was thus

changed to 10MHz so that at least two peaks would fit in the range, and the resolution bandwidth was consequently adjusted to a value of 50kHz, as mentioned in section 6.7.

7.3. Results

The fiber laser was stabilized using both the computer-controlled method and the circuit controlled method at 10GHz, 5GHz, and 2.5GHz. The computer-controlled method was already optimized, and the LabView™ program was basically the same as for the 40GHz setup except for the three modifications explained in section 7.2.4; no optimisation was required for this method.

For the circuit-controlled method however, the change in the modulation frequency and the change in the cavity length had to be considered for the selection of the gains in the *PI* controller. Without DSF, the total cavity length was shorter, which reduced the impact of temperature fluctuations on the fiber laser. Since the rate of change of the inter-mode frequency spacing had decreased, the P and the I needed to be readjusted and optimized for each of the three different frequencies.

7.3.1. Computer-Controlled Method

The experiments with the computer-controlled method turned out to be inaccurate for several reasons. The principal problem was related to the DC reference curve, since it was almost impossible to get a linear curve once the program was running. Figure 7.4 was a rare exception where the DC curve was found to be roughly linear.

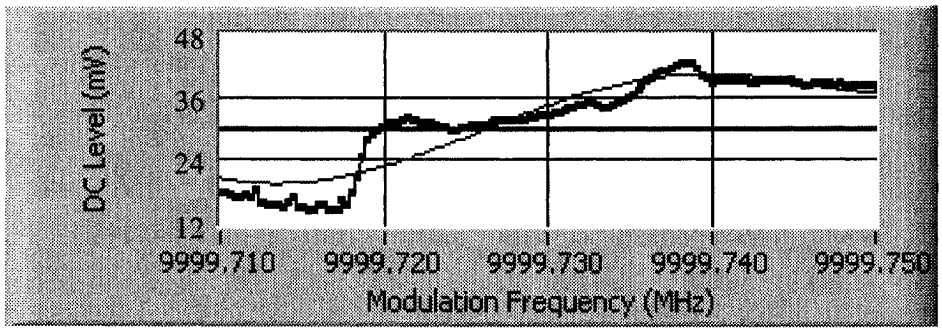

Figure 7.4: Typical curve of the DC level found at lower frequencies.

Figure 7.4 shows a typical example of a DC curve at the lower modulation frequencies. One problem was that the resolution bandwidth (RB) of the RF spectrum increased and resulted in a decrease of the RF spectrum resolution. Therefore, the LabView™ program did not appear to set the modulation frequency at the resonance frequency.

Another problem was the numerical filter, which induces noise inside the cavity since it is made of single-mode fiber. Noise peaks could be seen on the RF spectrum while the program was building the DC level curve. As a result, the curve exhibited non-linear behaviour.

Another, more subtle, problem was related to the phase shifter. Although the phase delay is limited to 0-125ps, for a modulation frequency of 10GHz, there is no problem since the phase can be delayed from 0-100ps. The problem arises when the modulation frequency is changed to 5GHz or 2.5GHz since their periods of phase delay, 200ps and 400ps respectively, are well outside the range of the phase shifter. The phase shifter cannot delay the phase of these two modulation frequencies over their whole period. This means that if the phase required to get the linear curve is found to be out of the range of the phase shifter, the computer-controlled method will not be able to stabilize the fiber laser. One

solution was to change the length of the electrical connections to try and get the phase delay required in the range of 0-125ps for the three modulation frequencies. This was a difficult task however, since the connectors have standard lengths that are not adjustable. Therefore, no optimized results were found.

A final problem was related to the mixer. Its input bandwidth was restricted between 5 and 45GHz, which implied that the desired 2.5GHz modulation frequency was out of its range. 2.5GHz was therefore not a good choice of modulation frequency for stabilizing the fiber laser and it was almost impossible for the computer-controlled method to stabilize the laser at that frequency.

Since the DC level curve is the most important parameter in the computer-controlled method, the non-linear curves found at the lower modulation frequencies could not stabilize the fiber laser over a long period of time. Nonetheless, some results of stabilization with the computer-controlled method for the three modulation frequencies – 10 GHz, 5GHz, and 2.5GHz – are shown in Figures 7.5, 7.6 and 7.7, respectively.

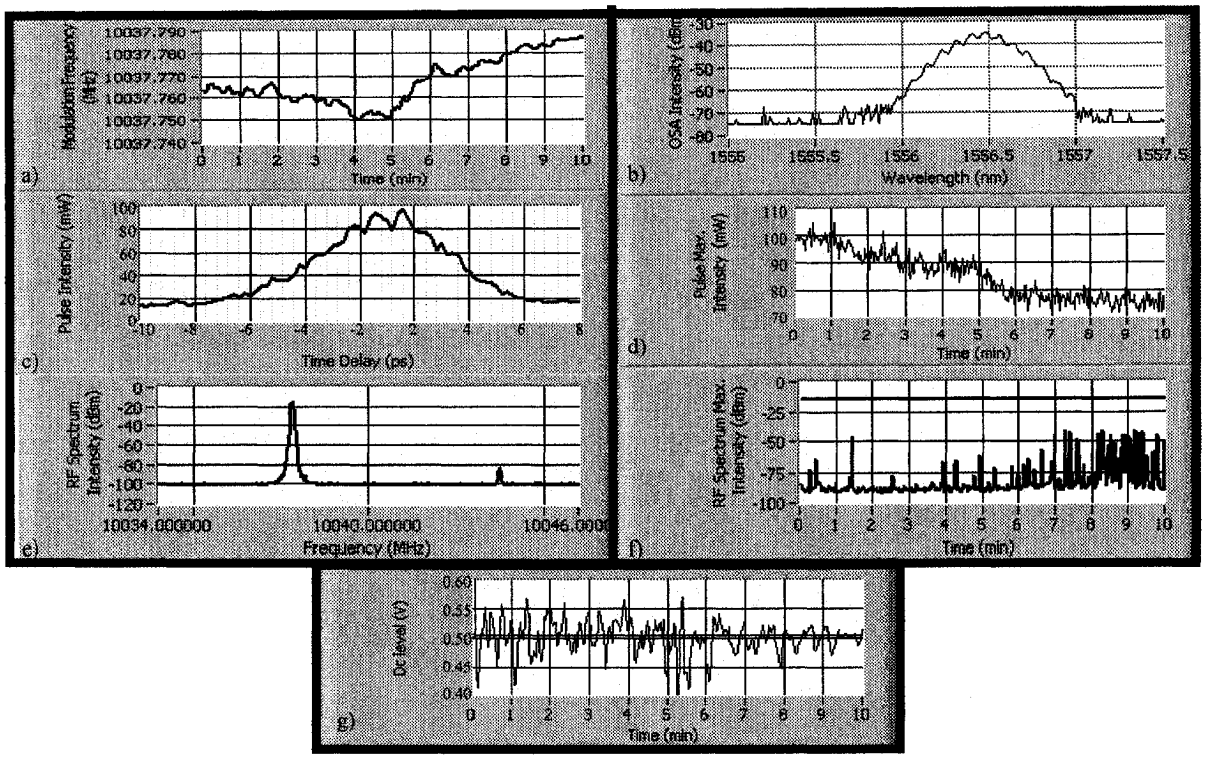

Figure 7.5: Results of a 10-minute experiment at 10GHz using the computer-controlled method for the (a) modulation frequency, (b) the optical spectrum, (c) and (d) the pulse characteristics, (e) and (f) the RF spectrum characteristics, and (g) the DC level.

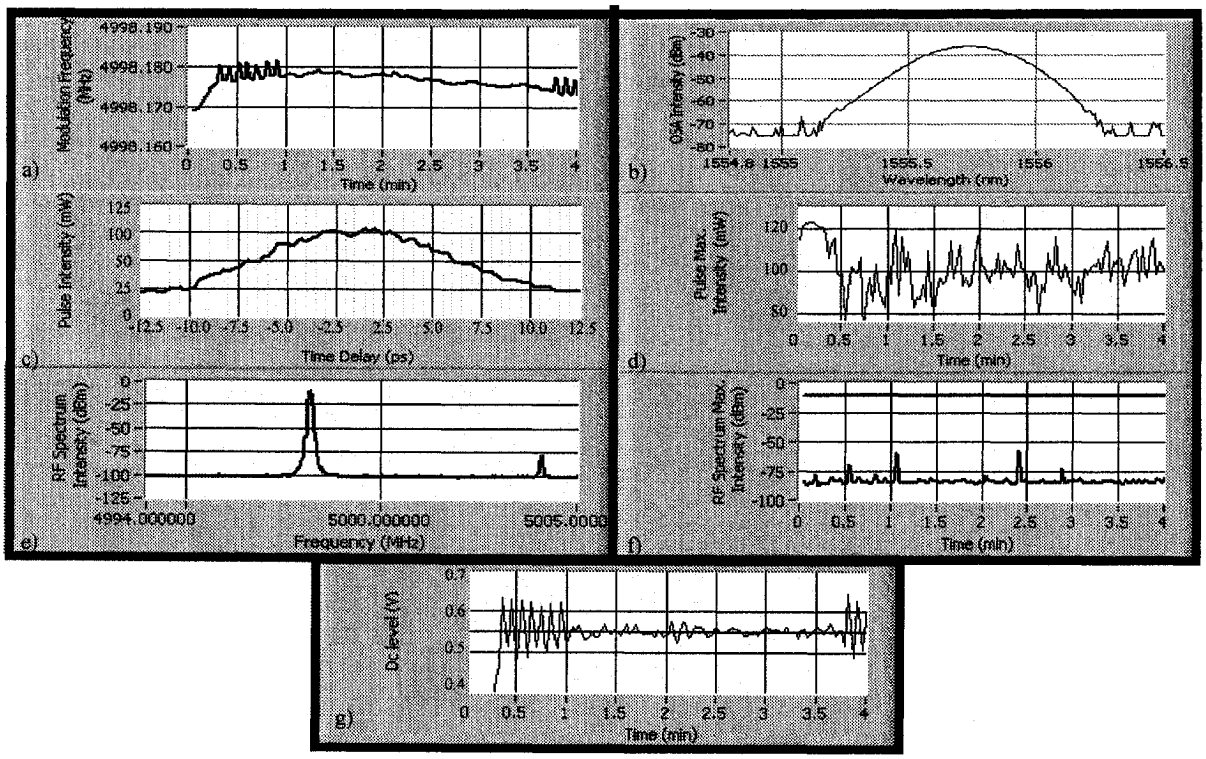

Figure 7.6: Results of a 4-minute experiment at 5GHz using the computer-controlled method for the (a) modulation frequency, (b) the optical spectrum, (c) and (d) the pulse characteristics, (e) and (f) the RF spectrum characteristics, and (g) the DC level.

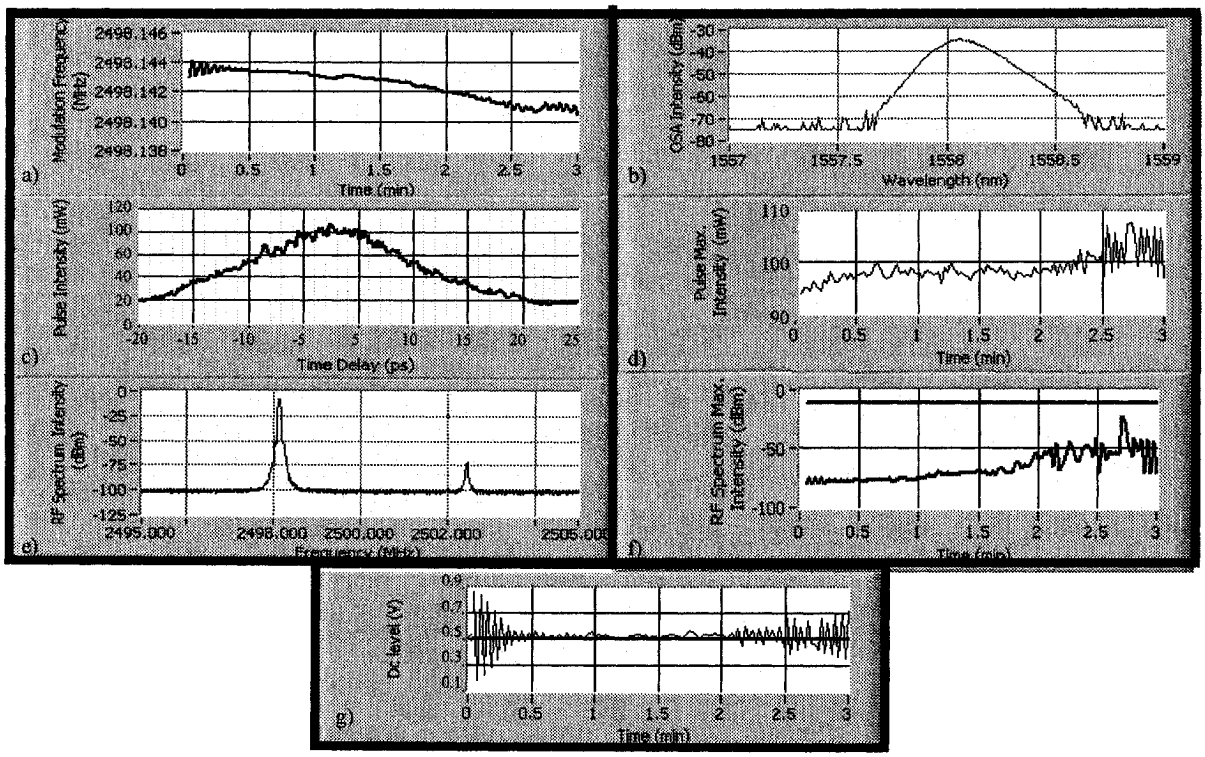

Figure 7.7: Results of a 3-minute experiment at 2.5GHz using the computer-controlled method for the (a) modulation frequency, (b) the optical spectrum, (c) and (d) the pulse characteristics, (e) and (f) the RF spectrum characteristics, and (g) the DC level.

From Figures 7.5(a), 7.6(a), and 7.7(a), it is possible to see that the fluctuations in temperature are less significant than they were at 40GHz. The signal-to-noise ratio was found to be 64dBm for all three new modulation frequencies, which is close to the 62dBm signal-to-noise ratio found with the 40GHz setup.

7.3.2. Circuit-Controlled Method

As with the computer-controlled method, the experiments with the circuit-controlled method turned out to be inaccurate. The reasons for this were similar to those for the computer-controlled method, since the *PI* controller requires a stable linear relationship between the DC level and the temperature fluctuation to be able to stabilize the fiber laser. Since the circuit-controlled method doesn't have to make decisions based on a pre-determined reference curve however, as is the case for the computer-controlled method, the circuit-controlled approach is more capable of adjusting to the fluctuations and stabilizing over more extended periods of time.

A problem encountered with the *PI* controller at the lower modulation frequencies was related to its speed of execution. The gains of the *PI* chosen for the circuit design at 40GHz were too high for the system at lower frequencies and hence, the fiber laser was never stable. The resistance of the *P* and the capacity of the *I* were manually exchanged for lower gains. For 10GHz, the reaction curve of the *PI* was captured to get a balance between the overshoot and the settling time.

Figure 7.8(a) shows a reaction curve that could not stabilize the laser for more than one minute. Since the gain of the *P* was very low, the *PI* controller in steady-state regime was unable to reach the setpoint of 3.1V. Figure 7.8(b) shows the optimum results of the *P* and *I* for 10GHz.

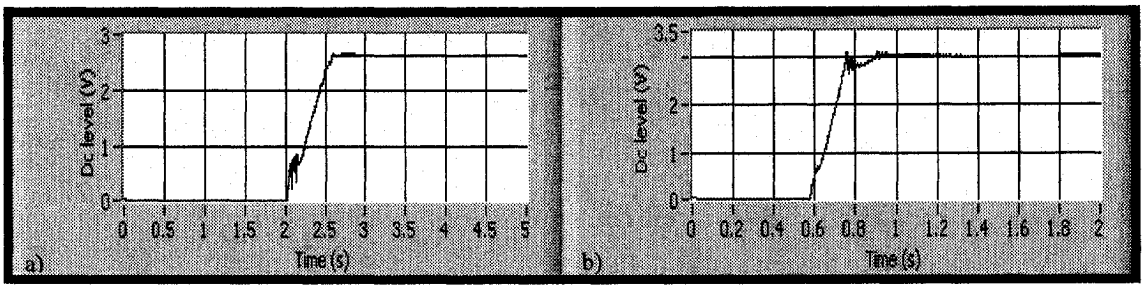

Figure 7.8: (a) Reaction curve for 10GHz with a resistance 400kΩ and a capacity of 5μF; (b) Reaction curve for 10GHz with a resistance 300kΩ and a capacity of 5μF.

Even with optimum values, it took the *PI* controller a relatively long period of time to stabilize the fiber laser at 10GHz due to the instabilities of the DC at the mixer. There were thus no practical reasons to continue to optimize the reaction curves for 5GHz and 2.5GHz. Figures 7.10, 7.11, and 7.12 show some basic results of stability for the fiber laser with modulation frequencies of 10GHz, 5GHz, and 2.5GHz.

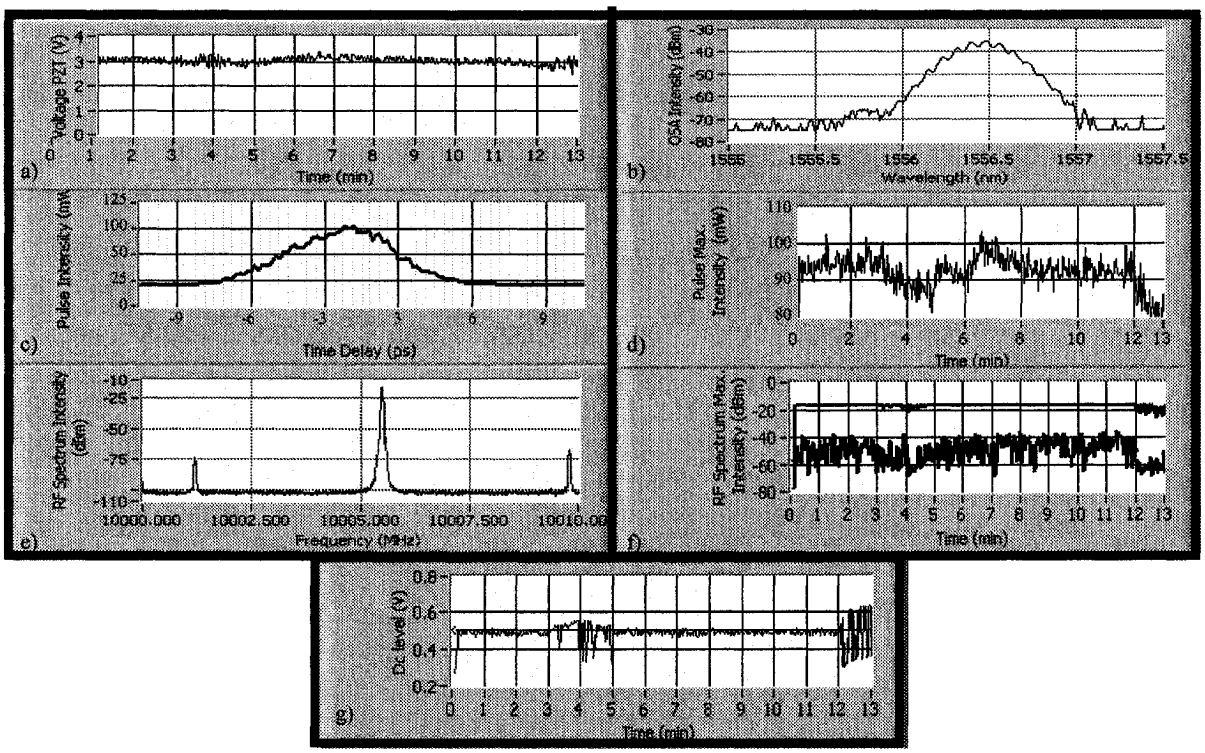

Figure 7.9: Results of a 13-minute experiment at 10GHz using the circuit-controlled method for the (a) voltage at PZT, (b) the optical spectrum, (c) and (d) the pulse characteristics, (e) and (f) the RF spectrum characteristics, and (g) the DC level.

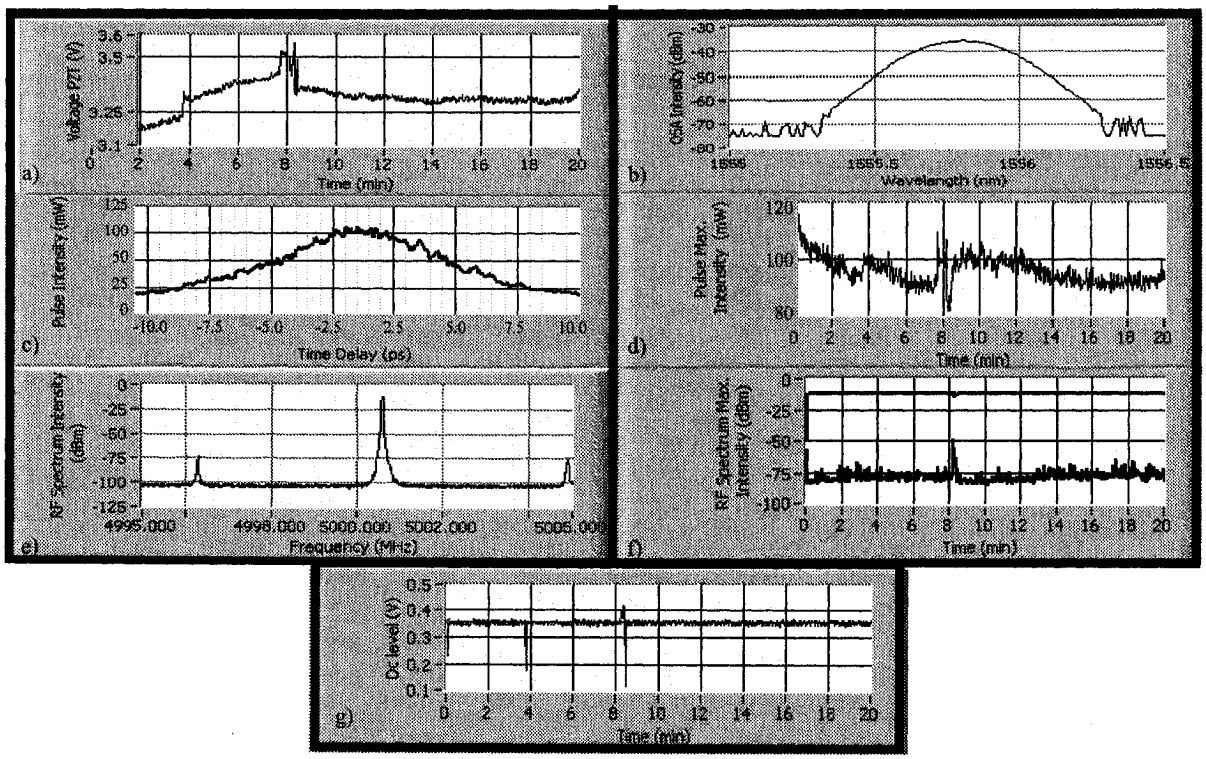

Figure 7.10: Results of a 20-minute experiment at 5GHz using the circuit-controlled method for the (a) voltage at PZT, (b) the optical spectrum, (c) and (d) the pulse characteristics, (e) and (f) the RF spectrum characteristics, and (g) the DC level.

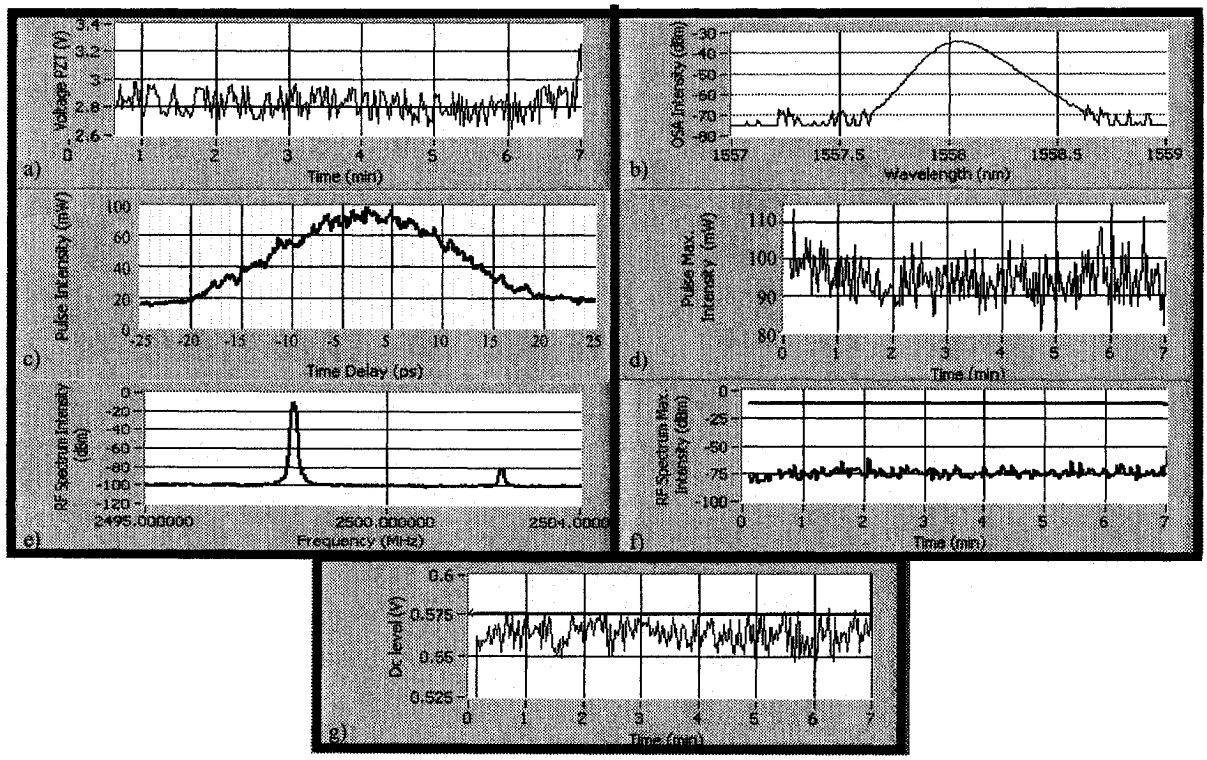

Figure 7.11: Results of a 7-minute experiment at 2.5GHz using the circuit-controlled method for the (a) voltage at PZT, (b) the optical spectrum, (c) and (d) the pulse characteristics, (e) and (f) the RF spectrum characteristics, and (g) the DC level.

As with the computer-controlled method, the variations in temperature do not cause as much fluctuation in the laser with the circuit-controlled approach at the lower modulation frequencies as much as with the 40GHz setup (see Figures 7.9 (a), 7.10(a) and 7.11(a)). Similarly, the signal-to-noise ratio was found to be the same as for the computer-controlled method. Finally, the period of stabilization of the laser using the circuit-controlled method was found to be better than for the computer-controlled method for all three of the lower modulation frequencies because of the dynamic reference curve of the circuit-controlled method.

7.4. Conclusion

The computer-controlled method and the circuit-controlled method for stabilizing the laser were generalized to three different modulation frequencies, 10GHz, 5GHz, and

2.5GHz. Although the results were found to be inaccurate, largely because of a cavity still designed for 40GHz operation, they imply that both stabilization methods could be generalized to other modulation frequencies for small periods of stabilization. Two important conclusions were drawn from the generalization process as well. First, the period of stabilization could be increased by either a re-adjustment of the dispersion inside the cavity or a change the fiber laser components. Second, the computer-controlled method was more versatile than the circuit-controlled method since the electrical circuit required a re-adjustment of its parameters at each new modulation frequency in order to stabilize the fiber laser.

8. Conclusion

Two methods were developed to stabilize a harmonic FM mode-locking fiber laser at 40GHz. A new approach (Ponomarev [14]) makes use of a LabView™ program to adjust the modulation frequency to follow temperature fluctuations and stabilize the laser. A second approach uses a *PI* controller and a piezo fiber stretcher to change the optical cavity length and stabilize the laser by maintaining the same operating mode. A hybrid approach, using the LabView™ program to control the piezo fiber stretcher, was also developed for experimental purposes. Comparison of the results for the two methods indicate that both the computer-controlled and the circuit-controlled methods are effective; the computer-controlled approach gives an unlimited time of stabilization, while being low-cost and simple, while the circuit-controlled approach has a fast time response and a stable repetition rate. The hybrid approach could stabilize the fiber laser, but it was not compared with the circuit-controlled method since its performance was comparable to that of the computer-controlled method.

Finally, an attempt was made to stabilize both the computer-controlled method and the circuit-controlled method at other modulation frequencies. From this frequency generalization process, it appeared that the computer-controlled method was more versatile. Although the results at 10GHz, 5GHz, and 2.5GHz were found to be inaccurate because of the 40GHz-specific cavity design, both methods could keep the fiber laser stable for small periods of stabilization at lower modulation frequencies. This proves that the generalization of the two stabilization methods at lower frequencies is possible.

9. Bibliography

Books

[1] Siegman, Anthony E. (1986), *Lasers*, Sausalito, University Science books.

[2] Agrawal, Govind P. (2001), *Applications of Nonlinear Fiber Optics*, San Diego, Academic Press.

[3] Yariv, Amnon (1997), *Optical Electronics in Modern Communications*, 5th edition, New York, Oxford University Press.

[4] Agrawal, Govind P. (2001), *Nonlinear Fiber Optics*, 3rd edition, San Diego, Academic Press.

[5] Åström, K. and T. HÄGGLUND (1995), *PID Controllers: Theory, Design, and Tuning*, 2nd edition, Research Triangle Park, ISA-The Instrumentation, Systems, and Automation Society.

[6] Agrawal, Govind P. (1997), *Fiber-Optic Communication Systems*, 2nd edition, New York, Wiley-Interscience.

[7] Rashid, Muhammad H. (1999), *Microelectronic Circuits: Analysis and Design*, Boston, PWS Publishing Company.

[8] Diels, Jean-Claude and Wolfgang RUDOLPH(1995), *Ultrashort Laser Pulse Phenomena: Fundamentals, Techniques, and Applications on a Femtosecond Time Scale*, San Diego, Academic Press.

[9] Ambardar, Ashok (1999), Analog *and Digital Signal Processing*, 2nd edition, Pacific Grove, Brooks/Cole Publishing Company.

[10] Saleh, B. E. A. and M.C. TEICH (1991), *Fundamentals of Photonics*, New York, Wiley-Interscience.

[11] Becker, Philippe C., N. Anders OLSSON and Jay R. SIMPSON (1999), *Erbium-Doped Fiber Amplifiers: Fundamentals and Technology*, San Diego, Academic Press.

[12] Paschotta, R. and Ursula KELLER (2003), *"Ultrafast Lasers: Technology and Applications"*, New York, Marcel Dekker inc.

[13] Hecht, Eugene (1987), *Optics*, Massachusetts, Addition-Wesley Publishing Company.

Articles

[14] E. A. Ponomarev, S. Yang, X. Bao, "Computer controlled harmonic FM mode-locking of 40 GHz repetition rate fiber laser," in Photonic Applications in Telecommunications, Sensors, Software, and Lasers, edited by J. Armitage, R. Lessard and G. Lampropoulos, Proc. SPIE 5579, 736-743 (2004).

[15] X. Shan, D. Cleland and A. Ellis, "Stabilizing Er fiber laser with pulse phase locking", Electronics Letters, vol.28, no. 2, 182-184 (1992).

[16] J. Li, P.A. Andrekson and B. Bakhshi, "Direct generation of subpicosecond chirp-free pulses at 10 GHz from nonpolarization maintaining actively mode-locked fiber ring laser", IEEE Photonics Technology Letters, vol. 12, no. 9, 1150-1152 (2000).

[17] E. Nakazawa, E. Yoshida, and K. Tamura, "Ideal Phase-Locked-Loop (PLL) Operation of a 10GHz Erbium-Doped Fiber Laser Using Regenerative Modelocking as an Optical Voltage Controlled Oscillator", Electro. Lett., vol. 33, no. 15, 1318-1320 (1997).

[18] D. Von Der linde, "Characterization of the Noise in Continuously Operating Mode-Locked Lasers", Appl. Phys. B, vol. 39, 201-217 (1986).

[19] E. Yoshida, M. Nakazawa: "Measurement of the Timing Jitter and Pulse Energy Fluctuation of a PLL Regeneratively Mode-Locked Fiber Laser", Electro. Lett., vol. 11, no. 5 (1999).

[20] S. Yang, E. A. Ponomarev, X. Bao, "Experimental study on relaxation oscillation in a detuned FM harmonic mode-locked Er-doped fiber laser," Optics commu., vol.245, 371-376 (2005).

[21] M. Horowitz, C.R. Menyuk, T. F. Carruthers and I. N. Duling, III, "Theoretical and experimental study of harmonically modelocked fiber lasers for optical communication systems", J. Lightwave Technology, Vol. 18, No. 11, pp. 1565-1574 (2000).

[22] H. Sotobayashi and K. Kikuchi, "Design theory of ultra-short pulse generation from actively mode-locked fiber lasers", IEICE Trans. Electron., Vol. E81-C, No. 2, pp. 201-207 (1998).

[23] J.S. Wey, J. Goldhar, D.W. Rush, M.W. Chbat, G.M. Carter and G.L. Burdge, "Performance characterization of a harmonically mode-locked erbium fiber ring laser", IEEE Photonics Technology Letters, Vol. 7, No. 2, pp.152-154 (1995).

[24] M. Nakazawa, E. Yoshida, E. Yamada and Y. Kimura, "A repetition-rate stabilized and tunable, regeneratively mode-locked fiber laser using an offset-locking technique", Jpn. J. Appl. Phys., Vol. 35, pp. L691-L694 (1996).

[25] E. Yoshida, K. Tamura and M. Nakazawa, "Intracavity dispersion effects of a regeneratively and harmonically FM mode-locked Erbium-doped fiber laser", IEICE Trans. Electron., Vol. E81-C, No. 2, pp. 189 - 194 (1998).

[26] M. Nakazawa, E. Yoshida and K. Tamura, "10 GHz, 2ps regeneratively and harmonically FM mode-locked erbium fibre laser", Electronics Letters, Vol. 32, No. 5, pp. 461-463 (1996).

[27] E. Yoshida, N. Shimizu and M. Nakazawa, "A 40-GHz 0.9-ps regeneratively mode-locked fiber laser with tuning range of 1530-1560 nm", IEEE Photonics Technology Letters, Vol. 11, No. 12, pp. 1587-1589 (1999).

[28] J. Li, P.A. Andrekson and B. Bakhshi, "Direct generation of subpicosecond chirp-free pulses at 10 GHz from nonpolarization maintaining actively mode-locked fiber ring laser", IEEE Photonics Technology Letters, Vol. 12, No. 9, pp. 1150-1152 (2000).

[29] M. Nakazawa, E. Yoshida, and Y. Kimura, "Ultrastable harmonically and regeneratively mode-locked polarisation-maintaining erbium fibre ring laser", Electronics Letters, Vol. 30, No. 19, pp. 1603-1605 (1994).

[30] L. A. Jiang and H. Yokoyama, "Timing jitter eater for optical pulse trains", Optics Letters, Vol. 28, No. 2, pp. 78-80 (2003).

[31] J. P. Gordon and H. A. Haus, "Random Walk of Coherently Amplified Solitons in Optical Fiber Transmission", Optics Letters, Vol. 11, No. 10, pp. 665-667 (1986).

[32] X. Shan, T. Widdowson, A. D. Ellis and A. S. Siddiqui, "Very simple method to stabilise mode-locked erbium fibre lasers", Electronics Letters, Vol. 32, No. 11, pp. 1015-1016 (1996).

[33] E. Yoshida and M. Nakazawa, "Wavelength tunable 1.0ps pulse generation in 1.530-1.555μm region from PLL, regeneratively modelocked fibre laser", Electronics Letters, Vol. 34, No. 18, pp. 1753-1754 (1994).

[34] E. Snitzer, "Proposed Fiber Cavities for optical masers", Journal of Applied Physics, Vol. 32, No. 1, pp. 36 (1961).

[35] L. Bouchard, S. Yang, E. A. Ponomarev, and X. Bao "Development and Performance Comparison of Two Different Approaches for Stabilizing a Harmonic Mode-Locking Fiber Laser at 40GHz", Journal of Applied Physics, accepted for publication (2005)

University Course Notes

[36] Desbiens, André, "Systèmes et commande linéaire", Québec, Université Laval (2001).

[37] Ganguly, Udaya S., "Électronique des composantes intégrés", Québec, Université Laval (2002).

Web sites

[38] xray.optic.rochester.edu/users/noddles/papers/jitter.pdf (Measuring Timing Jitter and Pulse Train Fluctuations)

[39] www.driedger.ca/Z-N/Z-N.html (Optimum Settings For Automatic Controllers)

[40] www.ecircuitcenter.com/Circuits/op_pid/op_pid.htm (PID Controller Design)

[41] www.engin.umich.edu/group/ctm/PID/PID.html (PID Tutorial)

[42] www.expertune.com/tutor.html (PID Tutorial)

[43] www.answer.com/topic/modelocking (Modelocking theory)